Studies on Nanomaterials Assemblies Composed of Silsesquioxane Derivatives

Asuman Celik Kucuk

Department of Applied Chemistry, Graduate School of Engineering

TOHOKU UNIVERSITY

September 2011

Studies on Nanomaterials Assemblies Composed of Silsesquioxane Derivatives

シルセスキオキサン誘導体からなるナノ集積体に関する研究

A Dissertation submitted for the Degree of

Doctor of Engineering

By

Asuman Celik Kucuk

Department of Applied Chemistry, Graduate School of Engineering

TOHOKU UNIVERSITY

September 2011

CONTENTS

1. CHAPTER 1: Introduction

1.1 Introduction

The study on the chemistry of compounds containing Si-O bonds has been dominated by silica, in which the formula unit is SiO_2, or by silicones, in which the formula unit is R_2SiO (R=organic substituent). However, within the last 10-15 years, the field of silsesquioxane chemistry, based on compounds with $RSiO_{1.5}$ repeat units, has grown dramatically. These compounds thus have a formula unit between that of the inorganic SiO_2 and the silicone polymers and have often been described as "hybrid" materials, that is, some from the chemically inert and thermally stable inorganic Si-O-Si fragment and some from the potentially reactive and readily modified R-Si fragment (Figure 1.1).[1-3]

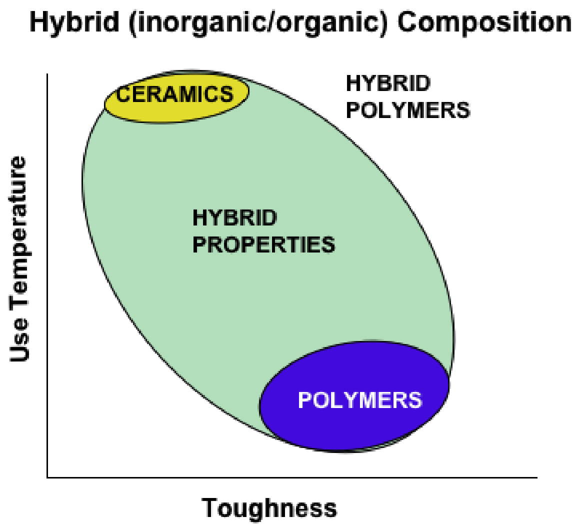

Figure 1.1 Hybrid properties of POSS

A variety of polymeric structures based on the $RSiO_{1.5}$ backbone has been readily prepared, from amorphous network[4-6] (Figure 1.2a) through ladder polymers[7, 8] (Figure 1.2b) to more highly ordered discrete molecular species with the general formula $(RSiO_{1.5})_n$ that is well known as polyhedral oligomeric silsesquioxanes (POSSs) [9-11] (Figure 1.2c-e). These cubic siloxane cages with readily functionalized substituents have thus become very popular as nanometer-scale building blocks or polymeric materials.[12-16]

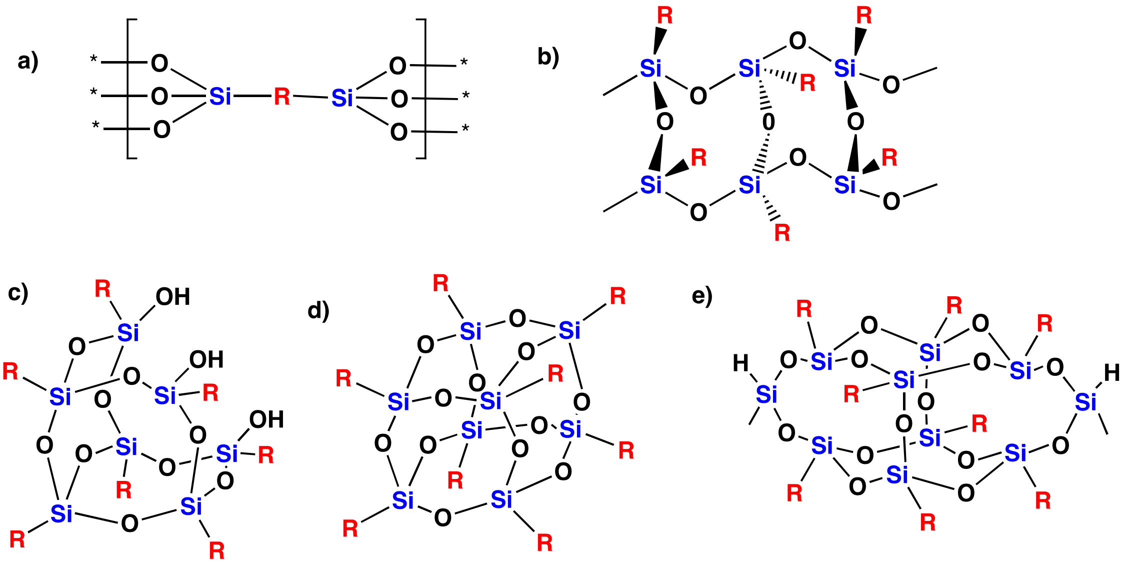

Figure 1.2 Possible structures of silsesquioxanes (a) amorphous network, (b) ladder polymer, (c) partially opened-cage POSS,[17, 18] (d) cubic POSS,[19, 20] and (e) double-decker type POSS.[21-23]

POSS densities are typically in the range of 1.12 g ml^{-1}. This is due to the fact that the core occupies only about 5% of the overall volume. Most of the volume is taken up by the organic R groups, which lie on the outside of the cage (Figure 1.3a).[24] The nature of the R groups, along with the topology of POSS cages, controls their physical states (solid, wax, liquid). POSS has a nanosize dimension, with diameters generally ranging from 0.7 nm to 5.0 nm, so they're smaller than a macromolecule, but larger than a small molecule (Figure 1.3b). This specific size regime enable a well compatibilization with conventional polymer to improve the physical properties as a nanofiller.

a) b)

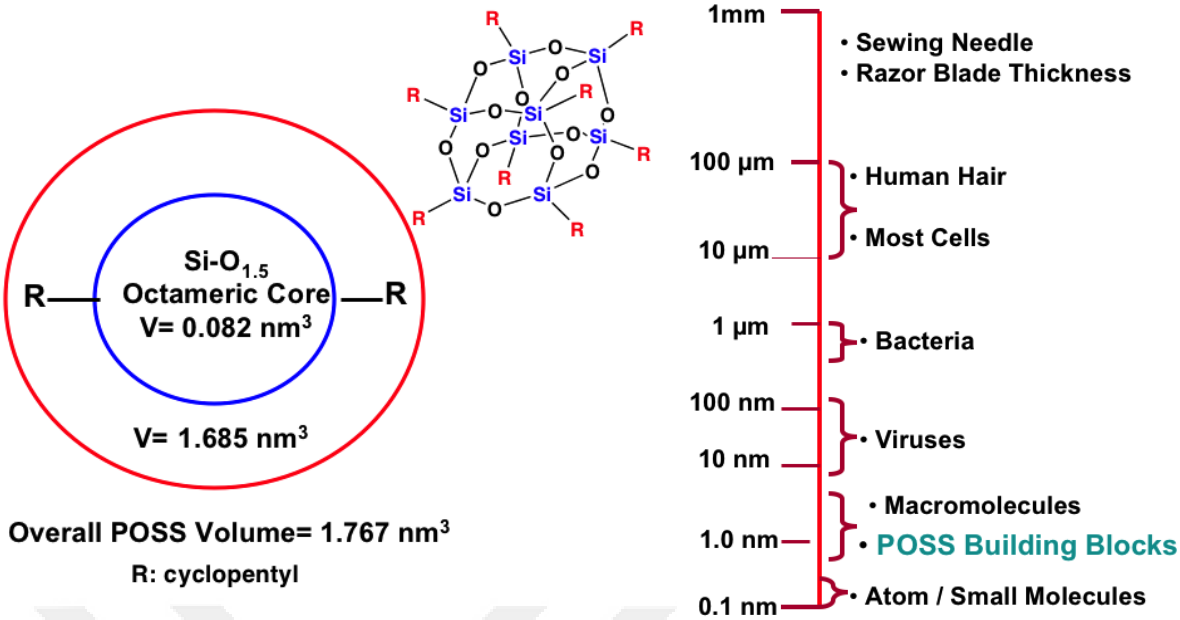

Figure 1.3 (a) Volume of POSS cage, (b) place of POSS in the size regime.

It is known that POSS architectures that POSS is core stays intact up to 550 °C.[16] The central core is externally functionalized with organic groups to provide compatibility with polymer[25] or biological materials.[26] The thermal stability of the organic group is compositionally dependent and ranges from 350 °C to 450 °C.[27] The average diameter of a POSS molecule is 1.5 nm.[28] Additionally, each POSS nanostructure can be manufactured to contain a chemically precise number of reactive groups that impart specific functionality to these building blocks. Thus POSS can be used as a monofunctional[29] or graftable monomer,[30] a difunctional comonomer,[31] a surface modifier,[32] or a polyfunctional crosslinker for polymers.[3, 20, 33, 34]

1.2 *Synthesis of POSSs*

1.2.1 *Fully Condensed Silsesquioxanes*

There are a great number of reactions leading to the formation of POSS and its derivatives[35-37] especially reviewed by Voronkov et al[38] and Feher and co-workers.[39] According to the these studies, silsesquioxanes are most often prepared via hydrolytic condensation reaction of trifunctional organosilicon monomers (e.g., $RSiCl_3$ or $RSi(OMe)_3$). These reactions can produce a wide variety of interesting products, ranging from small oligomers and discrete clusters to complex resins and "T-gels" (Scheme 1.1). It is difficult to make generalizations about these reactions because each reaction appears to be uniquely sensitive to a highly interdependent combination of experimental factors, including product solubilities, initial monomer concentration, nature and stability of the solvent, temperature, pH, the amount of free water available, and the type of catalyst (acid or base) used to facilitate condensation.

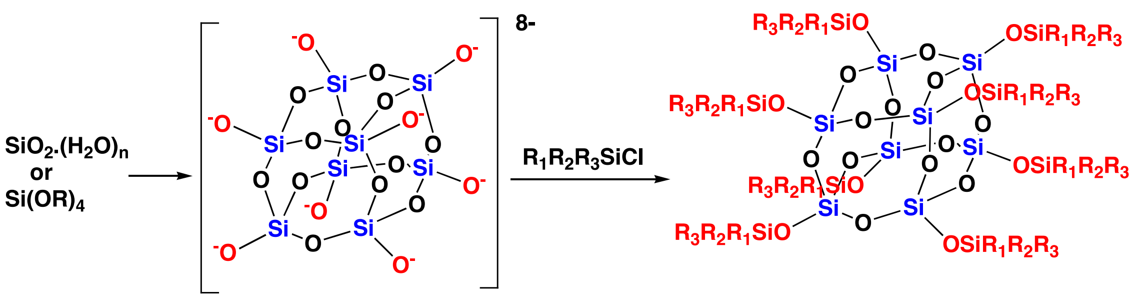

Scheme 1.1 Hydrolytic condensation reactions for POSS

Nevertheless, many hydrolytic condensation reactions produce synthetically useful quantities of fully-condensed POSS frameworks containing T_6, T_8, T_{10} and/or T_{12} Si atoms (Figure 1.4).

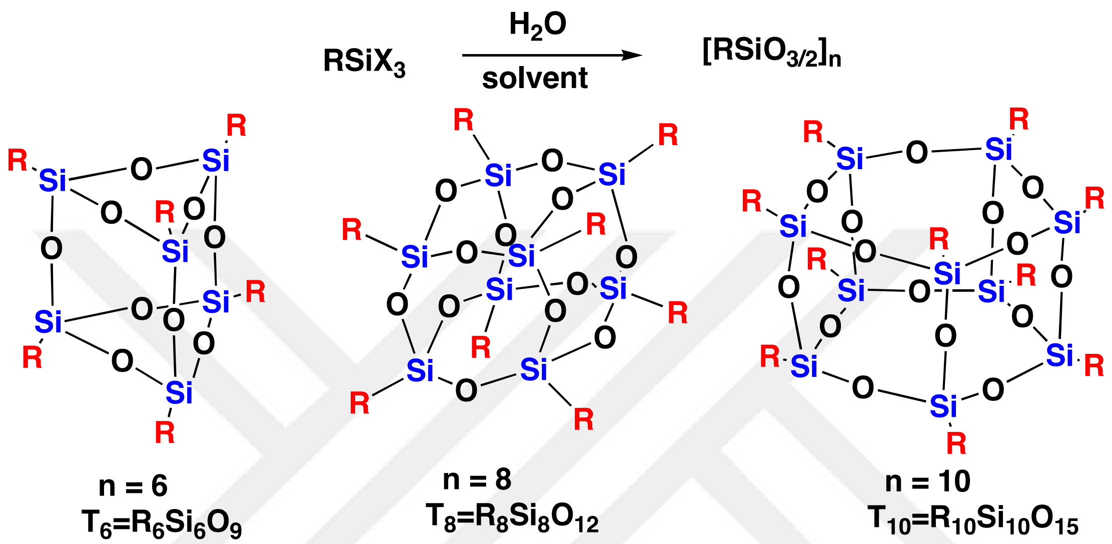

Figure 1.4 Structures of fully-condensed POSS frameworks

1.2.2 *Synthesis of Double-decker-shaped Silsesquioxane*

The structure and synthetic route of double-decker phenylsilsesquioxane is shown in Scheme 1.2. It is a reaction of phenyltrimethoxysilane in the medium of sodium hydroxide and 2-propanol. After the reaction, double-decker phenylsilsesquioxane sodium salt is precipitated and obtained as a colorless powder.[22]

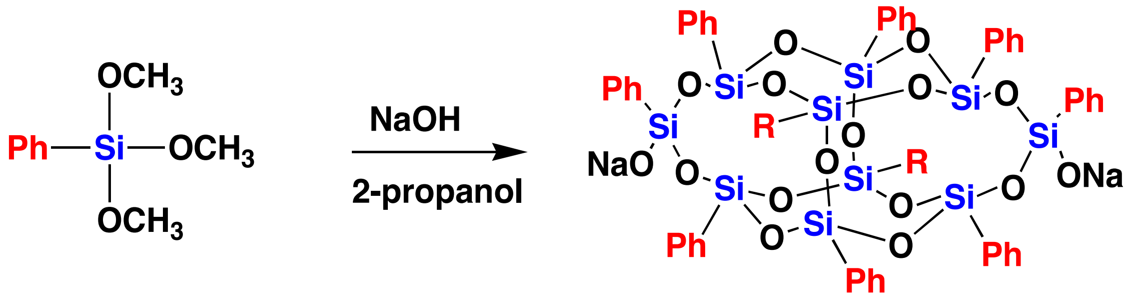

Scheme 1.2 Synthesis of tetrasodium salt of double-decker phenylsilsesquioxane

1.3. Functionalization of POSS Compounds by Hydrosilylation

1.3.1. Hydrosilylation Reactions Using Highly Reactive Pt(0) Catalyst Precursors

Hydrosilylation catalyzed by platinum catalyst promotes in high yield,[40] therefore, it is frequently used for functionalization, or polymerization of POSS. The Chalk-Harrod mechanism is the most commonly accepted mechanism for platinum catalyzed hydrosilylation and is based on elementary steps such as oxidative addition and reductive elimination, which are fundamental to organometallic chemistry for processes such as the hydrogenation of olefins.[41-43]

An overall reaction scheme is shown in Figure 1.5. During the induction period, the Pt(0) precatalyst undergoes dissociation of the bridging olefin to form a mononuclear, two coordinate complex. Oxidative addition of R_3SiH leads to formation of a Pt(II) complex which is followed by migratory insertion of the olefin into the Pt-H bonds. The reversibility of these steps is supported by the reaction with deuterosilane in which high levels of deuterium were incorporated in the hydrosilylation products of divinyltetramethyldisiloxane ($M^{vinyl}M^{vinyl}$). After hydrosilylation of the $M^{vinyl}M^{vinyl}$ ligand, which concludes the end the induction period, the catalytic cycle proceeds with the added olefin. Of course it cannot be ruled out that olefin exchange may also be occurring during the induction period.[44]

Steps in the catalytic cycle are similar to those occurring during the induction period. Evidence in support of the catalytic cycle includes kinetic data, which support a positive order in hydrosilane and an inverse dependence on olefin concentration. In situ Extanted X-ray Absorption Fine Structure (EXAFS) analysis indicate that the catalyst is mononuclear and contains Pt-C and Pt-Si bonds regardless of the stoichiometry of the reagents. The absence of vinylsilane products is consistent with migratory insertion of the olefin into the Pt-H bond. The observed kinetic isotope effect suggests that Si-H bond breaking occurs prior or during the rate determining step. The rate-determining step is most likely reductive elimination since no Pt-H bonds observed by NMR or IR spectroscopies.[44]

The platinum end products are dependent on the stoichiometry of the reagents. With high olefin concentration, a $Pt(olefin)_3$ complex is formed. Under conditions of high hydrosilane concentration, a multinuclear Pt cluster is formed with silyl ligands. The products can be interconverted by addition of the appropriate reagent probably through the intermediacy of species **4**. Conditions that favor formation of Pt complex 2 (absence of oxygen with poor reagents for hydrosilylation, excess hydrosilane, and poorly coordinating olefins) can result in low conversion and olefin bond isomerization.[44]

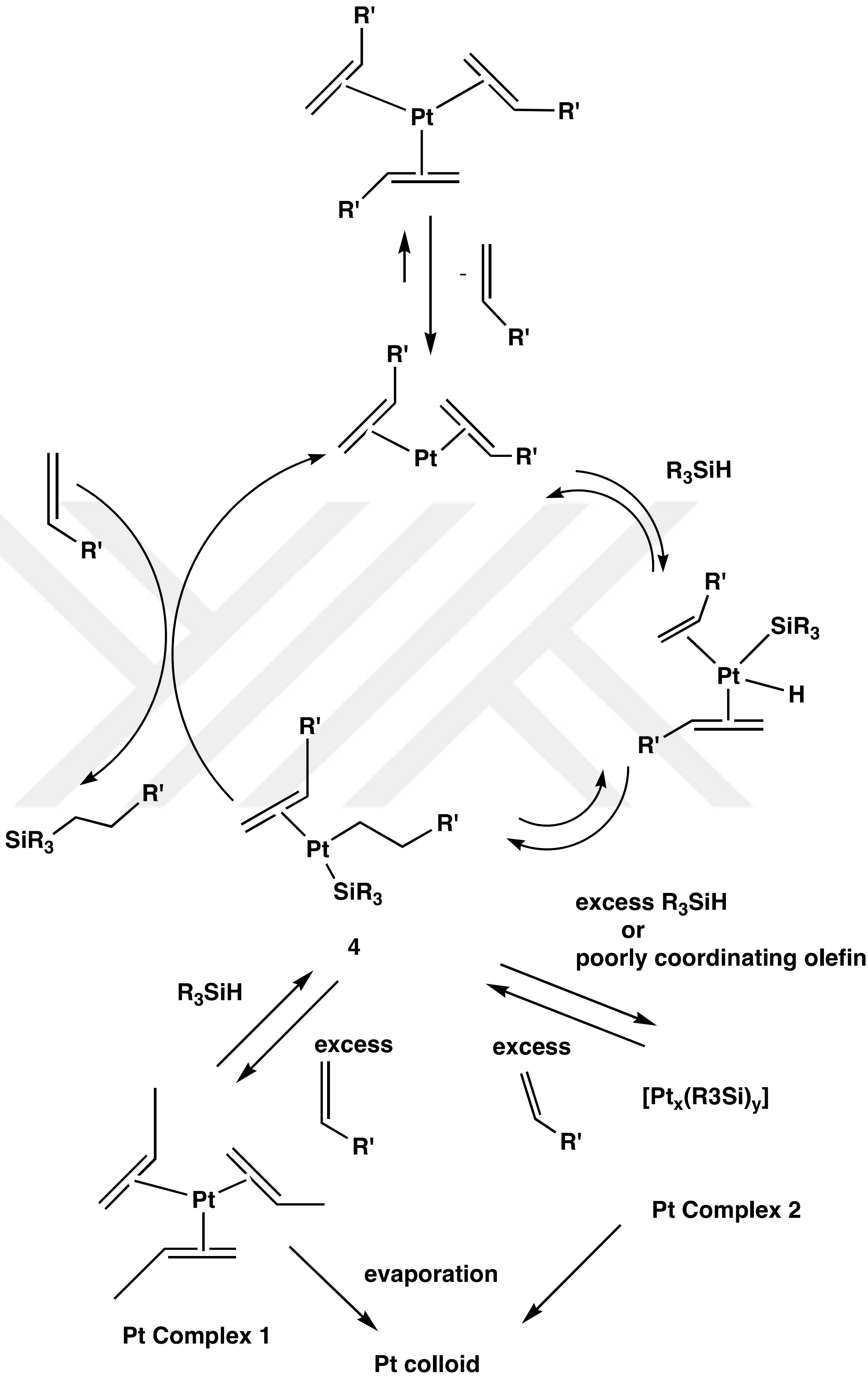

Figure 1.5 Overall reaction mechanism for hydrosilylation catalyzed Karstedt's

precatalyst.[44]

1.3.2 Hydrosilylation Reaction of T_8R_8 Compounds

Hydrosilylation is a simple, often platinum-catalyzed, reaction allowing the addition of a Si-H to an unsaturated compound such as an alkene or alkyne. In the case of T_8 derivatives, the general reaction can be summarized in Scheme 1.3. While the yields of such a reaction are often high,[45] reaction at an oxygen center, rather than the carbon-carbon double or triple bond, may occur when there is alcohol or carbonyl functionality present in the alkene or alkyne. On the other hand, Laine et al. reported that selective silylation to alkenes, alkynes can be acchived with selection of proper catalyst, concentration, and solvent.[46]

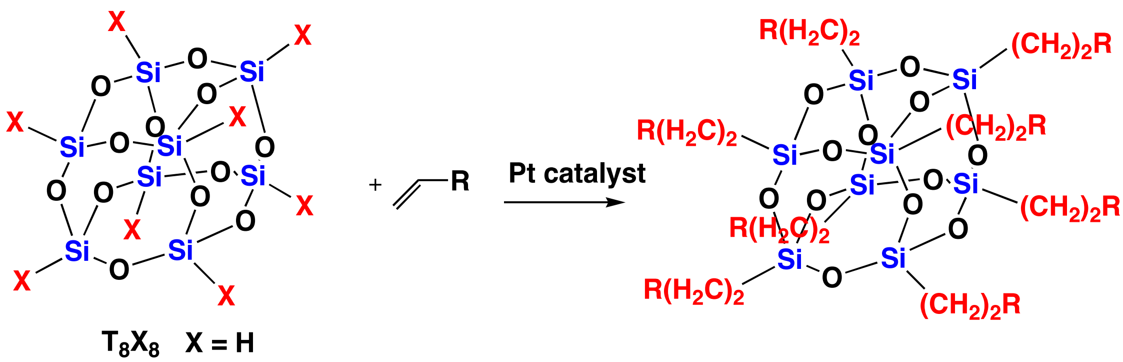

Scheme 1.3 Hydrosilylation reaction of POSS

1.4. Applications of POSS for Proton-conducting Material

The quest for clean and efficient sources of electrical energy and concerns about environmental pollution has intensified the research on hydrogen fuel cells. Among various types of fuel cells, the polymer electrolyte membrane or proton exchange membrane fuel cell (PEM) has the well-recognized potential to supply clean energy for transportation and portable electronic systems.[47, 48] The heart of this technology is a polymer membrane that selectively conducts protons.

PEM fuel cell contains two electrodes and a polymer membrane, which acts an electrolyte (Figure 1.6). PEM is sandwiched between two porous electrodes. When the PEM fuel cell is operated, hydrogen flows into the cell on the anode. A catalyst, typically Pt, facilitates the oxidation of the hydrogen gas to form the protons and electrons. Protons pass through the electrolyte, and combine with the oxygen and electrons at the cathode, with the help of another catalyst layer, producing water. Electrons flowing from the anode to cathode through an external circuit generate electrical power. The reactions, which occur at each electrode, are:

Anode $H_2 \rightarrow 2H^+ + 2e^-$

Cathode $1/2\ O_2 + 2H^+ + 2e^- \rightarrow H_2O$

Overall $H_2 + 1/2\ O_2 \rightarrow H_2O$ + Electrical energy

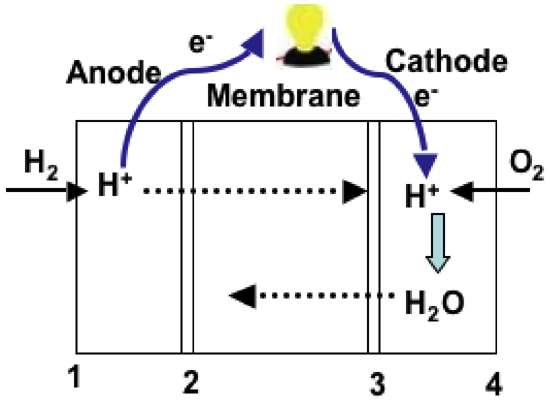

Figure 1.6 Proton exchange membrane fuel cell.

Conventional material used in PEM is Nafion, a perfluorosulfonic acid (PFSA) based polymer (Figure 1.7).[48] The major drawback Nafion is that they rely on water-assisted proton transport (PT) that is, the vehicular motion of hydronium ions,[49] which restricts the operational temperature to about 80 ˚C.[50] Hence, research efforts are being focused on developing new materials that are capable of conducting protons under anhydrous conditions that is via Grotthuss mechanism of proton transfer or framework proton conduction.[51]

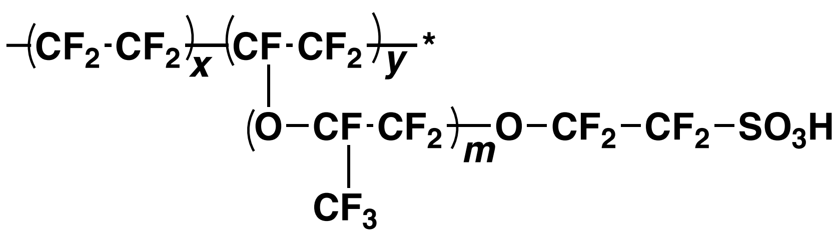

Figure 1.7 The chemical structure of Nafion.

Researches have incorporated POSS in polymer electrolyte to improve not only thermal and mechanical stability but also proton conductivity in intermediate temperature. For example, Choudhury et al.[52] reported that incorporation of sulfonated polyhedral oligomeric silsesquioxanes (POSS) into the Nafion using layer-by-layer technique has allowed them to achieve anhydrous conductivity and good mechanical integrity at high temperatures (5 mS cm^{-1} at 150 ˚C with 20% ionic liquid (IL)). They reported that ionic interaction between POSS, IL and Nafion membrane is the key for the increase in the proton conductivity and mechanical properties.

Moreover, in their other work, POSS has been used as a filler in sulfonated poly(ether ether ketone) (SPEEK) matrix. The composite membranes showed a three-fold increase in proton conductivity; that is 4.5 mS cm^{-1}, which is higher compared with SPEEK (1.5 mS cm^{-1}) and Nafion (3.4 mS cm^{-1} at 90 ˚C), with a significant decrease in methanol permeability.[53]

1.5. Preparation of Ultrathin Film Using the Langmuir-Blodgett Technique

1.5.1 *Monolayers*

Irving Langmuir demonstrated that amphiphilic molecules are able to form a monolayer at the air-water interface. Conventional amphiphilic molecules composed of two parts; non-polar “TAIL” group, which usually is a hydrocarbon chain and polar “HEAD” group, which is composed of hydroxyl, amine, carboxyl, etc. The amphiphilic molecules are dissolved in a volatile solvent (chloroform) and spread at the air-water interface. After the evaporation of solvent, a movable barrier compresses the monolayer at the air-water interface and surface pressure (π)-surface area (*A*) isotherm was measured. The π-A isotherm gives information about stability of the monolayer at the air-water interface, reorientation of molecules in the two-dimensional system, phase transition and conformational transformation. Surface pressure (π) is the conceptual inverse of surface tension (γ), which can be defined as the tendency of liquids to reduce their surface area. This value is represented quantitatively as

$$\Pi = \gamma_0 - \gamma \qquad (1\text{-}1)$$

where γ_0 is the surface tension of a pure liquid and γ is the surface tension of a liquid covered with a monolayer. As the surface tension of a pure liquid drops with the addition of a surfactant, the surface pressure similarly rises.

The area per molecule can be defined as the average area occupied by one molecule on the surface at a particular surface pressure. The gaseous phase is characterized by a random arrangement of molecules on the surface with a large area per molecule and low surface pressure (Figure 1.8, (G)). The liquid phase can be separated into two different phases for some molecules. A first order transition from the gas phase to the liquid-expanded phase is shown by a change in slope of the π-A isotherm (Figure

1.8, (L-G)). This phase is characterized by coherent fluidity with a smaller density than the liquid condensed phase or a bulk liquid as well as any corresponding solid bulk or surface phases. The liquid condensed phase results from an area per molecule that is small enough to restrict position but still allow for free molecular rotation on the surface (Figure 1.8, (L_1)).[54] The solid phase exists where molecules are highly ordered and packed as tightly together as possible (Figure 1.8, (L_2)). The limiting area per molecule permits no free movement within the dense, rigid film. When the areas per molecule become smaller than that of the solid phase, film collapse is observed. In the collapse regime, molecules cease to maintain their ordered in two-dimensional arrangement and begin to pile up on top of one another to eventually form multilayers (Figure 1.8, (S)).

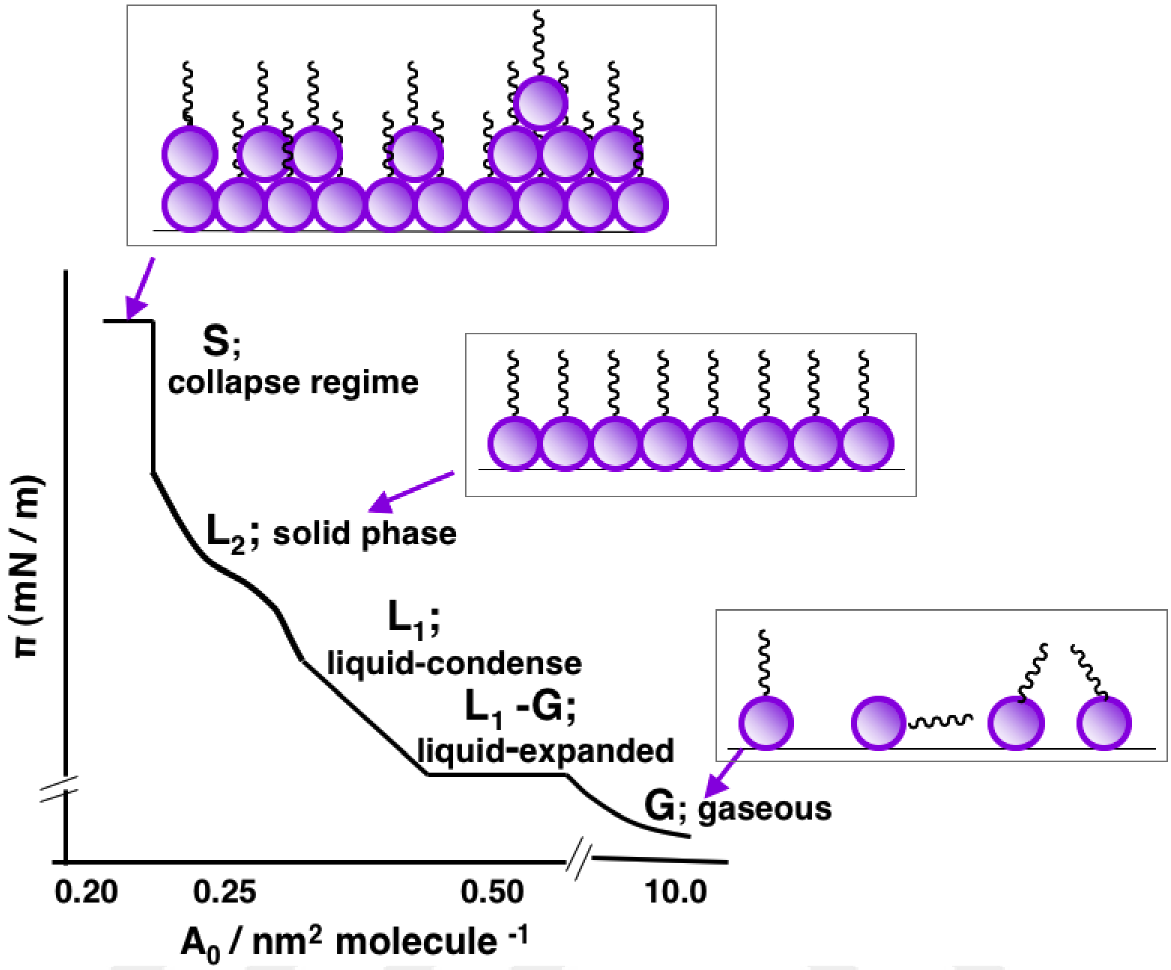

Figure 1.8 Generic π-A isotherm for amphiphilic molecules

1.5.2. Langmuir-Blodgett Films

When operating at a constant surface pressure, monolayers at the air-water interface can be deposited onto solid substrates by passing the substrate through the monolayer at the air-water interface by downward and upward strokes (LB technique). For a monolayer to be deposited onto a substrate, there are two factors, which must be considered. First, the monolayer must be hydrophobic enough to be largely insoluble in the water subphase. Second, the film must have enough rigidity to remain on the surface but must also have a low enough viscosity to be transferred onto the substrate without cracking. Film deposition can occur in one of three patterns: x-type, y-type, or z-type (Figure 1.9).

Y type film: Layers are deposited on the substrate during both up- and downstroke processes. When the substrate surface is hydrophilic, for instance, the first monolayer is transferred as it is raised through the air-water interface. Subsequently monolayers are deposited on each traversal of the interface. As shown in Figure 1.9, either a head-to head or tail-to tail film pattern is obtained.

X type film: It is obtained when the floating monolayer is only transferred to the substrate as it inserted into the subphase (downstroke process).

Z type film: It is obtained when the monolayer is only transferred to the substrate as it is removed from the water subphase (upstroke process).

The films deposited as a x-type or z-type film are sometimes determined to actually be a y-type film by x-ray analysis. The deposition type can also switch at some point during the deposition.[55] The major advantage of making films in this way is that each layer is deposited individually and is exactly one molecule thick. It follows that the number of molecular layers can be predetermined and highly ordered films of a controlled thickness can be obtained.

The surface pressure, at the deposition process, is an important factor since the arrangement of molecules on the subphase depends on the different pressures. The most desirable transfer occurs from the liquid condensed phase where the film has been compressed as densely as possible without collapsing into multilayers. A collapsed film or a film in which the molecules are loosely packed together will not produce uniform films on the surface of the solid substrate. The quality of the deposited film can be measure quantitatively through the transfer ratio (TR) given by

TR = decrease in Langmuir monolayer surface area/ total surface area of substrate

Transfer ratio of unity means stable LB film deposition on the substrate. Higher TR value than unity means dissolution of molecules in water or aggregation, whereas lower TR means incomplete coverage of the solid substrate.

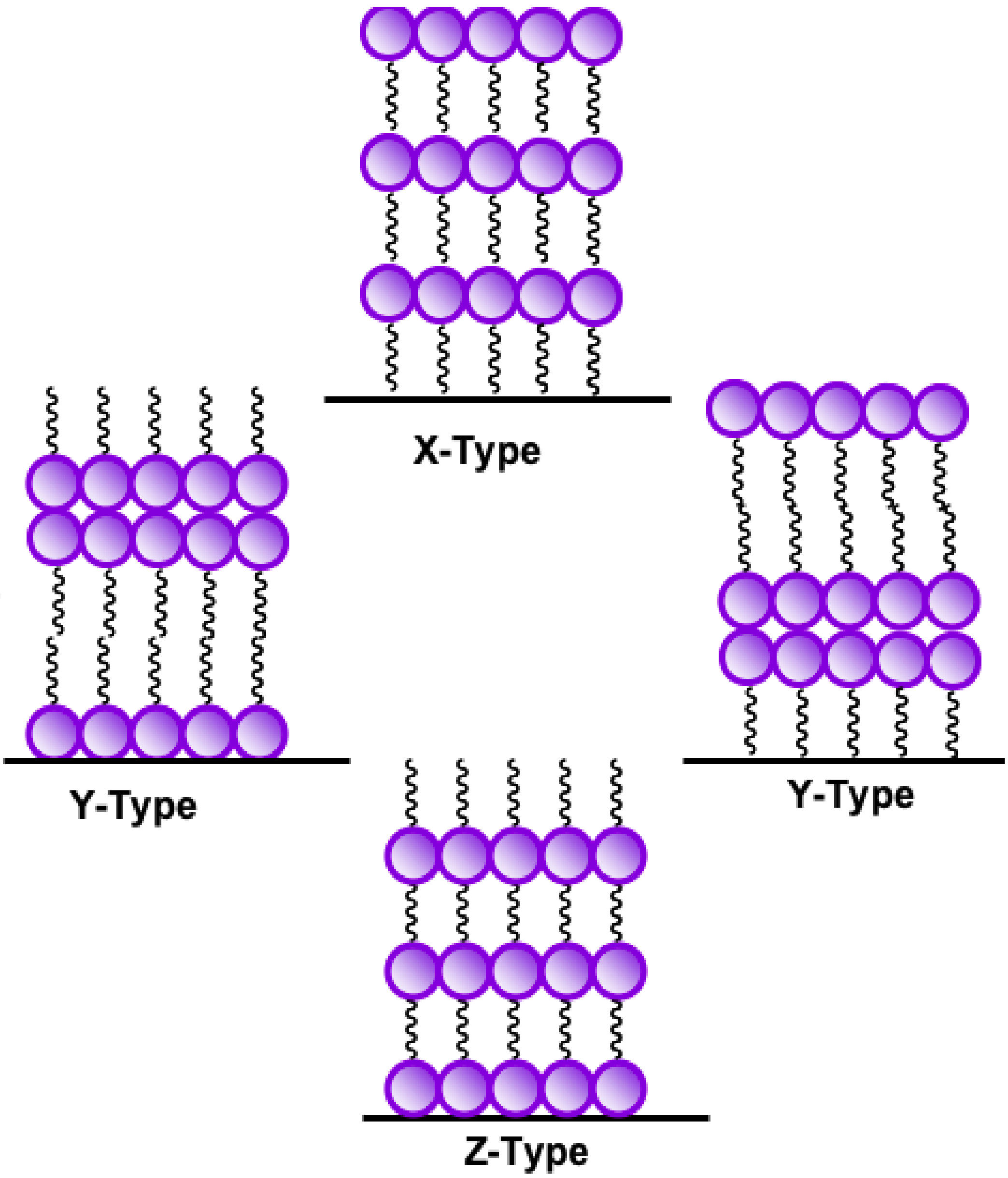

Figure 1.9 Film Deposition Types

1.6. Brewster Angle Microscopy

There are several methods of surface imaging that are compatible with Langmuir monolayer including fluorescence microscopy and Brewster angle microscopy (BAM). The advantage of BAM is that a Langmuir film can be studied *in situ* without further chemical perturbation or the deposition of the film onto a solid substrate. Since the reflectivity about Brewster's angle is associated with the angle of incidence and the angle of refraction, θ_0 and θ_1 respectively, the theory behind this technique can be related simply to Snell's Law written as

$$n_0 \sin\theta_0 = n_1 \sin\theta_1 \tag{1-2}$$

To define Brewster's angle (θ_b), $\tan\theta_b = n_1 / n_0$, it is important to note that light passing through a medium with a lower refractive index (air, n_0) into a medium with a higher refractive index (water, n_1) generally reflects *p*-polarized light. However, when operating a microscope at Brewster's Angle, no *p*-polarized light is reflected. The addition of a film to the surface introduces some reflectivity that is dependent upon the film thickness and the refractive index (Figure 1.10). The reflection caused by the monolayer increases as the film thickness and film index increase.[54]

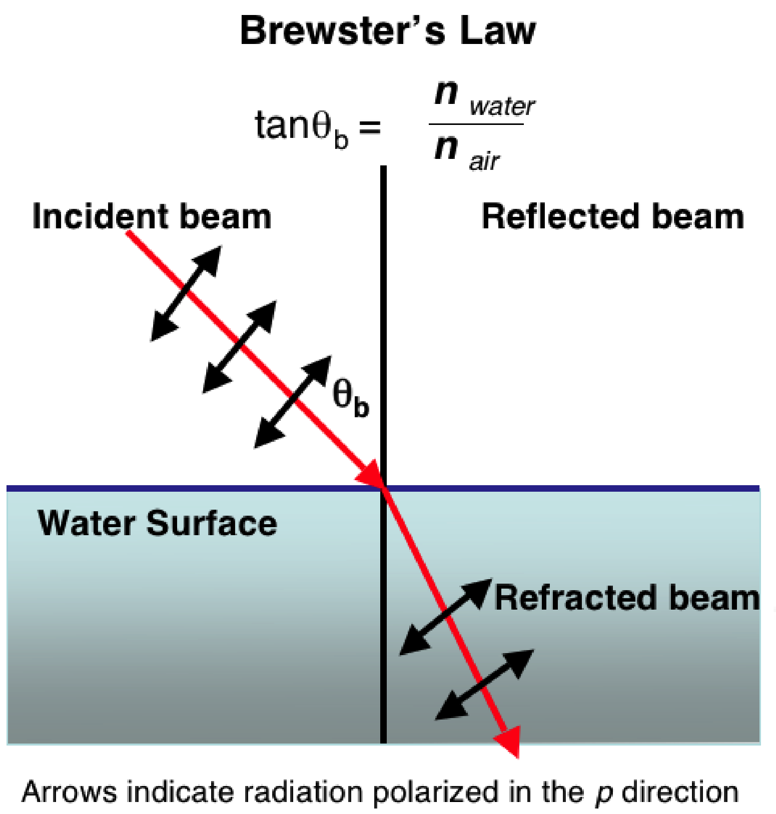

Figure 1.10 Light diagram in Brewster Angle Microscopy (BAM) condition

A Brewster angle microscope, as sketched in Figure 1.11 consists of the following basic components: a laser, a lens L_1 to collimate the beam, a polarizer, a lens L_2 to image the monolayer on a CCD camera. Optionally, one can use a second polarizer, on the reflected light, to probe any polarization change after reflection, which must be due to optical anisotropy in the film.

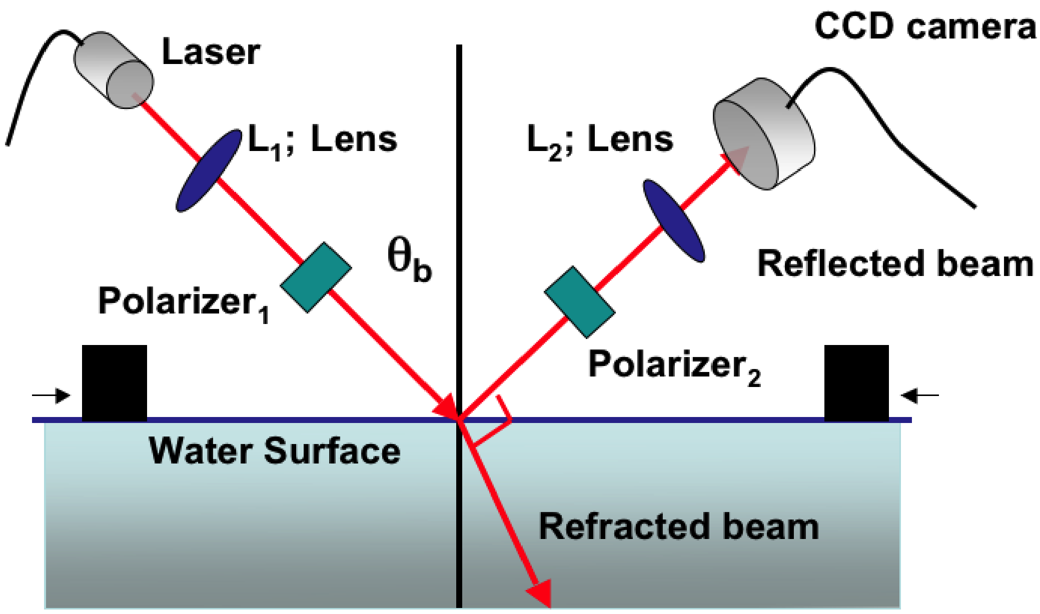

Figure 11. Set up for a Brewster angle microscope.

1.7. Outline of the Thesis

This thesis focuses on organizing silsesquioxanes at a nanometer scale using LB technique, since well-defined and oriented molecular films are extremely important to elucidate physical properties as well as to prepare hybrid nano materials. Conventional POSSs such as T_8, T_{10} and T_{12} have at least 8 reactive sites and generally they have rigid structures. Having many reactive sites makes their functionalization and purification difficult. Moreover, rigid structure easily causes aggregation of POSSs. As compared to conventional POSSs, one of the POSS members, double-decker-shaped silsesquioxanes (DDSQs) have structural differences, which may bring additional advantages.

In this thesis, DDSQ is used as a building block because of its uniformity, easy functionalization and less rigid structure. Unique "core-coronae" type amphiphilic hybrid DDSQ have been synthesized and their monolayer behaviors have been investigated. Additionally, DDSQ molecules are considered as proton-conducting materials and their potential capability of proton conductivity have been examined.

The thesis has been divided into 6 chapters. The outline of the chapters is as follows:

In the Chapter 2, amphiphilic DDSQs, which consist of DDSQ as a hydrophobic core and di(ethylene glycol) (DEG) units as hydrophilic coronae were synthesized. Hydrophilic DEG units were attached to the reactive hydrosilane groups using hydrosilylation reaction to prepare two and tetra-armed amphiphilic DDSQs, these are abbreviated as 2DEG-DDSQ and 4DEG-DDSQ, respectively. The amphiphilic DDSQs take "core-coronae" structure, where DDSQ core is the hydrophobic and DEG units are the hydrophilic coronae. Therefore, the study in the Chapter 2 proposes a new approach to form LB film using the core-coronae structure.

In the Chapter 3, the effects of subphases on the monolayer behavior of 4DEG-DDSQ have been investigated. There kinds solutes, phosphoric acid, 1,3-bis (hydroxymethyl)urea, and KCl, were added to the subphase and the change in the morphology of the monolayers has been investigated.

In the Chapter 4, to understand how subsistent effects on the monolayer behavior, hydroxyl groups of DEG in 2DEG-DDSQ and 4DEG-DDSQ were converted to ethyl carbamate.

In the Chapter 5, 4DEG-DDSQ was functionalized with phosphonic acid to prepare hybrid proton conductive membrane. The obtained compound (PHOS-DDSQ) was characterized by ^{1}H, ^{31}P NMR, FT-IR and MALDI-TOF mass spectrometry. The thermal stability and proton conductivity of new material (PHOS-DDSQ) were investigated under different humid and also non-humid conditions. The contribution of DDSQ, covalent bonded phosphonic acid, and effects of short-chain DEG units to the proton conductivity were also discussed.

In the chapter 6, the summary and conclusion of the thesis were described.

6. References

1. Wright, M. E.; Petteys, B. J.; Guenthner, A. J.; Fallis, S.; Yandek, G. R.; Tomczak, S. J.; Minton, T. K.; Brunsvold, A. *Macromolecules* **2006,** 39, 4710-4718.

2. Haddad, T. S.; Lichtenhan, J. D. *Macromolecules* **1996,** 29, 7302-7304.

3. Lichtenhan, J. D.; Otonari, Y. A.; Carr, M. J. *Macromolecules* **1995,** 28, 8435-8437.

4. Choi, J.; Tamaki, R.; Kim, S. G.; Laine, R. M. *Chemistry of Materials* **2003,** 15, 3365-3375.

5. Sanchez, C.; Soler-Illia, G. J. d. A. A.; Ribot, F.; Lalot, T.; Mayer, C. R.; Cabuil, V. *Chemistry of Materials* **2001,** 13, 3061-3083.

6. Pyun, J.; Matyjaszewski, K. *Chemistry of Materials* **2001,** 13, 3436-3448.

7. Fendler, J. H. *Chemistry of Materials* **2001,** 13, 3196-3210.

8. Maoz, R.; Sagiv, J. *Advanced Materials (Weinheim, Germany)* **1998,** 10, 580-+.

9. Murugavel, R.; Bhattacharjee, M.; Roesky, H. W. *Applied Organometallic Chemistry* **1999,** 13, 227-243.

10. Cordes, D. B.; Lickiss, P. D.; Rataboul, F. *Chemical Reviews (Washington, DC, United States)* 110, 2081-2173.

11. *Hybrid Plastics Home Page* *http://www.hybridplastics.com* (accessed Feb. 16, 2010).

12. Koh, K.; Sugiyama, S.; Morinaga, T.; Ohno, K.; Tsujii, Y.; Fukuda, T.; Yamahiro, M.; Iijima, T.; Oikawa, H.; Watanabe, K.; Miyashita, T. *Macromolecules* **2005,** 38, 1264-1270.

13. Leu, C.-M.; Reddy, G. M.; Wei, K.-H.; Shu, C.-F. *Chemistry of Materials* **2003,** 15, 2261-2265.

14. Leu, C.-M.; Chang, Y.-T.; Wei, K.-H. *Chemistry of Materials* **2003,** 15, 3721-3727.

15. Zhang, C.; Babonneau, F.; Bonhomme, C.; Laine, R. M.; Soles, C. L.; Hristov, H. A.; Yee, A. F. *Journal of the American Chemical Society* **1998,** 120, 8380-8391.

16. Xu, H.; Kuo, S.-W.; Lee, J.-S.; Chang, F.-C. *Macromolecules* **2002,** 35, 8788-8793.

17. Hottle, J. R.; Kim, H.-J.; Deng, J.; Farmer-Creely, C. E.; Viers, B. D.; Esker, A. R. *Macromolecules* **2004,** 37, 4900-4908.

18. Deng, J.; Farmer-Creely, C. E.; Viers, B. D.; Esker, A. R. *Langmuir* **2004,** 20, 2527-2530.

19. Knischka, R.; Dietsche, F.; Hanselmann, R.; Frey, H.; Mülhaupt, R.; Lutz, P. J. *Langmuir* **1999,** 15, 4752-4756.

20. Tsuchida, A.; Bolln, C.; Sernetz, F. G.; Frey, H.; Mülhaupt, R. *Macromolecules* **1997,** 30, 2818-2824.

21. Wu, S.; Hayakawa, T.; Kakimoto, M.-a.; Oikawa, H. *Macromolecules* **2008,** 41, 3481-3487.

22. Hoque, M. A.; Kakihana, Y.; Shinke, S.; Kawakami, Y. *Macromolecules* **2009,** 42, 3309-3315.

23. Sylvie Boileau, B. B., Francois Ganachaud, *Silicon Based Polymers*. Springer Science+Business Media B.V: 2008; p 205-211.

24. Laine, R. M. *Journal of Materials Chemistry* **2005,** 15, 3725-3744.

25. Lee, W.; Ni, S.; Deng, J.; Kim, B.-S.; Satija, S. K.; Mather, P. T.; Esker, A. R. *Macromolecules* **2007,** 40, 682-688.

26. Frankamp, B. L.; Fischer, N. O.; Hong, R.; Srivastava, S.; Rotello, V. M. *Chemistry of Materials* **2006,** 18, 956-959.

27. Sheen, Y.-C.; Lu, C.-H.; Huang, C.-F.; Kuo, S.-W.; Chang, F.-C. *Polymer* **2008,** 49, 4017-4024.

28. Waddon, A. J.; Coughlin, E. B. *Chemistry of Materials* **2003,** 15, 4555-4561.

29. Lichtenhan, J. D.; Vu, N. Q.; Carter, J. A.; Gilman, J. W.; Feher, F. J. *Macromolecules* **1993,** 26, 2141-2142.

30. Kim, Y.; Zhao, F.; Mitsuishi, M.; Watanabe, A.; Miyashita, T. *Journal of the American Chemical Society* **2008,** 130, 11848-11849.

31. Kopesky, E. T.; Haddad, T. S.; Cohen, R. E.; McKinley, G. H. *Macromolecules* **2004,** 37, 8992-9004.

32. Gonzalez, R. I.; Phillips, S. H.; Hoflund, G. B. *Journal of Spacecraft and Rockets* **2000,** 37, 463-467.

33. Mather, P. T.; Jeon, H. G.; Romo-Uribe, A.; Haddad, T. S.; Lichtenhan, J. D. *Macromolecules* **1999,** 32, 1194-1203.

34. Bizet, S.; Galy, J.; Gérard, J.-F. *Macromolecules* **2006,** 39, 2574-2583.

35. C. L. Frye and W. T. Collins. *J. Am. Chem. Soc.* **1970,** 92, 5586.

36. M. M. Sprung and F. O. Guenther. *Journal of the American Chemical Society* **1955,** 92, 3990.

37. J. F. Brown, J. *Journal of the American Chemical Society* **1965,** 87, 4317.

38. Lavrent'yev, M. G. V. a. V. L. *Topics Curr. Chem.* **1982,** 102, 199.

39. F. J. Feher, R. T., R. Jin, K. O. Wyndham, S. Lucke, R. Brutchey, and F. Nguyen,. *Polym. Mater. Sci. Eng.* **2000,** 82, 301.

40. Marciniec, B. G., J.; Urbaniak, W.; Kornetka, Z.W., *In Comprehensive Handbook on Hydrosilylation*. Marciniec, B., Ed.; Pergamon: Oxford: 1992.

41. I., O., *The Chemistry of Organic Silicon Compounds,*. Patai S.; Rappaport, Z. Eds.;Wiley Interscience: N.Y.,: 1989; Vol. 2.

42. Armitage, D. A., *In Comprehensive Organometallic Chemistry,*. Wilkinson, G.; Stone, F.G.A.;Abel, E.W., Eds.; Pergamon: Oxford,: 1982; Vol. 2.

43. Harrod, J. F. C., A.J., *In Organic Synthesis via Metal Carbonyls* . Wender, I.; Pino, P.,Eds., Wiley: N.Y.: 1977; Vol. 2.

44. Stein, J.; Lewis, L. N.; Gao, Y.; Scott, R. A. *Journal of the American Chemical Society* **1999,** 121, 3693-3703.

45. Hill, A. F., Fink, M. J., . *Academic Press: Oxford, U.K.* **2008,** 57, 1-116.

46. Zhang, C.; Laine, R. M. *Journal of the American Chemical Society* **2000,** 122, 6979-6988.

47. Hickner, M. A.; Ghassemi, H.; Kim, Y. S.; Einsla, B. R.; McGrath, J. E. *Chemical Reviews (Washington, DC, United States)* **2004,** 104, 4587-4612.

48. Steele, B. C. H. H., Angelika. *Nature* **2001,** 414, 345-352.

49. Kreuer, K.-D. *Chemistry of Materials* **1996,** 8, 610-641.

50. Mauritz, K. A.; Moore, R. B. *Chemical Reviews (Washington, DC, United States)* **2004,** 104, 4535-4586.

51. Ghosh, B.; Lott, K. F.; Ritchie, J. E. *Abstracts of Papers of the American Chemical Society* **2006,** 231, 2.

52. Subianto, S.; Mistry, M. K.; Choudhury, N. R.; Dutta, N. K.; Knott, R. *ACS Applied Materials & Interfaces* **2009,** 1, 1173-1182.

53. Chhabra, P.; Choudhary, V. *Journal of Applied Polymer Science* 118, 3013-3023.

54. Adamson, R. W. G., A. P. . *Physical Chemistry of Surfaces.*

55. Choi, J.-W. S., K.; Rhee, H. W.; Lee, W. H. . *Bull. Korean Chem. Soc.* **1998,** 19, 549-553.

2. CHAPTER 2: Langmuir-Blodgett Films Composed of Amphiphilic Double-Decker-Shaped Silsesquioxanes (DDSQ)

2.1. Introduction

Polyhedral oligomeric silsesquioxanes (POSSs) have attracted much interest because of their unique chemical structures and well-defined geometric shapes. POSSs consist of a rigid inorganic $SiO_{1.5}$ core with organic coronae. The $SiO_{1.5}$ core provides good thermal[1] and mechanical properties[2] as well as high optical transparency,[3] which are important for applications in optics,[4] catalysis[5] and electronics.[6] Organic coronae provide processability and compatibility with polymer materials, which are important for nanofillers.[7, 8] The well-defined organic-inorganic architecture is suitable for creating hybrid nanostructure blocks. Controlling a structure in nanometer scale provides higher homogeneity besides higher reproducibility and predictability, and gives an opportunity to tailor the properties of the materials.[9] In several reports, "bottom up" approach has already been applied to organization of POSSs at a nanometer scale.[9-12] For example, Caruso et al. [11] and Su et al. [12] used a layer-by-layer assembly technique to prepare POSS nanocomposite thin films. Mehl et al. [13] and Zhu et al. [14] attached liquid crystal mesogens to POSS and studied the self-assembled structure of the mesogen-substituted POSSs. Deng et al. used a trisilanol-POSS, a partial cage structure, to prepare a uniform Langmuir monolayer at the air-water interface. They carried out intensive study on the surface morphology and viscoelastic properties at the air-water interface of the trisilanol-POSS.[15-19] As far as we know, the trisilanol-POSS is the only monodisperse POSS material that can form a stable monolayer at the air-water interface. Unfortunately, transfer of a trisilanol-POSS monolayer onto a solid substrate to produce Langmuir-Blodgett (LB) film has not been achieved.

Polymer hybrid nano-sheets (LB films) containing POSS as a comonomer of an amphiphilic polymer have been already reported.[20] Esker et al.[21] also reported polymer LB film using a telechelic polymer whose endgroups were POSS. Tsukruk et al.[22] prepared LB film of organic-functionalized core-shell silsesquioxane. These studies reported monolayer behavior using POSS copolymers or mixed silsesquioxane as a core. The main objective of the present study was to prepare LB film of POSS with a well-defined molecular structure that does not show molecular weight distribution. LB films enable molecular ordering in one, two and three dimensions, which are important for better understanding and design of POSSs as nanobuilding blocks.[23]

In this study, LB films based on monodisperse double-decker shaped polyhedral oligomeric silsesquioxanes (DDSQs) molecules are prepared. DDSQs are new members of the POSS family that can be used to prepare organic-inorganic hybrid materials with several functions.[24] We synthesized amphiphilic DDSQs consisting of a DDSQ hydrophobic core and di(ethylene glycol) units as hydrophilic coronae. The DDSQs used in this study possessed precisely two or four reactive hydrosilane (SiH) groups. In this study, hydrophilic di(ethylene glycol) units were introduced to the hydrosilane groups using a hydrosilylation reaction to prepare amphiphilic DDSQs. The reactive units in DDSQs are smaller than the often-used octamer POSS $(RSiO_{1.5})_8$, which has eight reactive SiH groups. Moreover, the synthesized DDSQs are unique amphiphilic molecules in structure. Conventional amphiphiles take a "head-to-tail" structure, where polar hydrophilic group is a head and long hydrocarbon chain is a tail. On the other hand, the amphiphilic DDSQs take "core-coronae" structure, where DDSQ core is hydrophobic and di(ethylene glycol) units is hydrophilic part. Therefore, the present study proposes a new type of amphiphilic DDSQ derivatives composed of the core-coronae structure. The synthesized amphiphilic DDSQs were characterized by ^{1}H, ^{13}C and ^{29}Si NMR, FT-IR and MALDI-TOF mass spectrometry. Monolayer properties of amphiphilic DDSQs at the air-water interface were characterized by surface pressure (π)–area (A) isotherms and Brewster angle microscopy (BAM). The monolayer was transferred onto a solid substrate using a vertical dipping method. The surface morphology of the transferred film was characterized by AFM and UV-vis spectrophotometry.

2.2. Experimental Section

2.2.1. Materials.

Double-decker shaped oligomeric silsesquioxanes containing two SiH groups (2H-DDSQ) and four SiH groups (4H-DDSQ) are kindly donated by

Chisso Corp. Anhydrous tetrahydrofuran (THF) and toluene are purchased from Aldrich and Nacalai Tesque, Inc., respectively, and were used without further purification. Platinum divinyltetramethyldisiloxane (Pt(dvs), 3 wt% in xylene solution) is obtained from Umicore. Dichloromethane, chloroform and acetone are purchased from Kanto Chemical Co. Inc. and distilled before use. Spectroscopic grade chloroform (Dojindo Laboratories) was used as a spreading solvent. Pure distilled water with resistivity higher than 17.5 MΩ·cm (purified by RFD240RA and CPW-101 system; Advantec) was used as the subphase. Octadecyltrichlorosilane (Shin-Etsu Chemical Co. Ltd.) was used without further purification.

2.2.2. **General Methods.**

FT-IR spectra were obtained using an FT-IR spectrometer (FT/IR4200; Jasco Inc.). IR spectra of the amphiphilic DDSQs were recorded between 4000 and 750 cm^{-1} with 4 cm^{-1} resolution, under a continuous nitrogen purge. UV-vis absorption spectra of amphiphilic DDSQ LB films were obtained using a spectrophotometer (U-3000; Hitachi Ltd.). ^{1}H, ^{13}C and ^{29}Si NMR measurements were carried out with a JEOL JNM-AL 400 spectrometer, in $CDCl_3$ or CD_3OD without tetramethylsilane. For MALDI-TOF MS (Bruker Daltonics) analysis, the matrix α-cyano-4-hydroxycinnamic acid was dissolved in THF (10 mg ml^{-1}), and mixed with 0.2 μL of sample solution (100 μmol in THF) in 1:1 v/v ratio. The resultant solution was deposited on a stainless steel sample plate and dried. The measurement was done in linear mode with a N_2 laser (337 nm), and positive mode with an accelerating voltage 20 kV.

2.2.3. Substrate Preparation.

Quartz slides and silicon wafers (p-type; Ryoko Sangyo Corp.) were used as substrates for LB film deposition. The substrates were freshly cleaned using a UV ozone cleaner (UV253; Filgen), then washed with chloroform and acetone. The substrates were then immersed in a chloroform solution of trichlorooctylsilane (ca. 1.0×10^{-6} mol L^{-1}) for 12 h to obtain hydrophobic substrate. Finally, the hydrophobic substrates were washed with chloroform and dried with flowing nitrogen. The hydrophilic substrates were used directly after washing with chloroform and acetone without hydrophobic treatment.

2.2.4. Surface Pressure (π)- Surface Area (A) Studies and LB Film Deposition.

A dilute chloroform solution (ca. 1.2×10^{-3} mol L^{-1}) of amphiphilic DDSQ was spread on a water surface. π–A isotherms and LB film deposition were carried out using an automatically controlled Langmuir trough (FSD-220 and 21, USI Systems Ltd.). The surface pressure was measured using a paper Wilhelmy plate. The compression rate was 15 cm^2 min^{-1}. The monolayer was deposited on the solid substrates using a vertical dipping method with dipping speed 10 mm min^{-1}, maintaining surface pressure and temperature at 25 mN m^{-1} and 8 °C, respectively. Deposition of the monolayer film on a hydrophilic silicon substrate was performed as follows. The substrate was immersed in a water subphase and 4DEG-DDSQ/chloroform solution was spread on the water surface. The 4DEG-DDSQ monolayer was compressed at 25 mN m^{-1} and transferred onto the substrate by withdrawing the substrate from the water subphase (upstroke deposition). Deposition of the monolayer film on a hydrophobic silicon substrate was performed as follows; a 4DEG-DDSQ monolayer was compressed at 25 mN m^{-1} and deposited on the substrate by downward deposition. After 5-10 min, the monolayer at the air-water interface was aspirated and the substrate was withdrawn from the water subphase at a speed of 10 mm min^{-1}.

2.2.5. BAM.

BAM studies (Mini BAM; KSV) were carried out simultaneously during the isotherm measurements; the BAM images were taken with a CCD camera.

2.2.6. AFM Observation.

Surface morphology was characterized using atomic force microscopy (SPA400, Seiko Instruments Inc.). A silicon cantilever (14 nN m^{-1} and 132 kHz, Si-DFM20, Seiko Instruments Inc.) was used. The images were taken using the tapping mode, and all measurements were carried out at room temperature.

2.2.7. XPS Analysis.

X-ray photoelectron spectrometer (PHI 5600; PerkinElmer Inc.) was used to obtain XPS spectra. All binding energies in XPS measurements were referenced to the C 1s peak for neutral carbon, which was assigned as a value of 285.0 eV.

2.3. Synthesis and Characterization

2.3.1. Synthesis of Amphiphilic DDSQ with Two Di(ethylene glycol) Units (2DEG-DDSQ).

2H-DDSQ (0.5667 g, 0.491 mmol) and a 1.3-fold stoichiometric excess of di(ethylene glycol) vinyl ether (0.174 mL, 1.28 mmol) relative to Si-H were dissolved in toluene (10 mL) at 0 °C with stirring in an argon atmosphere. 10 μL of Pt(dvs) was added dropwise to the solution, and reaction was performed for 3.5 h at room temperature (Scheme 2.1).

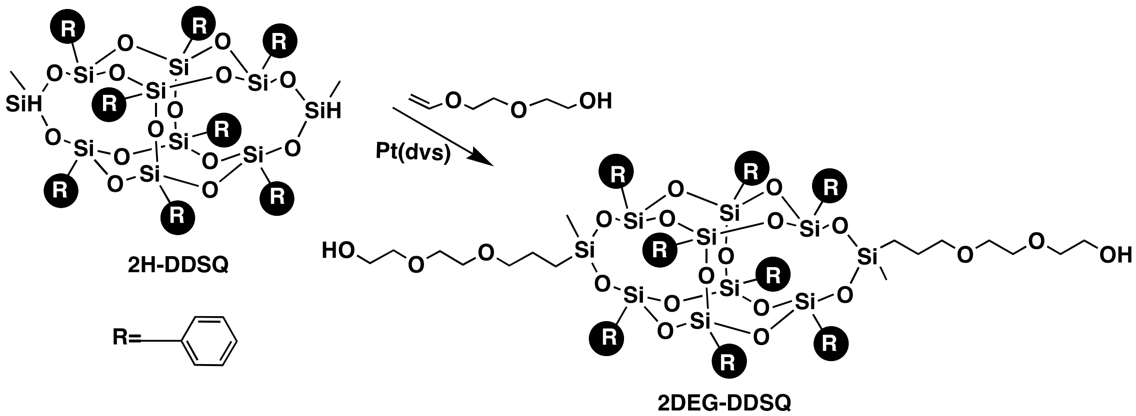

Scheme 2.1 Synthesis of amphiphilic DDSQ through direct hydrosilylation with di(ethylene glycol) vinyl ether.

The crude product was recrystallized from THF/n-hexane and dried under vacuum at 40 °C (yield: 94%).

2.3.2. FT-IR Spectrum of 2DEG-DDSQ

Figure 2.1 shows the FT-IR spectra of initial compound (2H-DDSQ) and obtained compound (2DEG-DDSQ). After hydrosilylation reaction, the strong Si-H peak related to the initial compound (2H-DDSQ) at 2145 cm^{-1} band disappears and OH vibration band related to the di(ethylenglycol) units appears at 3436 cm^{-1}. The peak between 1050 - 1140 cm^{-1} for Si-O-Si stretching of DDSQ core appears in each spectrum, suggesting that DDSQ core remained unchanged during the synthesis.

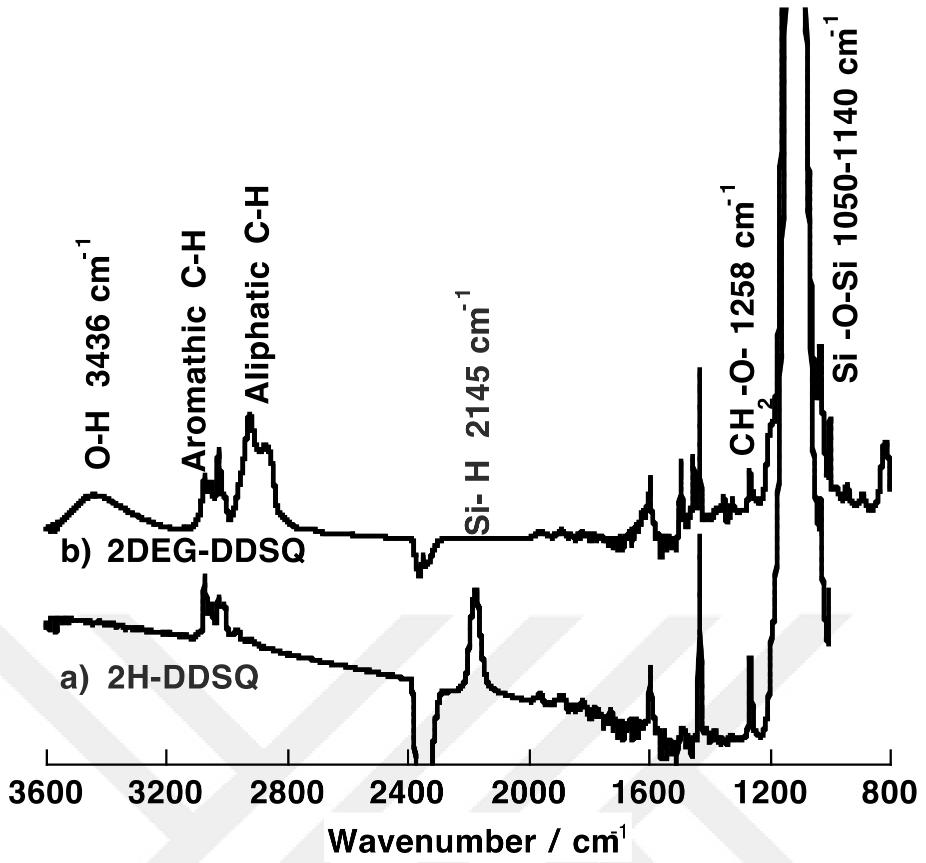

Figure 2.1 FTIR spectra of (a) 2H-DDSQ and (b) 2DEG-DDSQ.

[FTIR (cm^{-1}), ν=3436 (broad, O-H), ν =2974, 2935, 2879 (aliphatic C-H), ν =1272 (CH_2-O), ν =1098 (Si-O)]

2.3.3. ^{1}H and ^{13}C NMRs Spectra of 2DEG-DDSQ

^{1}H and ^{13}C NMR spectra (Figure 2.2 and 2.3) of 2DEG-DDSQ were taken in $CDCl_3$ and CD_3OD solvents. Both integration of aromatic peaks in $CDCl_3$ measurement and aliphatic protons peaks in DEG units in CD_3OD measurement are compatible with the theoretical calculation of the integrals. To check the stability of 2DEG-DDSQ against to back biting reaction catalyzed by base,[25] ^{1}H and ^{13}C NMR of the sample were taken periodically during 20 weeks. No change is observed either in location or integration of proton peaks.

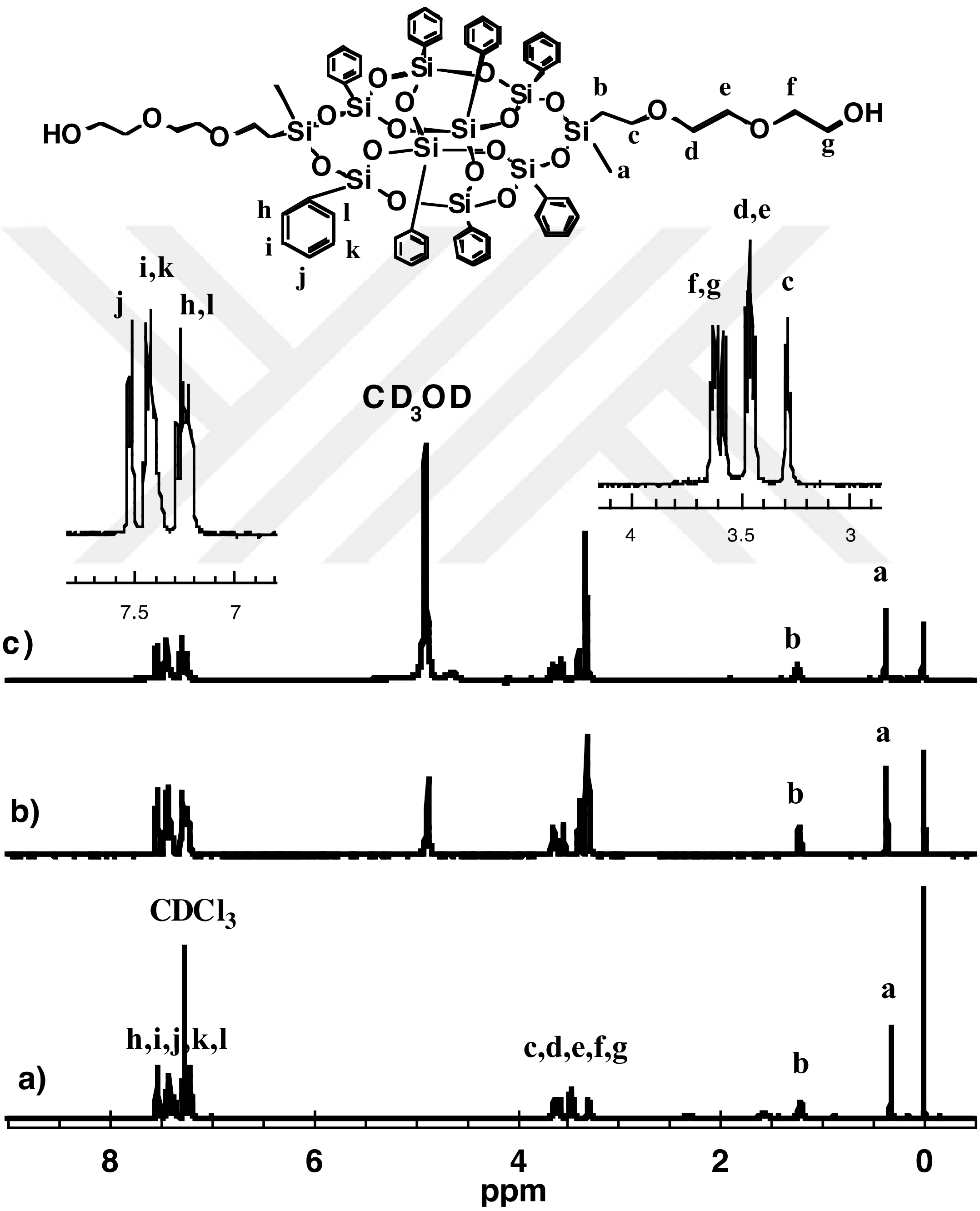

Figure 2.2 ^{1}H NMR of 2DEG-DDSQ (a) in $CDCl_3$ (b) in CD_3OD, and (c) 20 weeks layer in CD_3OD.

[^{1}H NMR (ppm) (400 MHz, $CDCl_3$, $CHCl_3$ ref) 7.25-7.60 (m, 40H, Ph), 3.4-3.7 (t, 20H CH_2-O), 1.22 (t, 4H, CH_2-Si), 0.36 (s, 6H, Si(CH_3)). NMR data in methanol: ^{1}H NMR (ppm), (400 MHz, CD_3OD), 7.25-7.60 (m, 40H, *Ph*), 3.4-3.7 (t, 20H C$\mathit{H_2}$-O), 1.22 (t, 4H, C$\mathit{H_2}$-Si), 0.36 (s, 6H, Si(C$\mathit{H_3}$))].

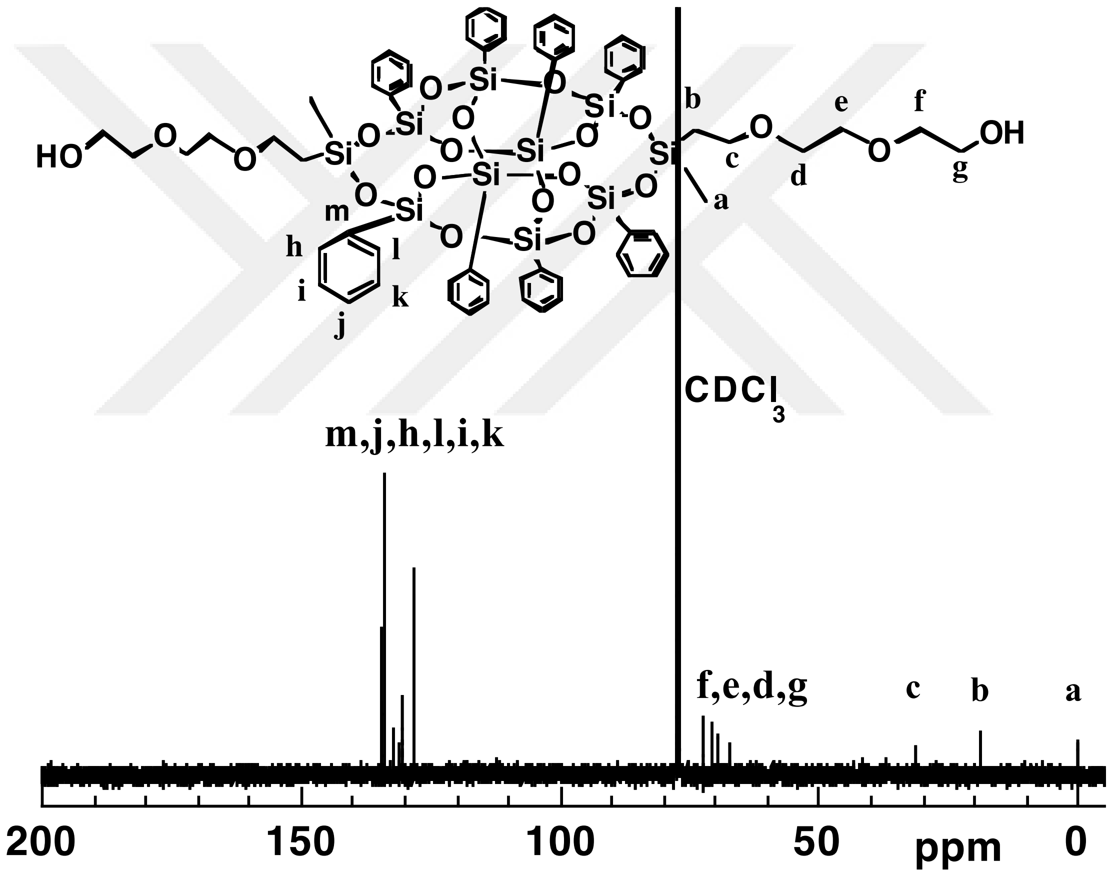

Figure 2.3 ^{13}C NMR of 2DEG-DDSQ in $CDCl_3$.

[^{13}C NMR (ppm), (100 MHz, $CDCl_3$, $CDCl_3$ ref) 128-134 (Ph), 65-73 (*C*H_2-O-*C*H_2), 31 (O-*C*H_2-CH_2-Si), 19 (*C*H_2-Si), 0.1 (Si (*C*H_3)$_2$). ^{13}C NMR (ppm), (100 MHz, CD_3OD) 128-134 (Ph), 65-73 ($\mathit{C}H_2$-O-$\mathit{C}H_2$), 31 (O-$\mathit{C}H_2$-CH_2-Si), 19 ($\mathit{C}H_2$-Si), 0.1 (Si ($\mathit{C}H_3$)$_2$)]

2.3.4. *Maldi-Tof MS Spectrum of 2DEG-DDSQ*

MALDI-TOF mass spectrum, which shows molecular ions at 1438 g mol^{-1} for [M + Na^+, calculated value 1439.2], strongly supports successfully attachment of DEG units to the DDSQ core (Figure 2.4).

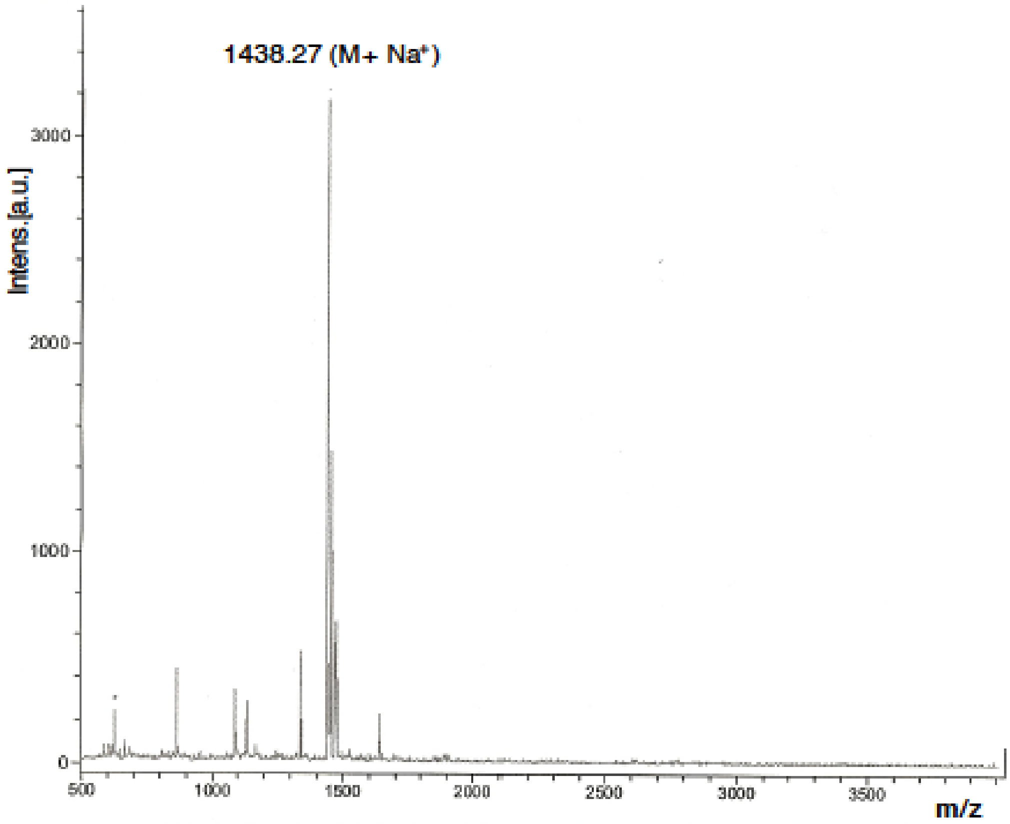

Figure 2.4 MALDI-TOF MS spectrum of 2DEG-DDSQ.

2.3.5. *Synthesis of Amphiphilic DDSQ with Four Di(ethylene glycol) Units (4DEG-DDSQ).*

4H-DDSQ (2.6 g, 0.008 mol, 1.6 M) and a 1.3-fold stoichiometric excess of di(ethylene glycol) vinyl ether (1.37 ml, 0.01 mmol, 2 M) relative to Si-H were dissolved in toluene (5 ml) at 0 °C with stirring in an argon atmosphere. 10 μl of Pt(dvs) was added dropwise to the solution and reaction was performed for 12 h at room temperature (Scheme 2.2). The crude product was purified by silica gel column chromatography eluted with THF/n-hexane and dried under vacuum at 40 °C (yield: 90%).

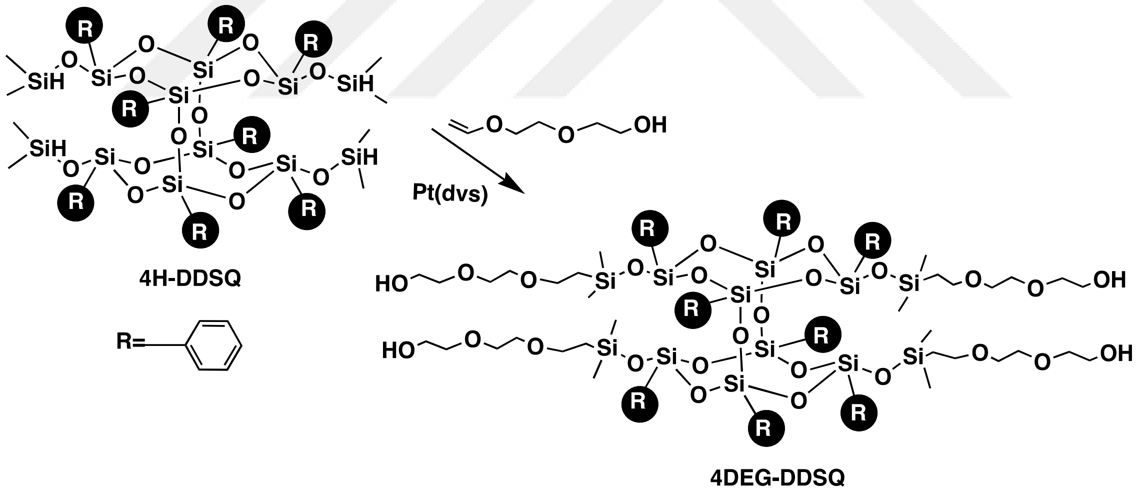

Scheme 2.2. Synthesis of amphiphilic DDSQ through direct hydrosilylation with di(ethylene glycol) vinyl ether.

2.3.6. *FT-IR Spectrum of 4DEG-DDSQ*

Figure 2.5 shows the FT-IR spectra of initial compound (4H-DDSQ) and obtained compound (4DEG-DDSQ). After hydrosilylation reaction, the strong Si-H peak related to the initial compound (4H-DDSQ) at 2145 cm^{-1} band disappears and OH vibration band related to the di(ethylenglycol) units appears at 3436 cm^{-1}. The peak between 1010 - 1140 cm^{-1} for Si-O-Si stretching of DDSQ core appears in each spectrum, suggesting that DDSQ core remained unchanged during the synthesis.

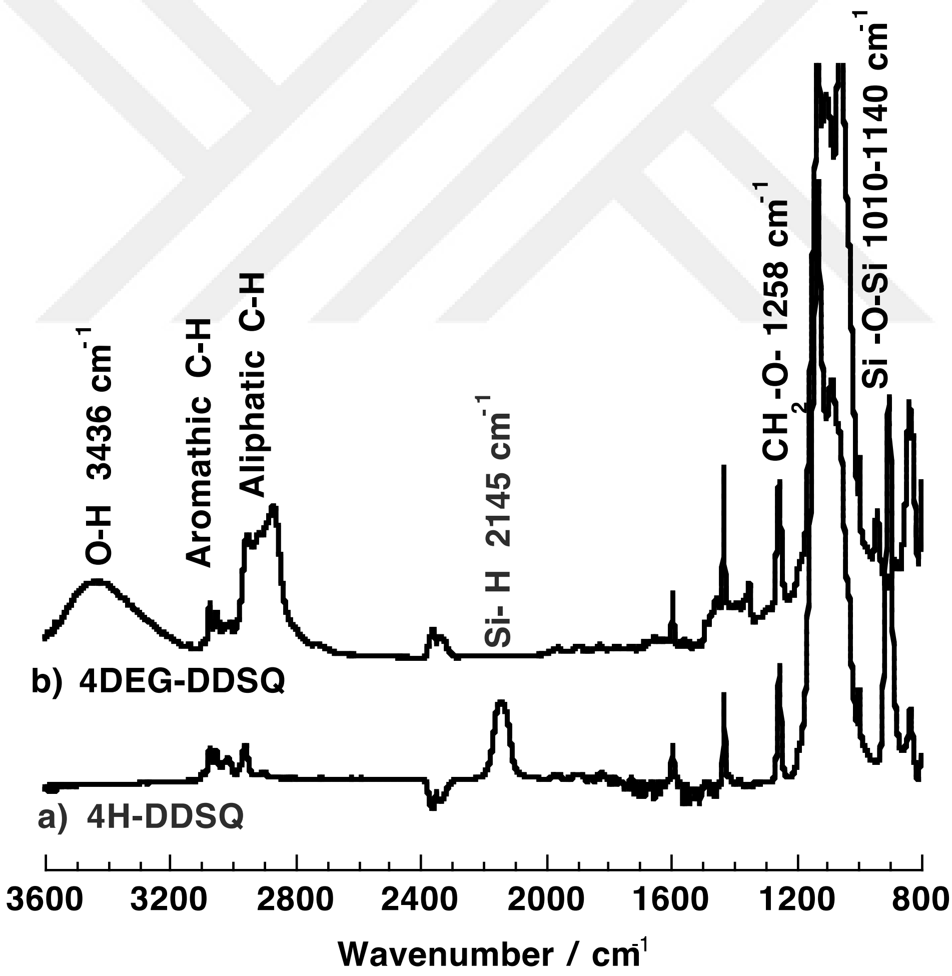

Figure 2.5 FTIR spectra of (a) 4H-DDSQ and (b) 4DEG-DDSQ.

(FTIR (cm^{-1}), ν =3442 (broad, O-H), n =2958, 2910, 2870 (aliphatic C-H), ν =1259 (CH_2-O), ν =1010 (Si-O), ν =1150 (Si-C)).

2.3.7. ^1H and ^{13}C NMR Spectra of 4DEG-DDSQ

^1H and ^{13}C NMR spectra (Figure 2.6 and 2.7) of 4DEG-DDSQ were taken in $CDCl_3$ and CD_3OD solvents. Both integration of aromatic peaks in $CDCl_3$ measurement and aliphatic protons peaks in DEG units in CD_3OD measurement are compatible with the theoretical calculation of the integrals. To check the stability of 4DEG-DDSQ against to the back biting reaction,[25] ^1H and ^{13}C NMR of the sample were taken periodically during 12 weeks. No change is observed either in location of proton or carbon peaks and integration of protons.

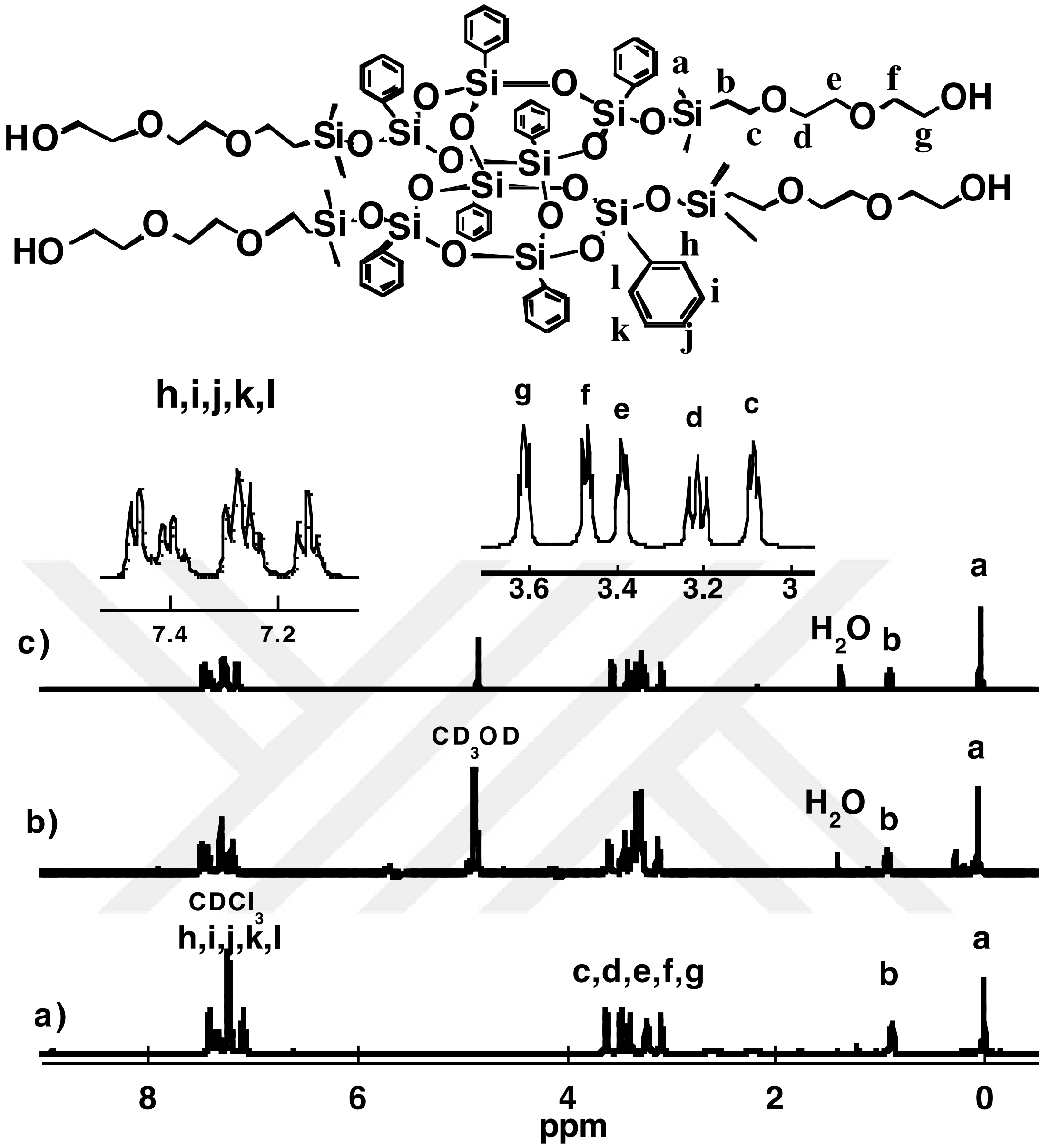

Figure 2.6 ^{1}H NMR of 4DEG-DDSQ (a) in $CDCl_3$ (b) in CD_3OD, and (c) 4 weeks layer in CD_3OD.

[^{1}H NMR (ppm), (400 MHz, $CDCl_3$, $CHCl_3$ ref) 7.26-7.76 (40H, Ph), 3.05-3.70 (40H, CH_2-O), 0.90 (8H, CH_2-Si), 0.01 (12H, Si(CH_3)$_2$. NMR data in methanol: ^{1}H NMR (ppm), (400 MHz, CD_3OD) 7.26-7.76 (40H, Ph), 3.05-3.70 (40H, CH_2-O), 0.90 (8H, CH_2-Si), 0.01 (12H, Si(CH_3)$_2$.

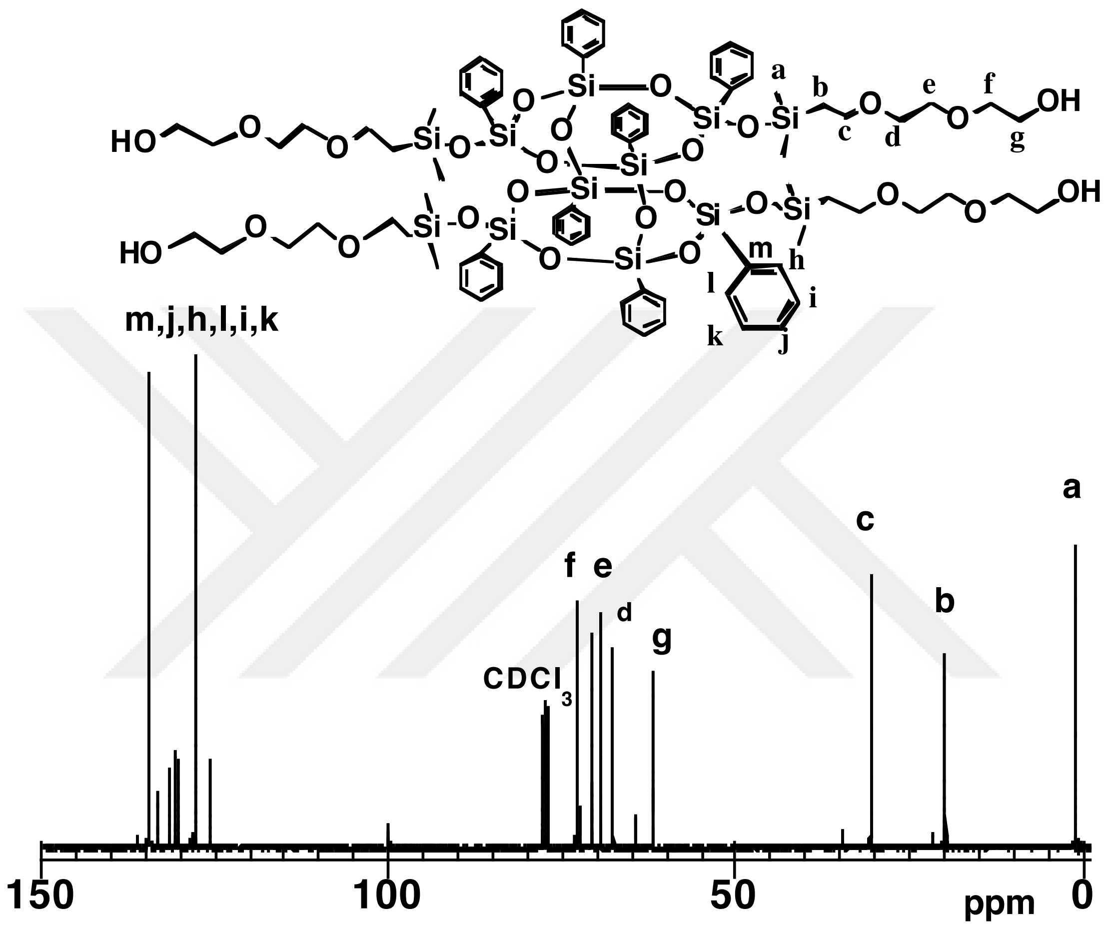

Figure 2.7 ^{13}C NMR of 4DEG-DDSQ in $CDCl_3$

^{13}C NMR (ppm), (100 MHz, $CDCl_3$, $CDCl_3$ ref) 125-140 (Ph), 60-70 ($\mathit{C}H_2$-O-$\mathit{C}H_2$), 30 (O-$\mathit{C}H_2$-CH_2-Si), 15 ($\mathit{C}H_2$-Si), 0.1 (Si ($\mathit{C}H_3)_2$). ^{13}C NMR (ppm), (100 MHz, CD_3OD, CD3OD ref) 125-140 (Ph), 60-70 ($\mathit{C}H_2$-O-$\mathit{C}H_2$), 30 (O-$\mathit{C}H_2$-CH_2-Si), 15 ($\mathit{C}H_2$-Si), 0.1 (Si ($\mathit{C}H_3)_2$)].

2.3.8. ²⁹Si NMR Spectrum of 4DEG-DDSQ

Figure 2.8 shows the [29]Si NMR spectra of 4DEG-DDSQ taken in CDCl3 and CD_3OD. ([29]Si NMR 71.5 MHz, $CDCl_3$, TMS ref) -98.45 (O*Si*$(CH_3)_2CH_2$), -183.70 (O_2*Si*(Ph)OSi$(CH_3)_2$), -186.3 (O_3*Si*(Ph)).

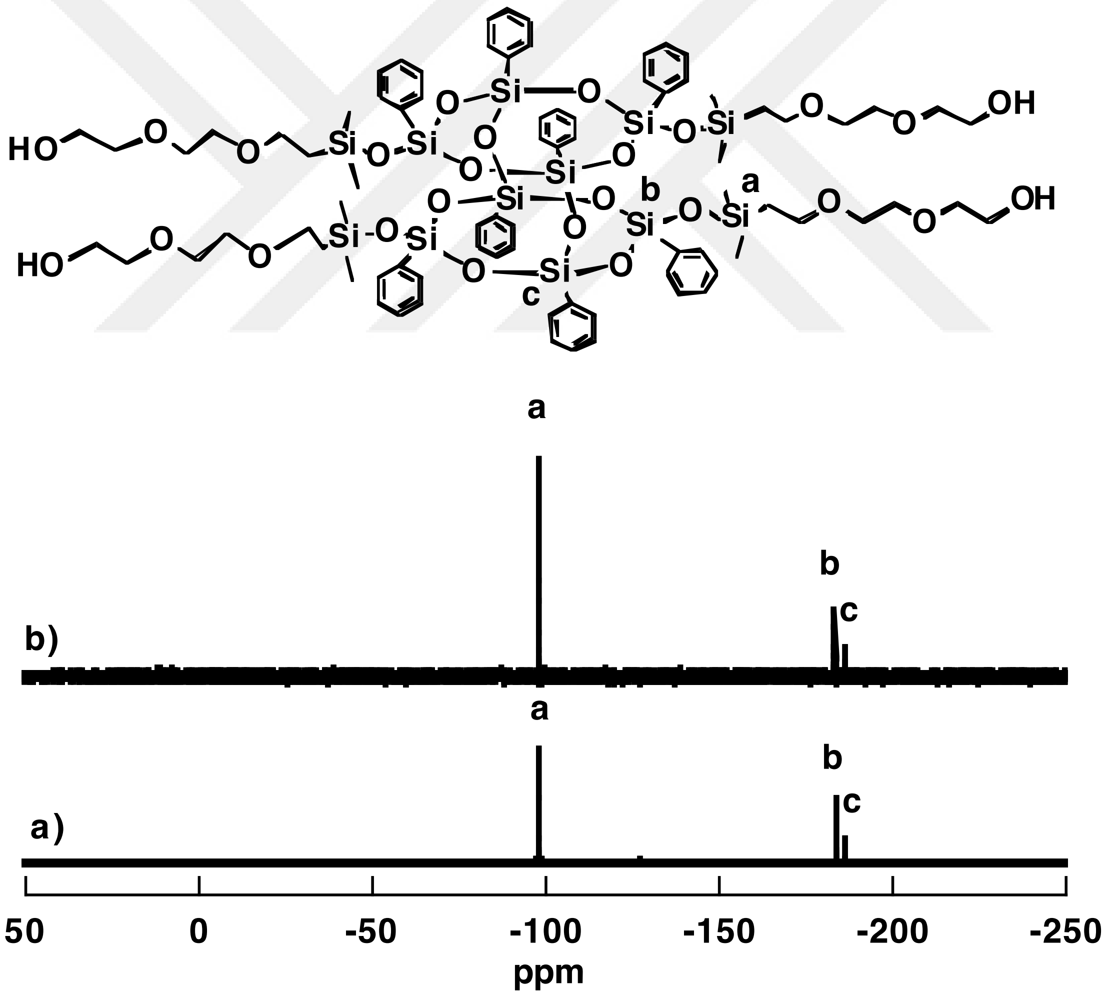

Figure 2.8. [29]Si NMR of 4DEG-DDSQ a) in $CDCl_3$ b) in CD_3OD.

2.3.9. Maldi-Tof MS Spectrum of 4DEG-DDSQ

MALDI-TOF mass spectrum, which shows molecular ions at 1849.5 g mol^{-1} for [M + Na^+, calculated value 1851.5], strongly supports successfully attachment of DEG units to the DDSQ core (Figure 2.9).

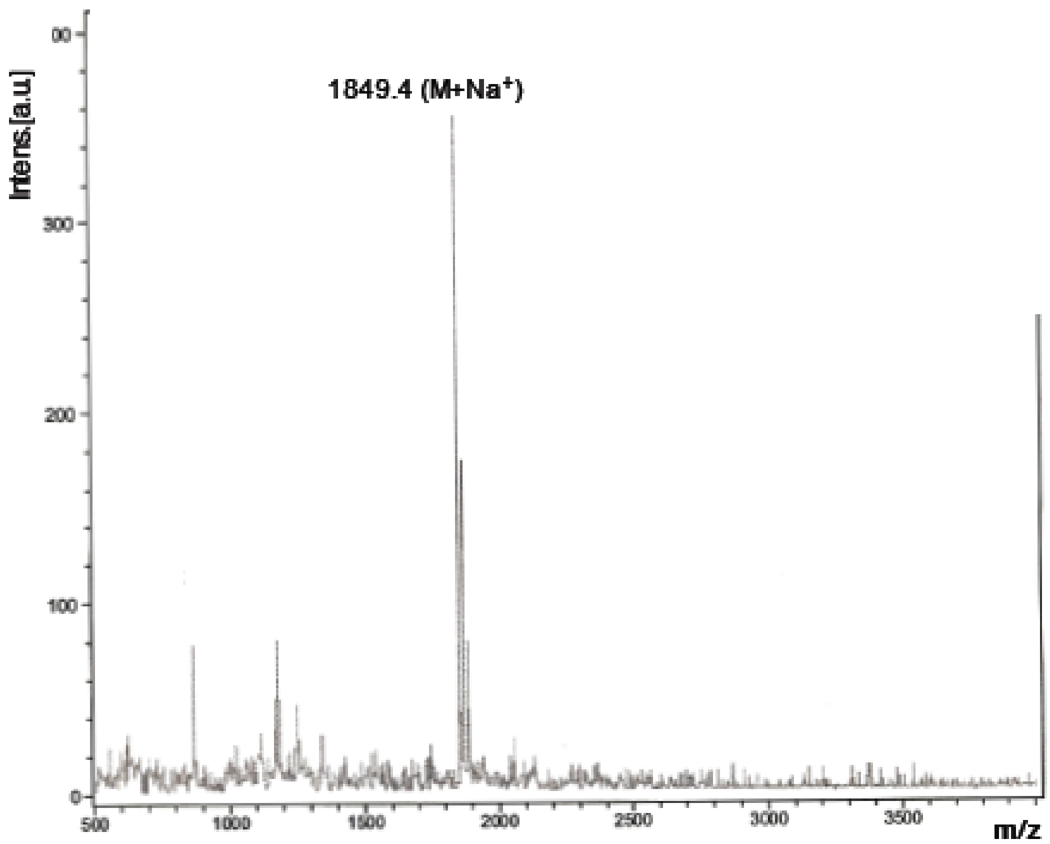

Figure 2.9 MALDI-TOF MS spectrum of 4DEG-DDSQ.

2.4. Surface Pressure (π)- Surface Area (A) Studies and LB Film Deposition.

A dilute chloroform solution (ca. 1.2×10^{-3} mol L^{-1}) of amphiphilic DDSQ was spread on a water surface. π–A isotherm measurements and LB film deposition were carried out using an automatically controlled Langmuir trough (FSD-220 and 21, USI Systems Ltd.). The surface pressure was measured using a paper Wilhelmy plate. The compression rate was 15 cm^2 min^{-1}. The monolayer was deposited on the solid substrates using a vertical dipping method with dipping speed 10 mm min^{-1}, maintaining surface pressure and temperature at 25 mN m^{-1} and 8 °C, respectively. Deposition of the monolayer film on a hydrophilic silicon substrate was performed as follows; the substrate was immersed in a water subphase and 4DEG-DDSQ/chloroform solution was spread on the water surface. The 4DEG-DDSQ monolayer was compressed at 25 mN m^{-1} and transferred onto the substrate by withdrawing the substrate from the water subphase (upstroke deposition). Deposition of the monolayer film on a hydrophobic silicon substrate was performed as follows; a 4DEG-DDSQ monolayer was compressed at 25 mN m^{-1} and deposited on the substrate by downward deposition. After 5-10 min, the monolayer at the air-water interface was aspirated and the substrate was withdrawn from the water subphase at a speed of 10 mm min^{-1}.

2.5. Results and Discussion

2.5.1. Synthesis and Characterization of 2DEG-DDSQ and 4DEG-DDSQ

Amphiphilic DDSQs, 2DEG-DDSQ and 4DEG-DDSQ were prepared by direct hydrosilylation reaction of DDSQs with di(ethylene glycol) vinyl ether (Scheme 2.1 and 2.2). The purity of 2DEG-DDSQ and 4DEG-DDSQ was confirmed by FT-IR, ^{1}H, ^{29}Si, ^{13}C NMRs, and MALDI-TOF MS spectra. As reported by Laine et al. [25] and Scott et al.,[26] O-silylation was totally suppressed by controlling the concentration of Pt(dvs) and di(ethylene glycol) vinyl ether. It was reported that direct hydrosilylation of vinyl alkyl alcohol is only possible with Q_8M_8H and T_8H which have a cage structure.[25] Because DDSQ has a similar cage structure, we succeeded in carrying out the direct hydrosilylation with high yield (more than 90%).

2.5.2. Monolayer Behavior of 2DEG-DDSQ and 4DEG-DDSQ at the Air-water Interface

A chloroform solution of DDSQs and amphiphilic DDSQs (1 mM) was spread on a water surface and π-A isotherms of the molecules were measured at 20 °C with compression rate of 15 cm^{2} min^{-1}. The π-A isotherms of 2H-DDSQ (Figure 2.10a) and 4H-DDSQ (Figure 2.11a) showed a rise in surface pressure at 0.28 nm^2 $molecule^{-1}$ and 0.90 nm^2 $molecule^{-1}$, respectively. These values are too small compared with their calculated molecular area based on the CPK model (Figures 2.10b, 2.11b), which indicates that DDSQs do not form a monolayer but aggregate at the air-water interface.

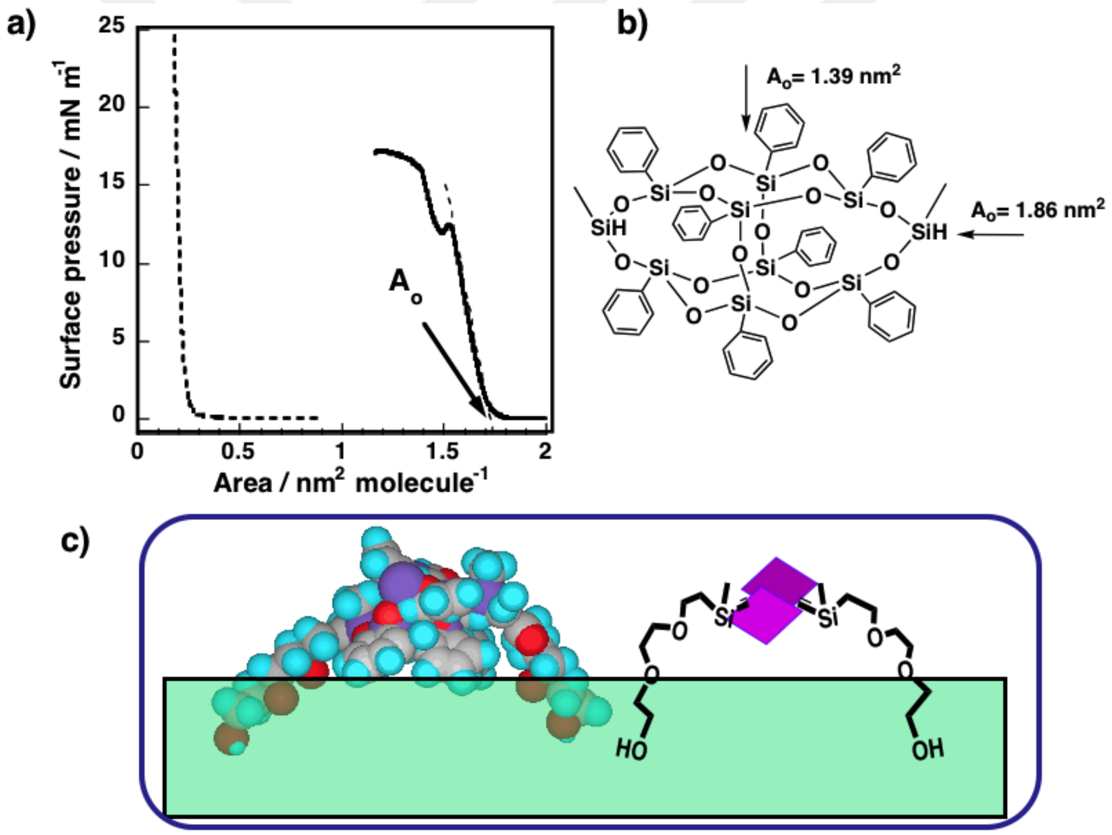

Figure 2.10. (a) Surface pressure (π)-area (A) isotherms for 2H-DDSQ (dotted line) and 2DEG-DDSQ (solid line) at 20 °C. (b) Calculated cross-sectional areas of 2H-DDSQ by CPK model. (c) Schematic illustration of the 2DEG-DDSQ monolayer at the air-water interface.

The BAM images of the DDSQs showed a heterogeneous surface, which is consistent with three-dimensional aggregates (Figures 2.12 and 2.13). On the other hand, the amphiphilic DDSQs show a lift-off surface pressure at high surface area (1.8 nm^2 $molecule^{-1}$ for 2DEG-DDSQ and 2.85 nm^2 $molecule^{-1}$ for 4DEG-DDSQ). The lift-off surface area values indicate that amphiphilic DDSQs spread uniformly on the air-water interface. The attachment of hydrophilic DEG units increases the hydrophilicity of DDSQs and prevents aggregation at the air-water interface. The limiting surface area, calculated by extrapolating the linear part of the π-A isotherm to zero pressure, was 1.72 nm^2 $molecule^{-1}$ for 2DEG-DDSQ and 2.56 nm^2 $molecule^{-1}$ for 4DEG-DDSQ. These values are larger than the calculated values of the cross-sectional area of the DDSQ cores (Figures 2.10b, 2.11b), which indicates that part of the DEG units were not submerged in the water subphase but were located at the air-water interface (Figures 2.10c, 2.11c).

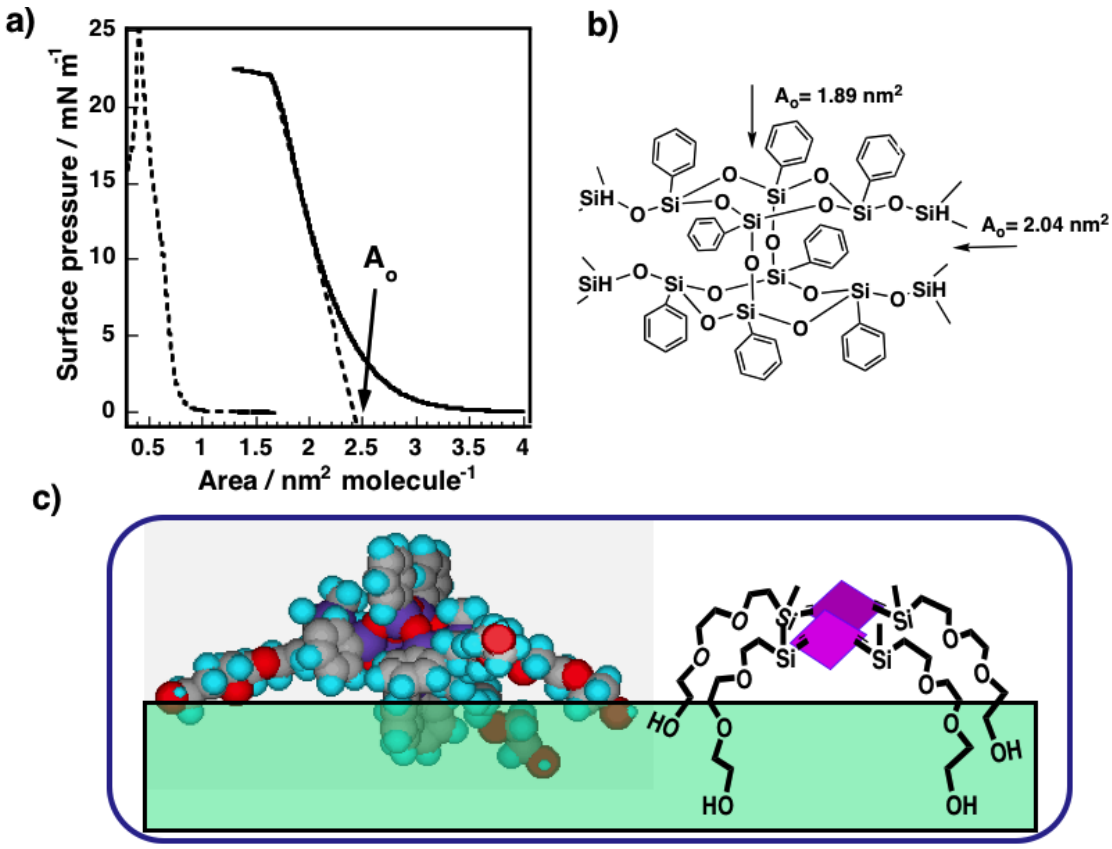

Figure 2.11. (a) Surface pressure (π)-area (A) isotherms for 4H-DDSQ (dotted line) and 4DEG-DDSQ (solid line) at 20 °C. (b) Calculated cross-sectional areas of 4H-DDSQ by CPK model. (c) Schematic illustration of the 4DEG-DDSQ monolayer at the air-water interface.

Figure 2.12 shows a typical BAM image of a 2DEG-DDSQ monolayer. At larger surface area, it formed a so-called island structure, with several sizes of domains with smoothly curved boundaries (Figure 2.12D), which are typical structures for a gas-liquid coexistence phase.[27] In the course of compression, the domains of the 2DEG-DDSQ monolayer coalesced (Figure 2.12E) and finally covered the whole measurement area (Figure 2.12F). In the close-packed film, small circular domains which were brighter than the surrounding area were formed. The circular domains are attributed to a liquid condensed (LC) phase of 2DEG-DDSQ monolayer

(Figure 2.12G). 4DEG-DDSQ showed a coexistence between gaslike and liquidlike domains at very large area (Figure 2.13D). After lift-off surface area, the film likely corresponds to a liquid expanded (LE) phase with small circular LC domains (Figure 2.13E). Further compression increased the number of LC domains, which were surrounded by the LE area (Figure 2.13F). The compression modulus ($|E|$)[28] calculated from the π–A isotherm using the equation $|E|=A(d\pi/dA)$ had a maximum value of 60 mN m^{-1} at 2.56 nm^2 for the 4DEG-DDSQ monolayer. This value supports the coexistence of LC domains and LE phase.[29] In a conventional amphiphilic molecule such as dipalmitoyl phosphatidylcholine (DPPC), the sizes of the LC domains increase with increasing surface pressure because of two-dimensional nucleation and growth.[30] On the other hand, 4DEG-DDSQ is a bulky molecule with high molecular weight, and we believe, therefore, that it was difficult to grow LC domains at the compression rate used. More brighter domains formation at the collapse region may be attributed to aggregation of 4DEG-DDSQ (Figure 2.13F). The 4DEG-DDSQ monolayer showed 2 times higher collapse pressure than the 2DEG-DDSQ monolayer because of the superior hydrophilic-hydrophobic balance. Consequently, further studies of LB film formation were carried out using 4DEG-DDSQ.

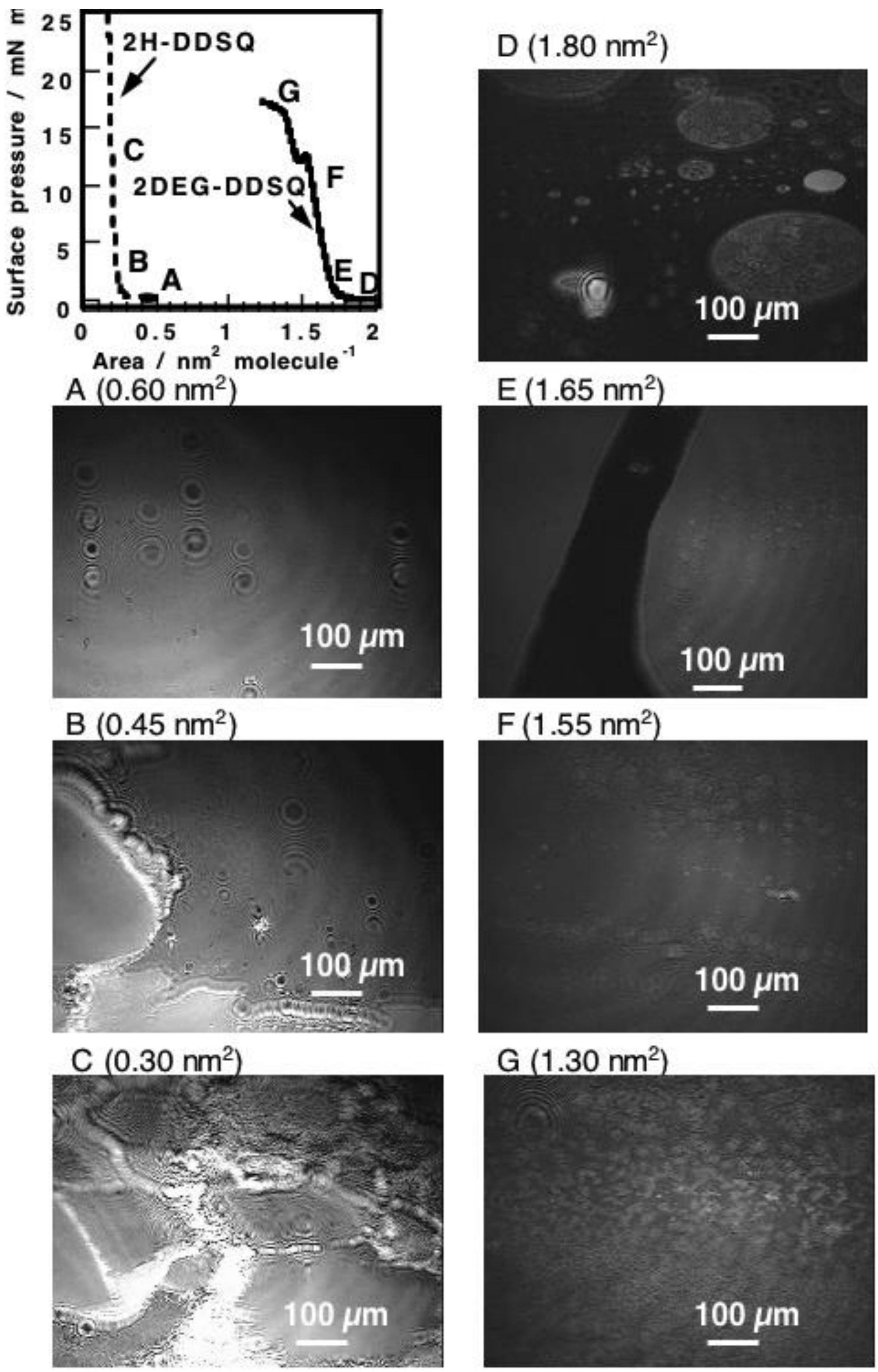

Figure 2.12. BAM images of 2H-DDSQ and 2DEG-DDSQ for different areas (A). The letters on the π-A isotherm were used to indicate each BAM images. The

position of the letters correspond to the A values, where the BAM images were taken.

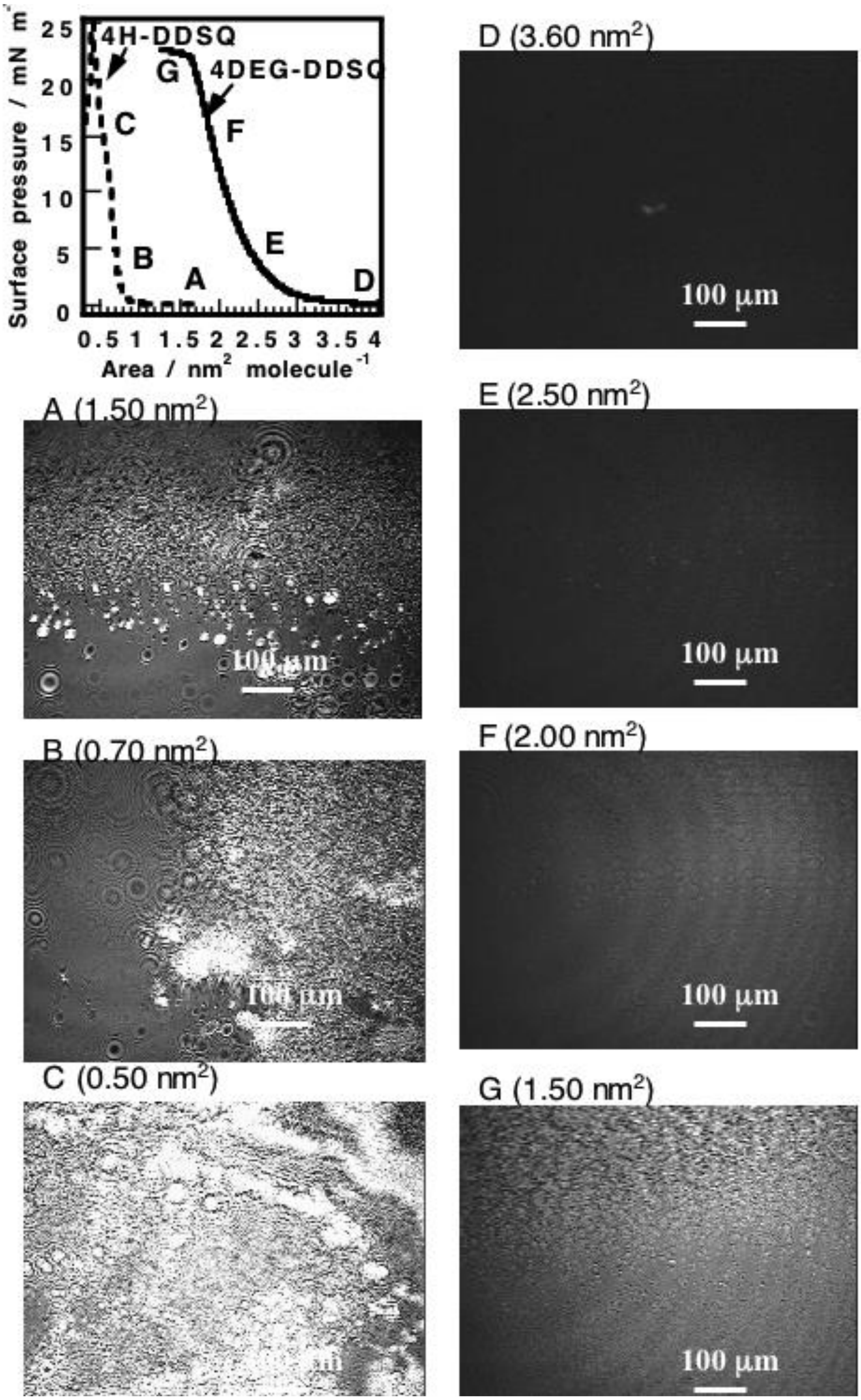

Figure 2.13. BAM images of 4H-DDSQ and 4DEG-DDSQ for different areas (A).

The letters on the π-A isotherm were used to indicate each BAM images. The position of the letters correspond to the A values, were the BAM images were taken.

π–A isotherms of 4DEG-DDSQ monolayers at various subphase temperatures, at constant compression rate, are shown in Figure 2.14. The collapse pressure increased with decreasing temperature of the subphase, whereas there was no significant change in the limiting area per molecule values at different temperatures. Reducing the temperature enhances the intermolecular interactions among the ethylene glycol units attached to the DDSQ cores, tending to make the monolayer more cohesive and ordered (at 8 °C). Cooling the system can be considered as increasing the compression rate.[31] The monolayer prepared at 8 ˚C can remain stable even after waiting several hours at constant pressure. However, a small increase in intermolecular interaction by reducing temperature by even 1 °C (at 7 °C) makes the monolayer unstable. This result shows that the suitable conditions for forming a stable monolayer are very limited.[32]

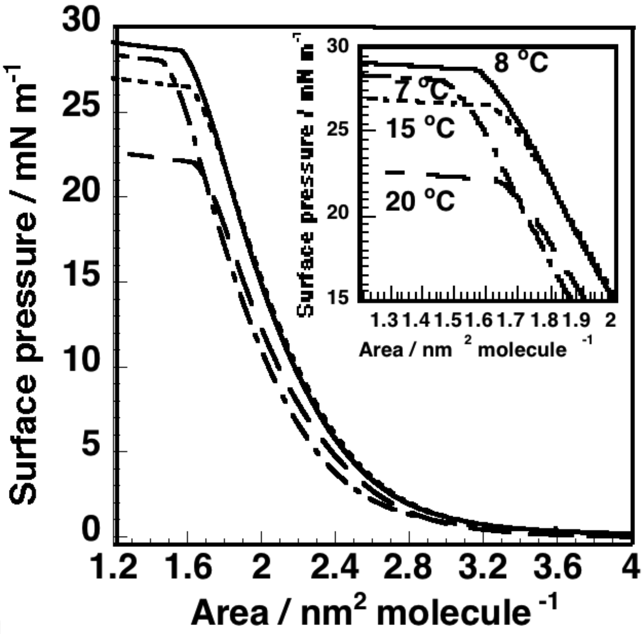

Figure 2.14. π-A isotherms of 4DEG-DDSQ at different temperatures. The temperatures correspond to 7.0 °C (dotted and solid line), 8.0 °C (solid line), 15.0 °C (dotted line), and 20 °C (dashed and solid line). The inset π-A graph is provided to clarify the differences around the collapse in the isotherm for the four temperatures studied.

2.5.3. Morphological Studies of 4DEG-DDSQ Langmuir Blodgett Films

One layer of 4DEG-DDSQ was transferred onto a hydrophilic substrate and the surface morphology of the film was characterized using AFM (Figure 2.15a). The AFM image showed a smooth and uniform surface with RMS=0.24 nm. This value is strong evidence of homogenous film formation on the hydrophilic substrate. The water contact angle of the substrate increased from 25.3 to 60.8° by monolayer deposition, which confirmed that the film covered the whole area of the substrate. On the other hand, a one-layer film of 4DEG-DDSQ deposited on a hydrophobic substrate showed a dot-like structure (Figure 2.15b). The height of the dots varied between 6 and 12 nm (Figure 2.15c). Considering that 4DEG-DDSQ formed a uniform film on the hydrophilic substrate, the dot-like structure was formed by dewetting of the water absorbed during the transfer process. The homogenous monolayer formation on a hydrophilic substrate was caused by hydrogen bonding interaction between ethylene glycol units and silanol groups at silicon surface.

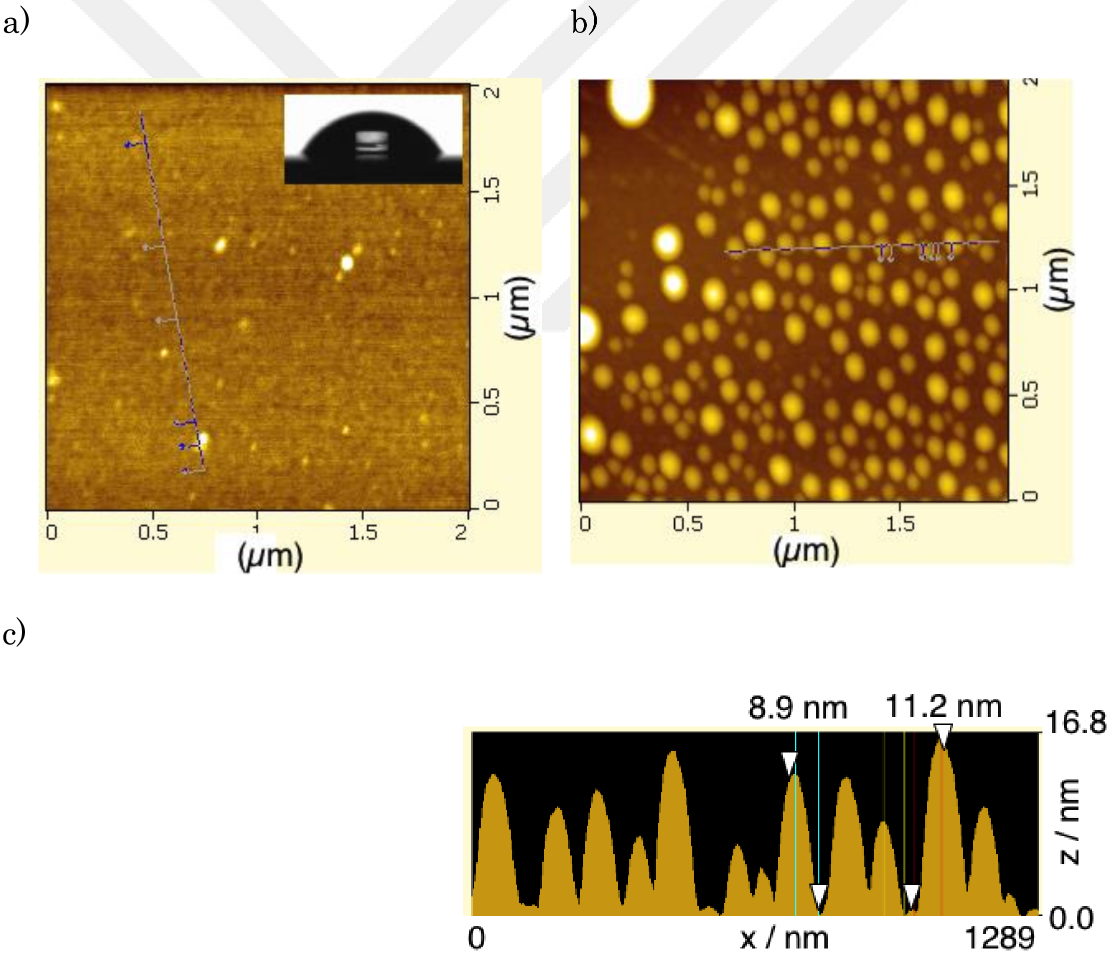

Figure 2.15. AFM images of a 1-layer 4DEG-DDSQ LB film deposited on (a) a hydrophilic silicon substrate, (b) a hydrophobic silicon substrate. (c) Cross-sectional profile of the dots on the hydrophobic substrate. Inset in (a): photograph

of water droplet on the monolayer deposited on the hydrophilic substrate.

Sequential deposition of 4DEG-DDSQ was carried out to prepare a multilayer film on a hydrophilic substrate. The transfer ratios estimated from the decrements of the surface area were almost zero at the downstroke and almost unity at the upstroke deposition. Thus the structure of the LB film was Z-type. The surface morphology of the multilayer film showed several voids and aggregates. The voids may be produced by exfoliating part of the deposited film and the exfoliated film formed the aggregates (Figure 2.16). The deposition of multilayer film onto a hydrophilic quartz substrate was not succeeded. The reason is unclear in present.

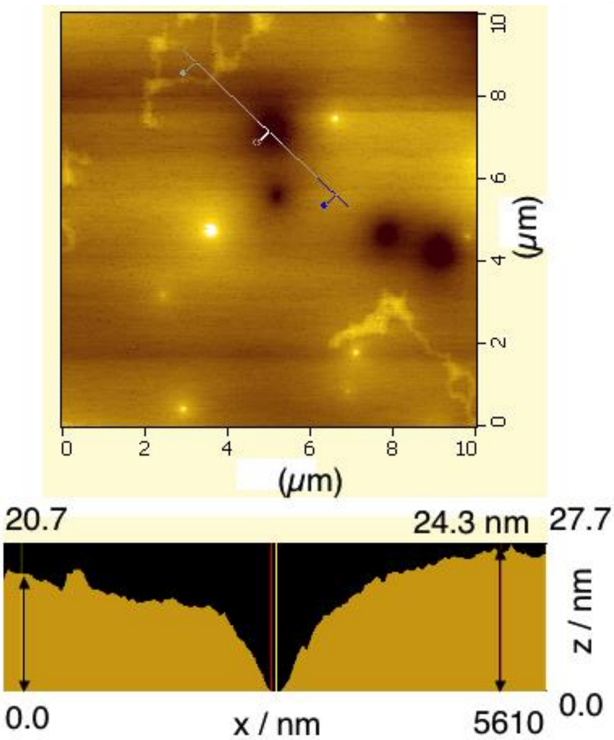

Figure 2.16. AFM image of a 21-layer 4DEG-DDSQ LB film deposited on a

hydrophilic silicon substrate and cross-sectional profile.

Multilayer deposition of 4DEG-DDSQ was also carried out using a hydrophobic substrate. Interestingly, the 4DEG-DDSQ monolayer was transferred as a Y-type film on hydrophobic substrates with a transfer ratio unity for upstroke and downstroke deposition. The UV-vis absorption spectra of 4DEG-DDSQ LB films with different numbers of layers showed an absorption peak at 210 nm, which is attributed to the π-π* absorption band of the phenyl group of DDSQ (Figure 2.17). The optical absorbance of the LB film at 210 nm increased linearly with increase in the number of deposited layers, which indicates that regular deposition is preceded onto the substrate in each deposition cycle.

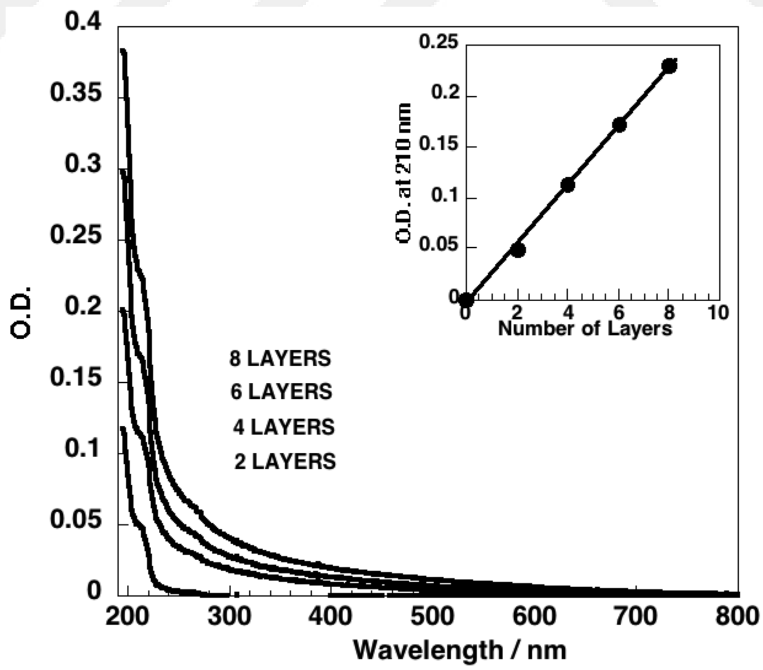

Figure 2.17. UV-vis spectra of the amphiphilic 4DEG-DDSQ LB films with different numbers of layers. Inset: Absorption intensity at 210 nm as a function of the number of layers.

Figure 2.18 shows AFM images of the multilayer film deposited on the hydrophobic silicon substrate. The images show that the size of dots increased, whereas the number of dots decreased with increase of the number of deposited layers. As discussed in the previous section, dewetting of the absorbed water produced the dots and dewetting occurred in each upward deposition. The dots pre-formed on the substrate were combined with each other through each dewetting process, which resulted in increase of the size and decrease in the number of the dots with increasing number of deposited layers.

a) b)

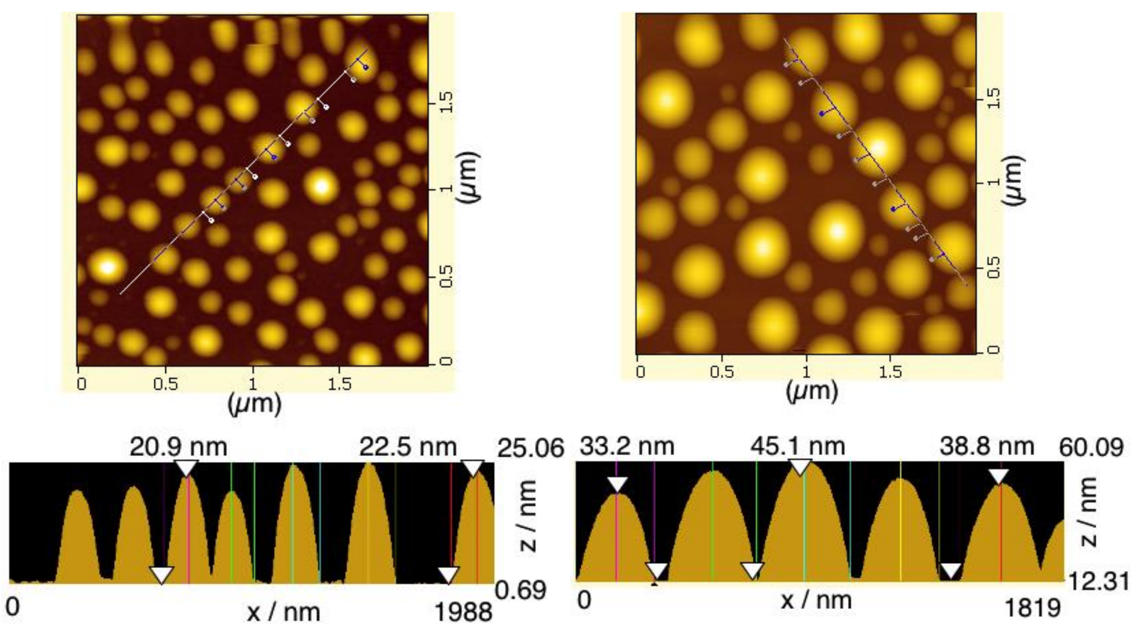

Figure 2.18. AFM image of (a) bi-layer, and (b) 8-layer 4DEG-DDSQ LB

films deposited on a hydrophobic substrate

2.6. Summary

New amphiphilic polyhedral oligomeric silsesquioxanes (POSSs) were synthesized, and their monolayer behavior on a water surface and Langmuir-Blodgett (LB) film formation were studied. Two kinds of amphiphilic POSS molecules, which have two or four di(ethylene glycol) units (2DEG-DDSQ and 4DEG-DDSQ, respectively), were synthesized by direct hydrosilylation of di(ethylene glycol) vinyl ether with double-decker shaped polyhedral oligomeric silsesquioxanes (DDSQs). Surface pressure (π)–area (A) isotherms and Brewster angle microscope (BAM) measurements indicated that both amphiphilic DDSQs form a stable monolayer at the air-water interface. In addition, 4DEG-DDSQ can be deposited on a solid substrate by the LB technique. Atomic force microscope (AFM) images of a one-layer 4DEG-DDSQ film showed a homogenous uniform surface on a hydrophilic silicon substrate, whereas nanometer scale dots were formed on a hydrophobic silicon substrate. The morphology difference is attributed to the difference in interaction between the monolayer and the substrate. Multilayer deposition on a hydrophobic substrate resulted in an increase of dot size with increasing deposition number of layers. Moreover, homogenous multilayer films with a few voids were obtained on a hydrophilic substrate. The results indicate that 4DEG-DDSQ is a good candidate for preparing hybrid nanoassemblies. Moreover, the amphiphilic DDSQ is unique amphiphile compared to conventional "head-to-tail" amphiphile. It takes "core-coronae" structure, where core is hydrophobic and coronae are hydrophilic. Our success in preparing LB film using the amphiphilic DDSQs suggests that the "core-coronae" type molecule is a new candidate for LB film forming materials.

2.7. References

1. Xu, H. Y.; Kuo, S. W.; Lee, J. S.; Chang, F. C. *Macromolecules* **2002,** 35, 8788-8793.
2. Pan, G. R.; Mark, J. E.; Schaefer, D. W. *Journal of Polymer Science Part B-Polymer Physics* **2003,** 41, 3314-3323.
3. Dodiuk, H.; Rios, P. F.; Dotan, A.; Kenig, S. *Polymers for Advanced Technologies* **2007,** 18, 746-750.
4. Atkins, G. R.; Krolikowska, R. M.; Samoc, A. *Journal of Non-Crystalline Solids* **2000,** 265, 210-220.
5. Duchateau, R. *Chemical Reviews (Washington, DC, United States)* **2002,** 102, 3525-3542.
6. Lo, M. Y.; Zhen, C. G.; Lauters, M.; Jabbour, G. E.; Sellinger, A. *Journal of the American Chemical Society* **2007,** 129, 5808-+.
7. Joshi, M.; Butola, B. S. *Journal of Macromolecular Science-Polymer Reviews* **2004,** C44, 389-410.
8. Turri, S.; Levi, M. *Macromolecules* **2005,** 38, 5569-5574.
9. Laine, R. M. *Journal of Materials Chemistry* **2005,** 15, 3725-3744.

10. Brick, C. M.; Chan, E. R.; Glotzer, S. C.; Marchal, J. C.; Martin, D. C.; Laine, R. M. *Advanced Materials (Weinheim, Germany)* **2007,** 19, 82-+

11. Cassagneau, T.; Caruso, F. *Journal of the American Chemical Society* **2002,** 124, 8172-8180.

12. Wu, G. J.; Su, Z. H. *Chemistry of Materials* **2006,** 18, 3726-3732.

13. Mehl, G. H.; Saez, I. M. *Applied Organometallic Chemistry* **1999,** 13, 261-272.

14. Cui, L.; Collet, J. P.; Xu, G. Q.; Zhu, L. *Chemistry of Materials* **2006,** 18, 3503-3512.

15. Deng, J. J.; Hottle, J. R.; Polidan, J. T.; Kim, H. J.; Farmer-Creely, C. E.; Viers, B. D.; Esker, A. R. *Langmuir* **2004,** 20, 109-115.

16. Deng, J. J.; Polidan, J. T.; Hottle, J. R.; Farmer-Creely, C. E.; Viers, B. D.; Esker, A. R. *Journal of the American Chemical Society* **2002,** 124, 15194-15195.

17. Deng, J. J.; Viers, B. D.; Esker, A. R.; Anseth, J. W.; Fuller, G. G. *Langmuir* **2005,** 21, 2375-2385.

18. Deng, J. J.; Farmer-Creely, C. E.; Viers, B. D.; Esker, A. R. *Langmuir* **2004,** 20, 2527-2530.

19. Yin, W.; Deng, J.; Esker, A. R. *Langmuir* **2009,** 25, 7181-7184.

20. Mitsuishi, M.; Zhao, F.; Kim, Y.; Watanabe, A.; Miyashita, T. *Chemistry of Materials* **2008,** 20, 4310-4316.

21. Lee, W.; Ni, S. L.; Deng, J. J.; Kim, B. S.; Satija, S. K.; Mather, P. T.; Esker, A. R. *Macromolecules* **2007,** 40, 682-688.

22. Gunawidjaja, R.; Huang, F. F.; Gumenna, M.; Klimenko, N.; Nunnery, G. A.; Shevchenko, V.; Tannenbaum, R.; Tsukruk, V. V. *Langmuir* **2009,** 25, 1196-1209.

23. Zheng, L.; Hong, S.; Cardoen, G.; Burgaz, E.; Gido, S. P.; Coughlin, E. B. *Macromolecules* **2004,** 37, 8606-8611.

24. Yoshida, K. H., T.; Ootake, N.; Tanaka, R.; Matsumoto, H, *Silsesuioxane-based polymers: Synthesis of phenylsilsesquioxanes with Double-decker structure and their polymers*. Springer: 2008; p 205-211.

25. Zhang, C. X.; Laine, R. M. *Journal of the American Chemical Society* **2000,** 122, 6979-6988.

26. Stein, J.; Lewis, L. N.; Gao, Y.; Scott, R. A. *Journal of the American Chemical Society* **1999,** 121, 3693-3703.

27. Broniatowski, M.; Macho, I. S.; Minones, J.; Dynarowicz-Latka, P. *Journal of Physical Chemistry B* **2004,** 108, 13403-13411.

28. Dervichian, D. G. *Journal of Chemical Physics* **1939,** 7, 931-948.

29. Harkins, W. D., In *The Physical Chemistry of Surface Films*, Reinhold: New York, 1952; p 107.

30. Minones, J.; Patino, J. M. R.; Conde, O.; Carrera, C.; Seoane, R. *Colloids and Surfaces a-Physicochemical and Engineering Aspects* **2002,** 203, 273-286.

31. Deng, J.; Hottle, J. R.; Polidan, J. T.; Kim, H.-J.; Farmer-Creely, C. E.; Viers, B. D.; Esker, A. R. *Langmuir* **2003,** 20, 109-115.

32. Miyashita, T. *Progress in Polymer Science* **1993,** 18, 263-294.

3. CHAPTER 3: Effects of Subphase Composition on the Monolayer Properties of Amphiphilic DDSQ

3.1. Introduction

Polyhedral oligomeric silsesquioxanes (POSSs), which consist of a rigid inorganic $SiO_{1.5}$ core with flexible and reactive organic coronae, have attracted much attention because of their unique structures,[1, 2] in addition to their physical properties such as a low dielectric constant,[3, 4] and high thermal stability.[5] Based on these unique properties, POSSs have been applied variously as nanofillers, catalytic supports, and surface coatings. Nanometer scale organization of POSS is important to improve their performance. Organization of POSSs can be achieved using, self-assembly, layer-by-layer assembly, or Langmuir–Blodgett (LB) technique. Among these techniques, the LB technique offers the possibility of preparing homogeneous thin films with well-defined layered structures and precise control of the thickness and composition.[6-8]

In the Chapter 2, it was shown that DDSQs substituted with DEG units form uniform monolayers at the air-water interface.[9] It is well known that intermolecular interactions in a monolayer film can be controlled by addition of some solute in the subphase.[10] Usually, ions are added to the subphase to control monolayer properties, such as monolayer stability, monolayer phase (liquid expand to liquid condensed) etc.

In the Chapter 3, we studied the effects of subphase composition on the monolayer behavior of amphiphilic 4DEG-DDSQ, which contains four DEG units as the coronae at the air–water interface. Solutes of three kinds (phosphoric acid, 1,3-bis(hydroxymethyl)urea, and potassium chloride) were added to the subphase to control intermolecular interactions in the 4DEG-DDSQ monolayer using hydrogen-bonding (phosphoric acid 1,3-bis (hydroxymethyl)urea) or ion-dipole (potassium chloride) interactions. The monolayers prepared on different subphase were deposited onto a solid substrate. Then the film surface morphology was observed using atomic force microscopy (AFM). Results showed that all the interactions hindered the layer disruption which occurs during the water deposition. The interactions were confirmed using FT–IR measurements.

3.2. Experimental Section

3.2.1. Materials.

1,3-Bis (hydroxymethyl)urea, phosphoric acid and potassium chloride (KCl) are purchased from Aldrich. Dichloromethane, chloroform, and acetone are purchased from Kanto Chemical Co. Inc. and distilled before use. Spectroscopic grade chloroform (Dojindo Laboratories) was used as a spreading solvent. Pure distilled water with resistivity higher than 17.5 MΩ·cm (purified using a RFD240RA and CPW-101 system; Advantec Toyo Kaisha Ltd.) was used as the subphase.

3.2.2. General Methods

BAM, AFM, and FT-IR measurements have been done as described in Chapter 2.

3.2.3. Isotherm Studies and LB Film Deposition

A dilute chloroform solution (ca. 1.2×10^{-3} mol L^{-1}) of the amphiphilic DDSQs was spread on aqueous 0.5 M phosphoric acid, 0.5 M 1,3-bis (hydroxymethyl)urea or 0.01 M potassium chloride solution. Then π–A isotherm measurements and LB film deposition were carried out using an automatically controlled Langmuir trough (FSD-220 and 21; USI Systems). The surface pressure was measured using a paper Wilhelmy plate. The compression rate was 15 cm^2 min^{-1}. The monolayer was deposited onto a hydrophobic solid substrate using vertical dipping at a dipping speed of 10 mm/min under surface pressure of 20 mN/m at 8 ˚C. Before using the substrates, they were washed with chloroform and acetone and then dried with flowing nitrogen.

3.2.4. Extraction Measurements.

Twenty mL of 0.01 M KOH aqueous solution containing picric acid (7×10^{-5} M) was added to a 20 mL of CH_2Cl_2 solution which contains 7.5×10^{-3}, 5×10^{-3}, 5×10^{-4}, and 2.5×10^{-4} M of 4DEG-DDSQ, respectively. The mixed solution was stirred vigorously and the water phase was collected. The ion conductivity of water phase was measured using an ion conductivity meter (MM-60R; TOA DKK) and converted to ion concentration using a calibration curve. The calibration curve was prepared by measuring ion conductivity of 0.001, 0.01, 0.05, 0.1, 0.5, and 1 M of KOH solution respectively.

3.3. Result and Discussion

3.3.1. Monolayer Behavior of 4DEG-DDSQ Prepared on Different Subphases

4DEG-DDSQ was dissolved in $CHCl_3$ and spread onto pure water or water subphases containing 0.5 M of phosphoric acid, 0.5 M of 1,3-bis (hydroxymethyl)urea, or 0.01 M of KCl. The π–A isotherms of 4DEG-DDSQ measured using phosphoric acid and 1,3-bis (hydroxymethyl)urea subphase were shifted toward the region of lager surface area compared to the isotherm of materials spread on pure water (Figure 1). However, no noticeable effect of KCl was evident on the π–A isotherm (Figure 1). The limiting surface areas (A_{limt}), as calculated by extrapolating the linear part of the π–A isotherm to zero pressure, were found respectively to be 2.63 nm^2 on pure water, 3.60 nm^2 on phosphoric acid, and 3.71 nm^2 on 1,3-bis (hydroxymethyl)urea subphase. The calculated cross-sectional area of 4DEG-DDSQ was 3.96 nm^2, which is based on a model where DEG units take a fully stretched (all-trans) conformation (Figure 3.1b).

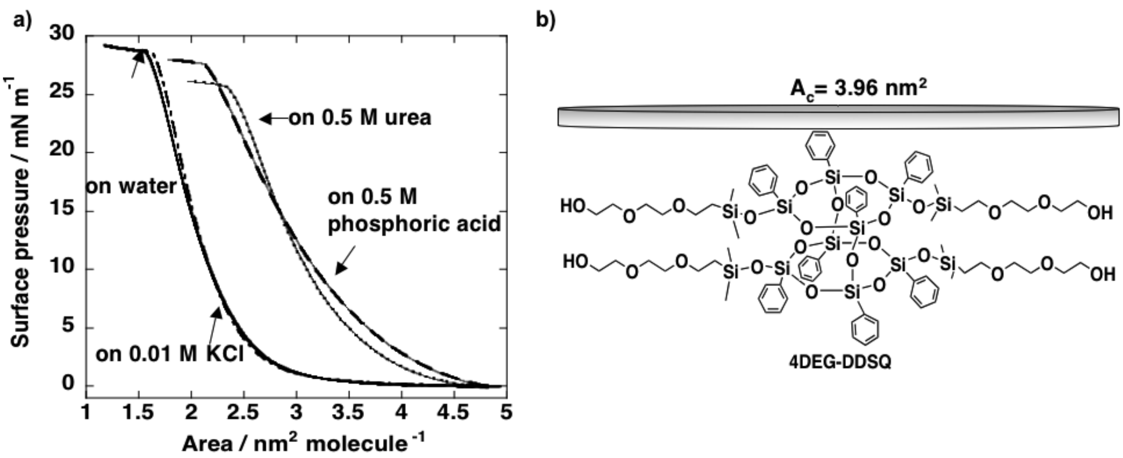

Figure 3.1. (a) π–A isotherms for 4DEG-DDSQ spread on pure water (solid line), 0.5 M 1,3-bis (hydroxymethyl)urea (dashed line), 0.5 M phosphoric acid (dotted line), and 0.01 M potassium chloride (dotted and dashed lines) aqueous solution at 8 °C. (b) CPK models calculation of cross-sectional area of the fully stretched 4DEG-DDSQ.

From the limiting surface area, it can be inferred that 4DEG-DDSQ takes the stretched conformation on the phosphoric acid and 1,3-bis (hydroxymethyl) urea subphase. Results of a previous study revealed that the DEG units of 4DEG-DDSQ on pure water are partially submerged into the water, which results in smaller A_{limt} than that in the fully stretched conformation (Scheme 3.1a). The strong hydrogen-bonding interaction between the OH groups at the DEG units and phosphoric acid or 1,3-bis(hydroxymethyl)urea on the subphase results in expansion of the limiting surface area (Schemes 3.1b, c). Although phosphoric acid is an anionic molecule, whereas 1,3-bis(hydroxymethyl)urea is a nonionic molecule, the electrostatic repulsion between the phosphoric acid groups seems to have a small effect on the monolayer property.

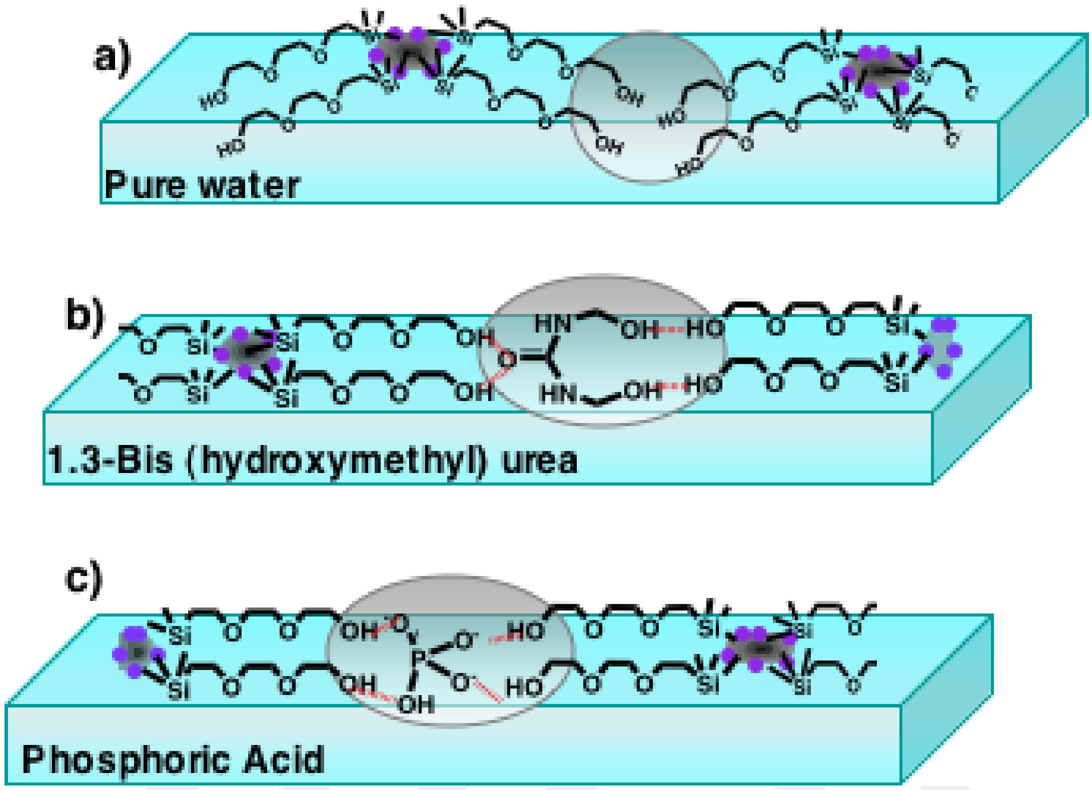

Scheme 3.1. Schematic illustration of the 4DEG-DDSQ monolayer in the (a) water, (b) 1,3-bis (hydroxymethyl)urea, and (c) phosphoric acid solution.

Surface morphologies of the monolayers spread on different subphases were observed using BAM (Figure 3.2). The BAM images of 4DEG-DDSQ spread on a KCl subphase show a liquid expanded (LE) phase with small circular liquid condensed (LC) domains at a lift-off surface area (Figure 3.2B). Further compression increased the number of LC domains (Figure 3.2C). This feature resembles that observed on pure water subphase, as reported previously.[9] The LC domains consist of POSS nanocrystal because of their high aggregation property.[11-13] However, the BAM images of 4DEG-DDSQ spread on the phosphoric acid and 1,3-bis (hydroxymethyl)urea subphase show a decrease of the LC domains and LE phase dominates the morphology with compression (figure 3.3b(B) and 3b(B)). The strong interaction between OH groups of DEG units and the solutes suppressed the POSS unit crystallization.

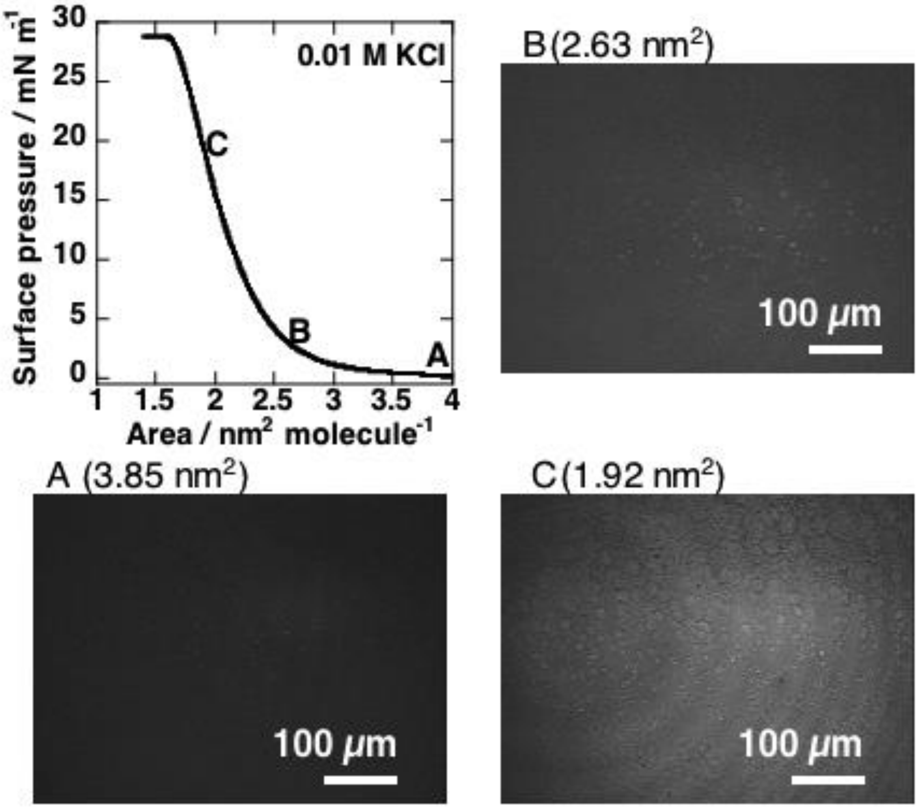

Figure 3.2. BAM images of 4DEG-DDSQ for different areas (A) on KCl aqueous subphase. Letters on the π–A isotherm were used to indicate each BAM image. The positions of letters correspond to the A values, where BAM images were taken.

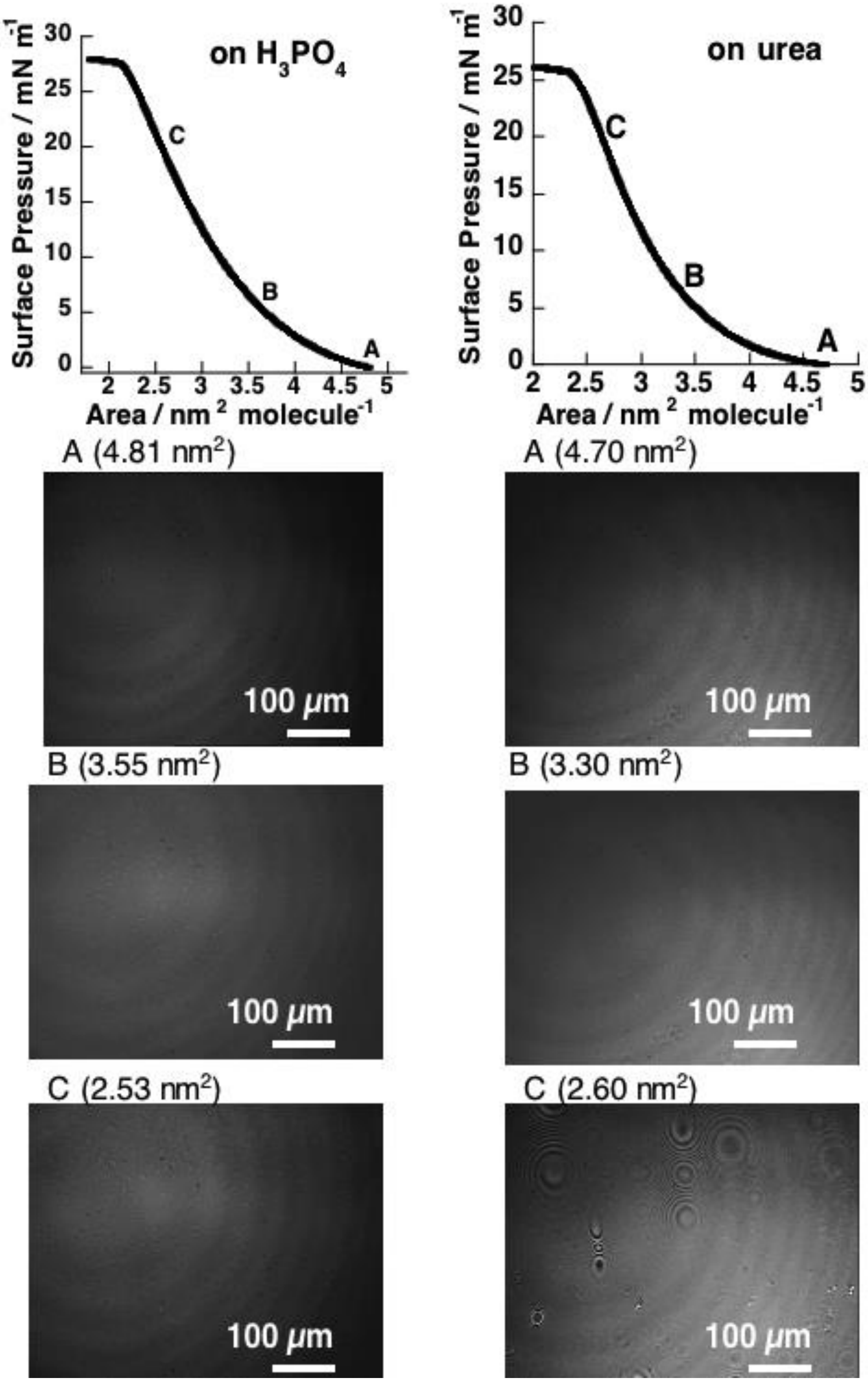

Figure 3.3 BAM images of 4DEG-DDSQ for different areas (A) on (a) phosphoric acid, and (b) 1,3-bis(hydroxymethyl)urea aqueous subphase. Letters on the π–A isotherm were used to indicate each BAM image. The letter positions correspond to the A values where the BAM images were taken.

The monolayers prepared on different subphases were deposited onto a solid substrate at 20 mN m^{-1} and 8 °C by the LB technique. The transfer ratios of upward and downward depositions are almost unity (Y-type film). The AFM images of the bilayer film deposited onto a silicon substrate show nanodots formation irrespective of the subphase composition (Figure 3.4). Previously, it had been concluded that nanodots were found by dewetting of water during the transfer process: because the interaction between 4DEG-DDSQs and the substrate is weak, the molecules on the substrate aggregate during the vaporization of water (dewetting phenomena). As discussed in the π–A isotherm, the 4DEG-DDSQ monolayer prepared using phosphoric acid and 1,3-bis (hydroxymethyl)urea have strong intermolecular interaction. That strong interaction prevents disruption of the layer structure during the evaporation of water, which produces smaller domain size and higher domain density than that on pure water subphase (Figures 3.4b and 3.4c). The AFM image of the film deposited using KCl subphase shows a similar morphological change. Even the π–A isotherm shows no noticeable difference compared to that on pure water (Figure 3.4d). The morphology change probably results from coordination of K+ with DEG groups.

To confirm the coordination, we performed extraction experiments. KOH aqueous solution of 0.01 M was mixed with chloroform solutions, which respectively contain 7.5×10^{-3}, 5×10^{-3}, 5×10^{-4}, and 2.5×10^{-4} M of 4DEG-DDSQ. The mixed solution was stirred vigorously. Then the water phase was collected. The ion conductivity of water phase was measured using an ion meter. The conductivity of water phase was decreased concomitantly with increasing 4DEG-DDSQ concentration in $CHCl_3$ (Figure 3.5a). It is particularly interesting that the conductivity value become constant when the 4DEG-DDSQ molar amount become greater than twice the K^+ molar amount. Considering the 4DEG-DDSQ structure, it is assumed that two DEG units coordinated with one K^+ ion to form a 2:1 coordination compound (Figure 3.5b). The K^+ coordination to DEG groups decreases the amount of absorbed water. Therefore, dewetting was hindered. The coordination structure is reasonable to explain the results of the π–A isotherm and the BAM measurements. Two DEG units attached onto the same DDSQ coordinates with one K^+. Therefore, the intermolecular interaction between 4DEG-DDSQs is similar to that prepared on the pure water subphase.

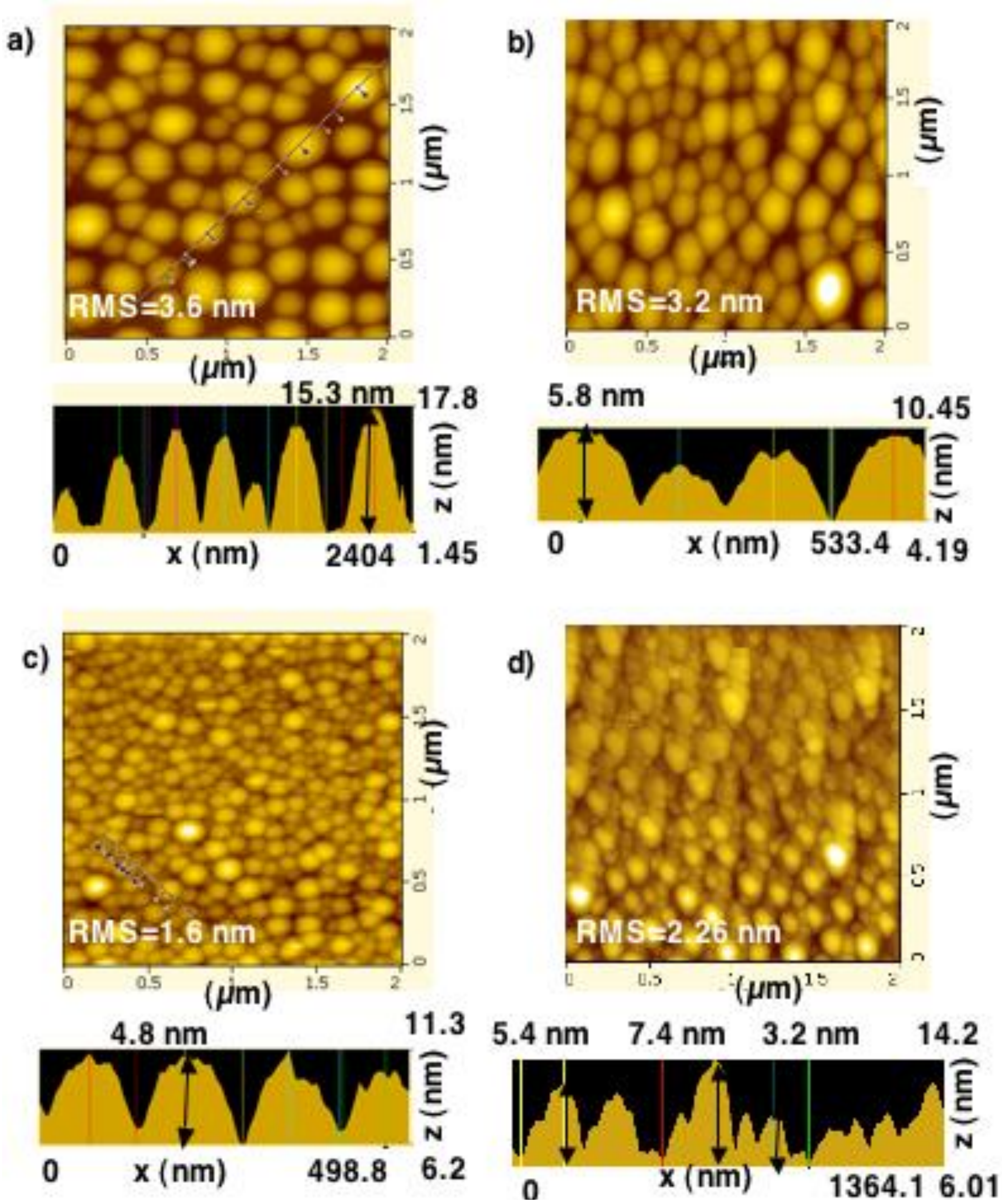

Figure 3.4. AFM images of bi-layer 4DEG-DDSQ LB film deposited on a hydrophobic silicon substrate prepared in the (a) water, (b) 0.5 M 1,3-bis (hydroxymethyl)urea, (c) 0.5 M phosphoric acid, and (d) 0.01 KCl solution together with cross-sectional profile of the dots.

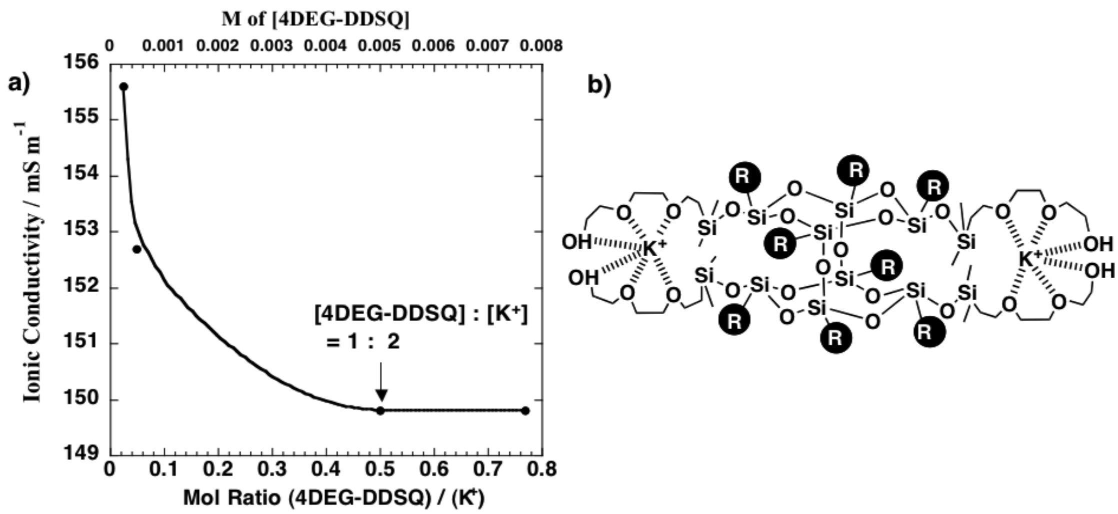

Figure 3.5 (a) Equivalent conductance of the 4DEG-DDSQ - KCl system. (b) Expected complexation mechanism of K^+ with DEG units.

3.3.2. Characterization of the Interactions by FT-IR Measurements

Interactions of the solutes to the monolayer film were discussed using FT-IR spectra measurements. Multilayer deposition of 4DEG-DDSQ using pure water and urea subphase onto CaF_2 was unsuccessful. Therefore, 4DEG-DDSQ cast film was used as a reference and compared with 20 layers of 4DEG-DDSQ deposited onto a CaF_2 substrate using phosphoric acid and KCl subphases. Figure 3.6 shows FT–IR spectra of the LB films and cast film of 4DEG-DDSQ. The FT–IR shows peaks related respectively to Si–O–Si at 1140–1030 cm^{-1}, CH_2–O–CH_2 at 1253 cm^{-1}, phenyl at 3040 cm^{-1}, and OH at 3345 cm^{-1}. The former three peaks show absorption at the same wavenumber in the entire film, whereas the later OH absorption band is dependent on the film structure. The 4DEG-DDSQ cast film shows broad absorption centered at 3345 cm^{-1}. However, the OH absorption band of the LB film deposited from phosphoric acid subphase was much broader than that of the cast film because of a wide distribution of hydrogen-bonding in the film.[14, 15] The OH absorption of the LB film prepared from KCl subphase shows a broad peak centered at 3345 cm^{-1} with a shoulder at 3320 cm^{-1}. The smaller wavenumber indicates that strong hydrogen bonds were formed in the LB film. The coordination of K^+ to 4DEG-DDSQ puts two OH groups close mutually. Therefore the hydrogen bond strength between the OH groups in the same DDSQ molecule becomes strong.

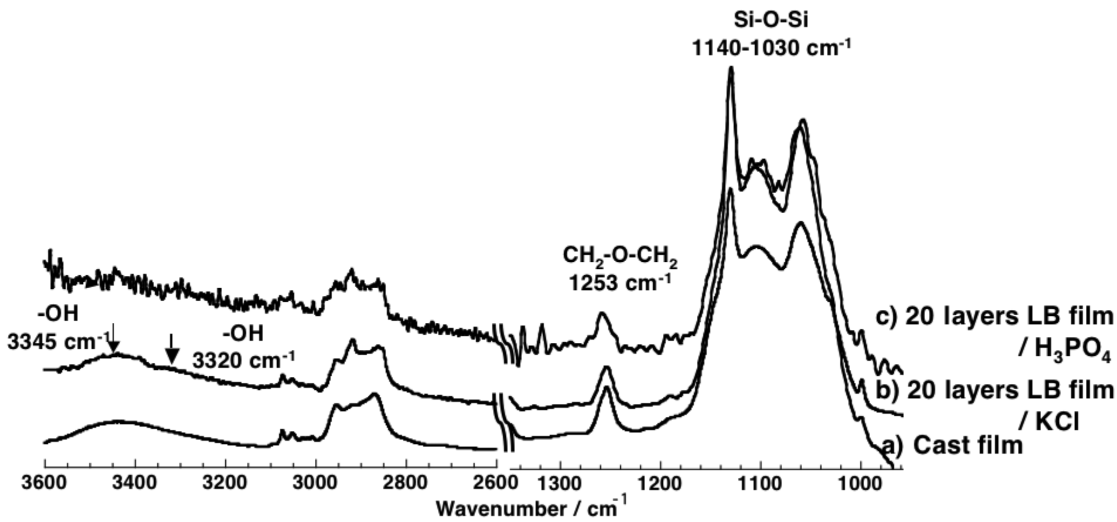

Figure 3.6. FT-IR spectra recorded at room temperature in the 800–3600 cm^{-1} region for (a) 4DEG-DDSQ cast film, and 20 layers LB film of 4DEG-DDSQ prepared in the (b) 0.01 M KCl and (c) 0.5 M phosphoric acid solution.

3.4. Summary

The monolayer behavior of 4DEG-DDSQ spread on subphase of three kinds (0.5 M phosphoric acid, 0.5 M 1,3-bis(hydroxymethyl)urea, and 0.01 M potassium chloride) was studied. The monolayer film prepared in phosphoric acid or 1,3-bis(hydroxymethyl)urea subphase shows an increase in A_{lim} compared to that prepared in pure water subphase. This fact can be attributed to the formation of hydrogen-bonding between the solutes and DEG units of 4DEG-DDSQ molecules. Although the addition of KCl to the subphase shows no drastic change in the π–A isotherm, coordination between K^+ and 4DEG-DDSQ with the ratio of 2:1 was confirmed by extraction measurement. Because the layer structure was disrupted by the dewetting of water, the bilayer films of 4DEG-DDSQ deposited onto a solid substrate formed nanodots irrespective of the subphase composition. However, the interactions between 4DEG-DDSQ and the solutes hinder disruption of the layer structure, which results in decreased size and increased density of the nanodots. This result demonstrates that the subphase composition is important for morphological control of "core–coronae" type amphiphiles.

3.5. ***References***

1. Lichtenhan, J. D. *Comments on Inorganic Chemistry* **1995,** 17, 115-130.

2. Gonzalez, R. I.; Phillips, S. H.; Hoflund, G. B. *Journal of Spacecraft and Rockets* **2000,** 37, 463-467.

3. Leu, C.-M.; Chang, Y.-T.; Wei, K.-H. *Macromolecules* **2003,** 36, 9122-9127.

4. Leu, C.-M.; Chang, Y.-T.; Wei, K.-H. *Chemistry of Materials* **2003,** 15, 3721-3727.

5. Mantz, R. A.; Jones, P. F.; Chaffee, K. P.; Lichtenhan, J. D.; Gilman, J. W.; Ismail, I. M. K.; Burmeister, M. J. *Chemistry of Materials* **1996,** 8, 1250-1259.

6. Mizuta, Y.; Matsuda, M.; Miyashita, T. *Langmuir* **1993,** 9, 1158-1159.

7. Yatsue, T.; Miyashita, T. *Journal of Physical Chemistry* **1995,** 99, 16047-16051.

8. Qian, P.; Matsuda, M.; Miyashita, T. *Journal of the American Chemical Society* **1993,** 115, 5624-5628.

9. Kucuk, A. C.; Matsui, J.; Miyashita, T. *Journal of Colloid and Interface Science* **2011,** 355, 106-114.

10. Ulman, A., *An Introduction to ultrathin Organic Films from Langmuir-Blodgett to Self-Assembly*. Academic Press, inc.: San Diego, 1991; Vol. 0-12-708230-1.

11. Deng, J. J.; Hottle, J. R.; Polidan, J. T.; Kim, H. J.; Farmer-Creely, C. E.; Viers, B. D.; Esker, A. R. *Langmuir* **2004,** 20, 109-115.

12. Deng, J. J.; Viers, B. D.; Esker, A. R.; Anseth, J. W.; Fuller, G. G. *Langmuir* **2005,** 21, 2375-2385.

13. Deng, J. J.; Polidan, J. T.; Hottle, J. R.; Farmer-Creely, C. E.; Viers, B. D.; Esker, A. R. *Journal of the American Chemical Society* **2002,** 124, 15194-15195.

14. Mishra, A. K.; Chattopadhyay, D. K.; Sreedhar, B.; Raju, K. V. S. N. *Progress in Organic Coatings* **2006,** 55, 231-243.

15. Coleman, M. M.; Lee, K. H.; Skrovanek, D. J.; Painter, P. C. *Macromolecules* **1986,** 19, 2149-2157.

4. Chapter 4: Monolayer Behavior of Amphiphilic DDSQ Containing Urethane Groups

4.1. Introduction

Organization of organic and polymeric materials at a molecular level[1-3] enables their potential technological applications in optical devices,[4] biomimetic surfaces,[5] and electronic[6] processes. The bottom-up approach can be achieved using self-assembly processes, such as layer-by-layer (LbL), and Langmuir–Blodgett (LB) techniques. The LB technique is an efficient process to construct well-organized and highly oriented uniform films. At a fundamental level, well-defined and oriented molecular films are extremely important to elucidate physical properties at surfaces and interfaces.

Polyhedral oligomeric silsesquioxanes (POSSs), which consist of a rigid inorganic $SiO_{1.5}$ core with flexible and reactive organic coronae, have attracted much attention because of their unique structures,[7, 8] in addition to their physical properties such as a low dielectric constant[9, 10] and high thermal stability.[11] The well-defined organization of POSSs is important for applying their unique properties to organic–inorganic nanohybrid materials. For example, Caruso et al. and Su et al. used an LbL technique to prepare nanocomposite ultrathin films.[12, 13] Banaszak Holl et al. fabricated self-assemble monolayer at the gold substrate using the vapor deposition method.[14, 15] Deng et al. discovered that trisilanol-POSSs form uniform Langmuir monolayers at the air–water interface. They conducted intensive studies of the surface morphology and viscoelastic properties of the trisilanol-POSSs.[16-20] Esker et al. blended amphiphilic trisilanolisobutyl-POSS or nonamphiphilic octaisobutyl-POSS with amphiphilic poly(dimethylsiloxane) to investigate the compatibility of POSS with the polymer.[21-23] In Chapter 2, it is shown that double-decker shaped polyhedral oligomeric silsesquioxanes (DDSQs) substituted with di(ethylene glycol) (DEG) units formed uniform monolayers at the air–water interface. The synthesized DDSQs are unique amphiphilic molecules in contrast to conventional "head-to-tail" amphiphiles because they are core–corona amphiphiles, in which DDSQ is hydrophobic core and DEG units are hydrophilic coronae. Reportedly, DDSQ substituted with four DEG units can be transferred onto the solid substrate.[24] However the film morphology was not uniform due to the weak multilayer interaction. In chapter 3, it is shown that addition of some solutes to the subphase improves the monolayer stability. In this chapter, we prepared 2DEGNH-DDSQ and 4DEGNH-DDSQ, which contain a urethane group at the end of the hydrophilic corona. Because urethane groups are well-known to form a directional hydrogen bonding, the surface pressure (π)–area (A) isotherm and Brewster angle microscope (BAM) images of 2DEGNH-DDSQ or 4DEGNH-DDSQ were obtained and compared with those of 2DEG-DDSQ or 4DEG-DDSQ to elucidate the effects of hydrogen-bonding interactions on monolayer properties. The mixed film was characterized using atomic force microscopy (AFM), X-ray photoelectron spectroscopy (XPS), and FT-IR spectroscopy.

4.2. Materials and Methods.

All the equipments used in this study such as AFM, XPS, FT-IR are the same as Chapter 2. Ethyl isocyante is purchased from Aldrich and used as received. Other chemicals are purchased from the same company as mentioned in Chapter 2.

4.3. Synthesis and Characterization (2DEGNH-DDSQ, 4DEGNH-DDSQ)

4.3.1. Synthesis of amphiphilic DDSQ with Amide Groups at the End of the Di(ethylene glycol) Units (2DEGNH-DDSQ).

2DEG-DDSQ (0.35 g, 0.247 mmol) was dissolved in toluene at 0 °C and stirred in argon atmosphere. Then ethyl isocyanate (0.06 ml, 0.740 mmol) was added dropwise to the reaction mixture. The reaction was conducted at room temperature for 1 day (Scheme 4.1). Unreacted isocyanate was removed by evaporation. The crude product was recrystallized from THF/n-hexane and dried under vacuum at 40 °C (yield: 97 %).

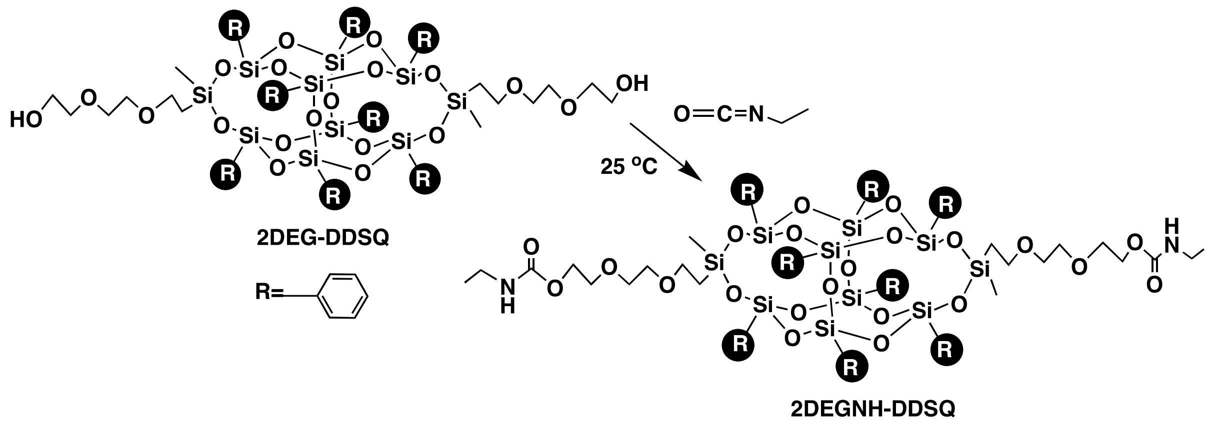

Scheme 4.1 Functionalization of 2DEG-DDSQ.

4.3.2. FT-IR Spectrum of 2DEGNH-DDSQ

Figure 4.1 shows the FT-IR spectra of 2DEG-DDSQ and 2DEGNH-DDSQ. The O-H peak related to DEG units at 3440 cm^{-1} band shifts at 3335 cm^{-1}, which is attribute to the NH vibration in 2DEGNH-DDSQ or 4DEGNH-DDSQ. The peak between 1050 - 1140 cm^{-1} for Si-O-Si stretching of DDSQ core appears in each spectrum, suggesting that DDSQ core remained unchanged during the synthesis. [FT-IR (cm^{-1}), ν =3335 (urethane, N-H), ν =3075–3010 (aromatic, Ph), ν =2974, 2935, 2879 (aliphatic C-H), ν =1697 (C=O), ν =1520 (-NH), ν =1262 (CH_2-O), ν =1098 (Si-O)].

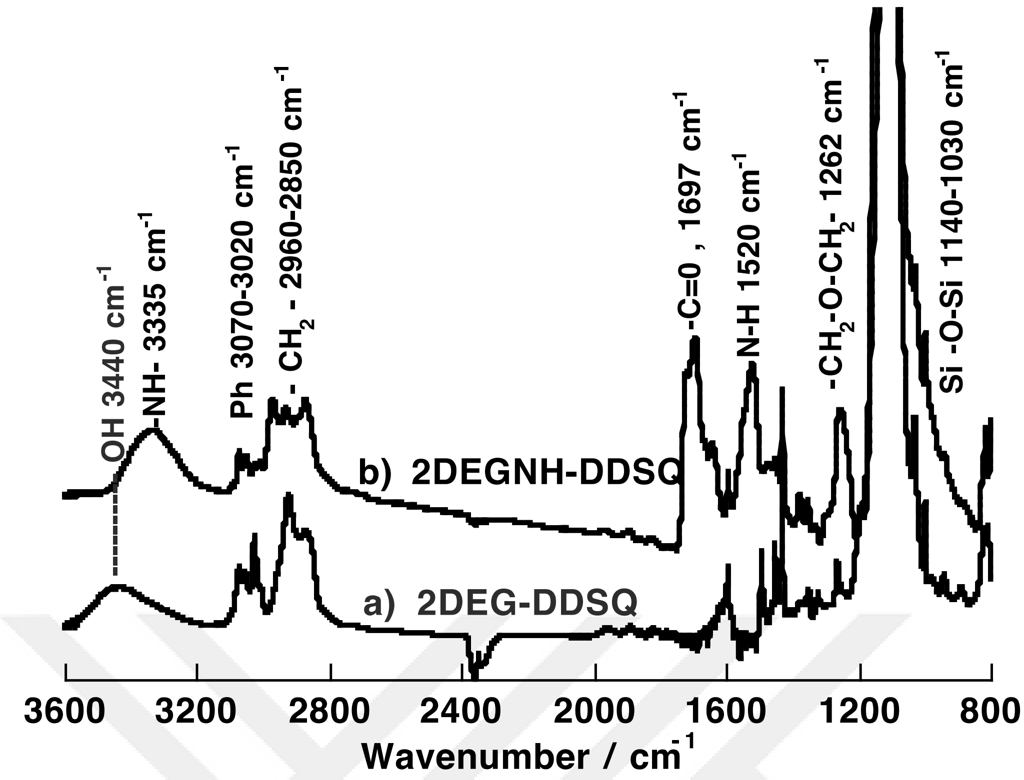

Figure 4.1. FTIR spectra of (a) 2DEG-DDSQ and (b) 2DEGNH-DDSQ.

4.3.3. ^{1}H and ^{13}C NMR spectra of 2DEGNH-DDSQ

^{1}H and ^{13}C NMR spectra (Figure 4.2) of 2DEGNH-DDSQ were taken in $CDCl_3$. The integration of protons peaks is compatible with the theoretical calculation of the integrals. After the reaction, *g* (–CH_2-O-CO-) and i (–CH_3) protons appeared at 4.16 and 1.08 ppm, respectively. [^{1}H NMR (ppm) (400 MHz, $CDCl_3$, $CHCl_3$ ref) 7.25–7.60 (m, 40H, Ph), 3.4–3.7 (t, 20H CH_2-O), 1.58 (t, 4H, NH-CH_2), 1.22 (t, 4H, CH_2-Si), 1.08 (t, 6H, CH_2-CH_3), 0.36 (s, 6H, Si(CH_3)). ^{13}C NMR (ppm), (100 MHz, $CDCl_3$, $CDCl_3$ ref) 128–134 (Ph), 65–73 (*C*H_2-O-*C*H_2), 36 (O-*C*H_2-CH_2-Si), 19 (*C*H_2-Si), 16 (*C*H_2-CH_3), 0.1 (Si (*C*H_3)$_2$)].

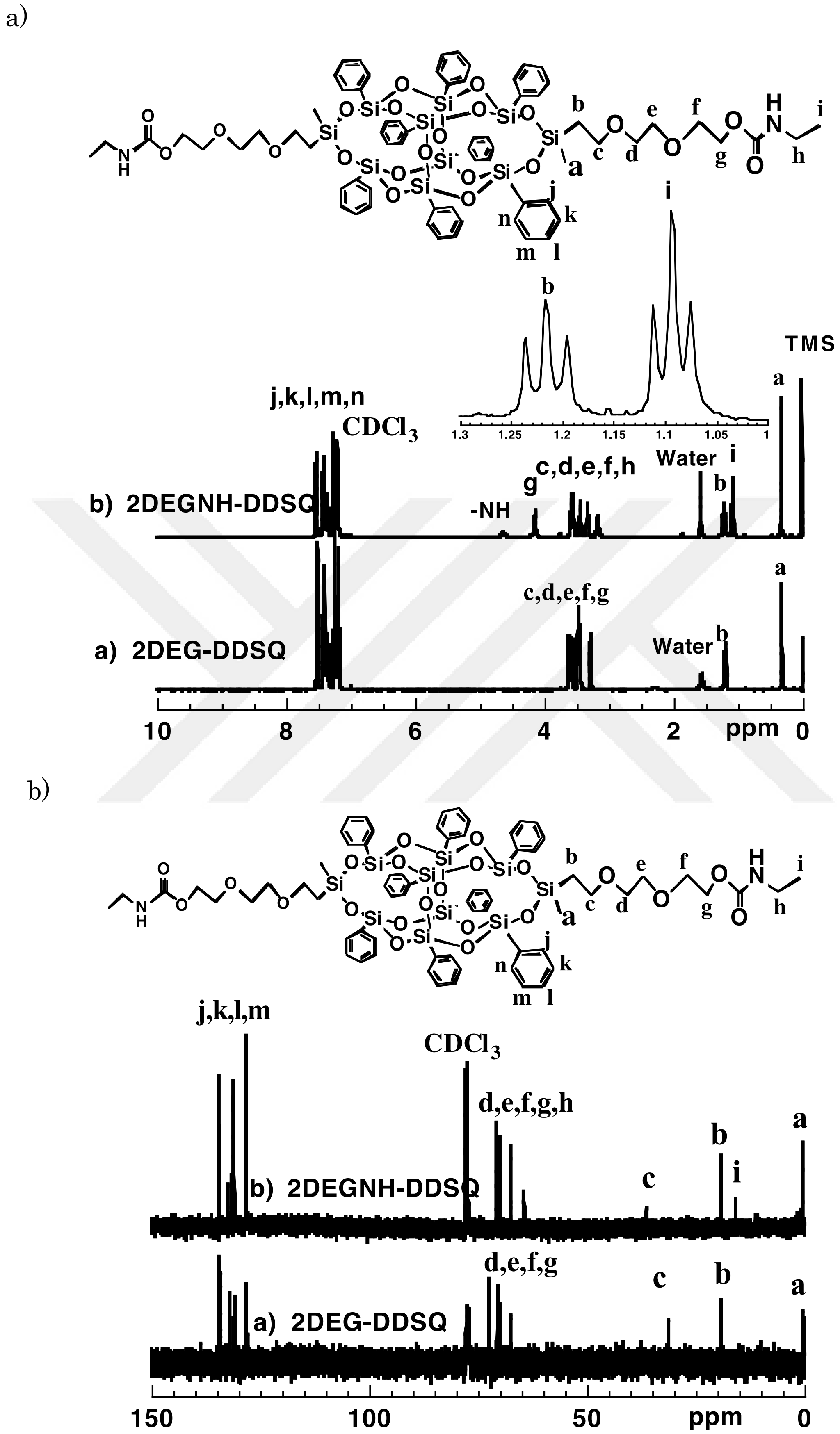

Figure 4.2. (a) ^{1}H NMR, (b) ^{13}C NMR of 2DEGNH-DDSQ in $CDCl_3$.

4.3.4. Synthesis of Amphiphilic DDSQ with Amide Groups at the End of the Di(ethylene glycol) Units (4DEGNH-DDSQ).

4DEG-DDSQ (1.5 g, 0.82 mmol) was dissolved in toluene at 0 °C and stirred in argon atmosphere. Then ethyl isocyanate (0.39 ml, 4.9 mmol) was added dropwise to the reaction mixture. The reaction was conducted at room temperature for 1 day (Scheme 4.2). Unreacted isocyanate was removed by evaporation. The crude product was dried under vacuum at 40 °C (yield: 95%).

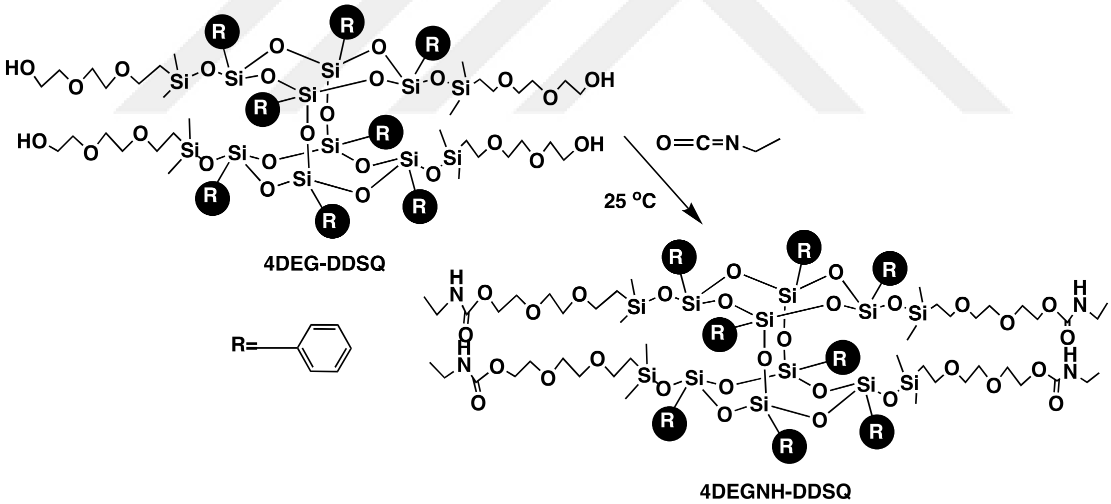

Scheme 4.2. Functionalization of 4DEG-DDSQ

4.3.5. FT-IR spectrum of 4DEGNH-DDSQ

Figure 4.3 shows the FT-IR spectra of initial compounds (4DEG-DDSQ) and obtained compound (4DEGNH-DDSQ). The O-H peak related to DEG units at 3444 cm^{-1} band shifts at 3343 cm^{-1}, which is attribute to the NH vibration in 4DEGNH-DDSQ. The peak between 1030 - 1140 cm^{-1} for Si-O-Si stretching of DDSQ core appears in each spectrum, suggesting that DDSQ core remained unchanged during the synthesis. [FT-IR (cm^{-1}), ν =3343 (urethane, N-H), ν =3075–3010 (aromatic, Ph), ν =2974, 2935, 2879 (aliphatic C-H), ν =1725 (C=O), ν =1531 (-NH), ν =1262 (CH_2-O), ν =1098 (Si-O)].

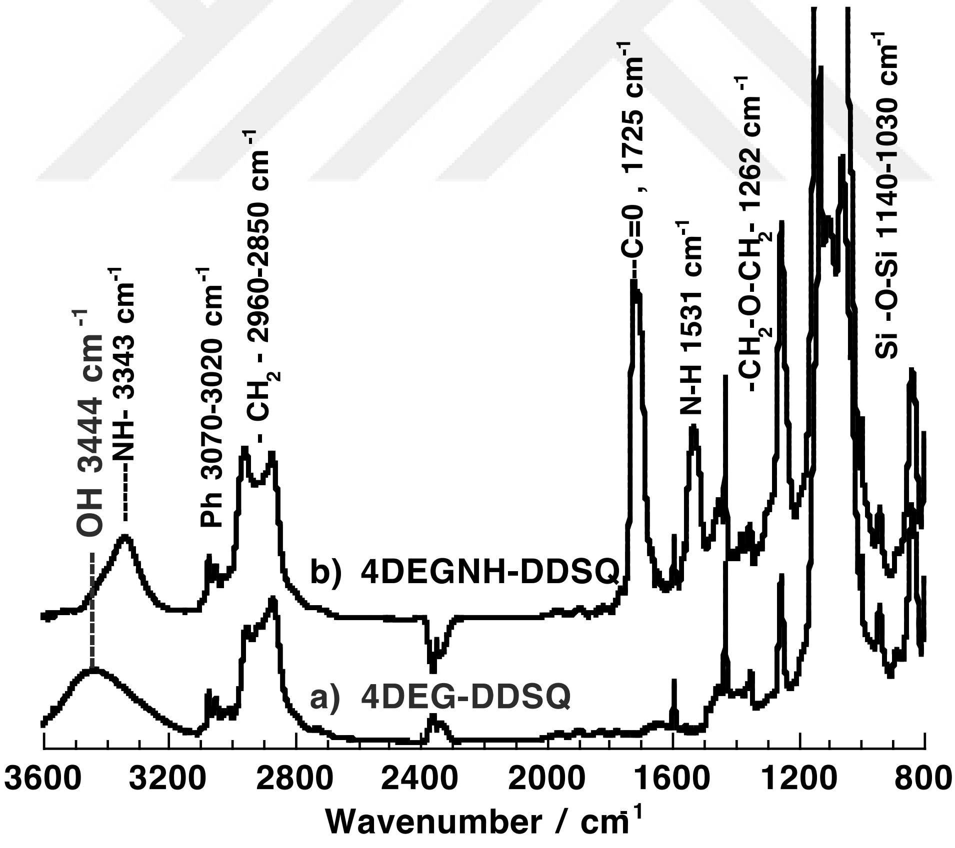

Figure 4.3. FTIR spectra of (a) 4DEG-DDSQ and (b) 4DEGNH-DDSQ.

4.3.6. ^{1}H NMR spectrum of 4DEGNH-DDSQ

^{1}H NMR spectrum (Figure 4.4) of 4DEGNH-DDSQ was taken in $CDCl_3$. The integration of protons peaks is compatible with the theoretical calculation of the integrals. After the reaction, *g* (–C*H₂*-O-CO-) and i (–CH_3) protons appeared at 4.16 and 1.08 ppm, respectively. [^{1}H NMR (ppm) (400 MHz, $CDCl_3$, $CHCl_3$ ref) 7.25–7.60 (m, 40H, Ph), 3.4–3.7 (t, 20H CH_2-O), 1.58 (t, 4H, NH-CH_2), 1.22 (t, 4H, CH_2-Si), 1.08 (t, 6H, CH_2-CH_3), 0.36 (s, 6H, Si(CH_3)).

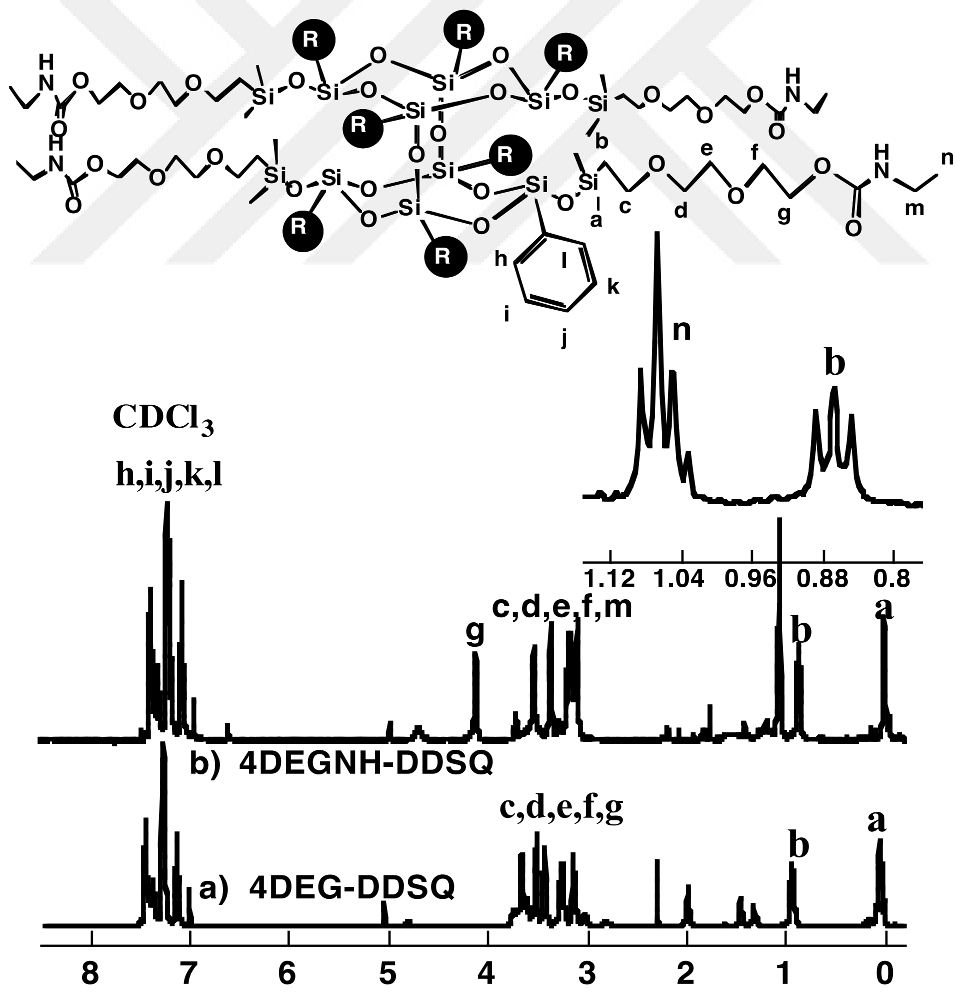

Figure 4.4. ^{1}H NMR of 4DEGNH-DDSQ in $CDCl_3$.

4.4. Results and Discussion

4.4.1. Monolayer Behavior of 2DEGNH-DDSQ at the Air–water Interface

A chloroform solution of amphiphilic DDSQs (1 mM) was spread on a water surface and π–A isotherms of the molecules were measured at 20 °C with a compression rate of 15 cm^2 min^{-1}. In chapter 2, it is described that 2H-DDSQ is not surface active, although amphiphilic 2DEG-DDSQ formes a uniform monolayer with a good balance between the hydrophobic DDSQ core and the hydrophilic DEG corona. The collapse pressure is identified as a spike in the π-A isotherm. The lift-off surface pressure is defined as a surface area where the surface pressure starts to increase. Comparing 2DEG-DDSQ with 2DEGNH-DDSQ (Figure 4.5a), the introduction of amide groups onto the end of the DEG units engenders a slight increase in the collapse pressure and the area of the lift-off in the surface pressure. The limiting surface area (A_{limt}), which is calculated by extrapolating the linear part of the π–A isotherm to zero pressure, was found to be 1.72 nm^2 for 2DEG-DDSQ and 1.81 nm^2 for 2DEGNH-DDSQ. These values are greater than the calculated values of cross-sectional areas of DDSQ core based on the CPK model (Figure 4.5b). However, the calculated cross-sectional area of 2DEG-DDSQ is 2.49 nm^2, which is based on a model where DEG units take a fully stretched (all-trans) conformation. This result indicates that the hydrophilic DEG units are partially submerged in the water subphase (Figure 4.5c,d).

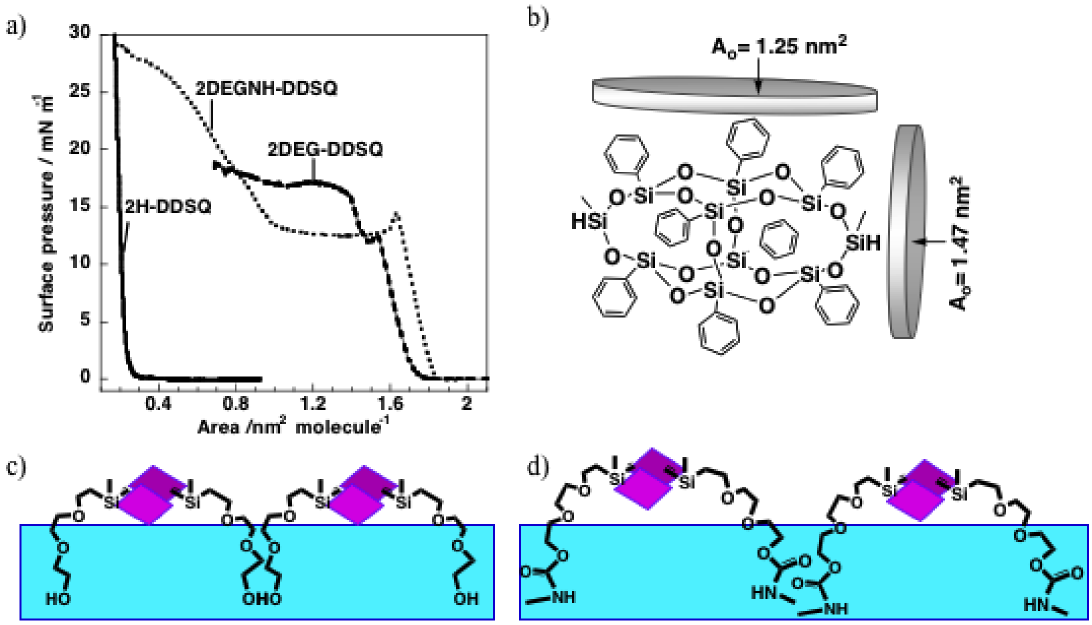

Figure 4.5. (a) Surface pressure (π)–area (A) isotherms for 2H-DDSQ (solid line), 2DEG-DDSQ (dashed line), and 2DEGNH-DDSQ (dotted line) at 20 °C. (b) Calculated cross-sectional areas of 2H-DDSQ using the CPK model. Schematic illustration of (c) 2DEG-DDSQ and (d) 2DEGNH-DDSQ monolayers at the air–water interface.

Figure 4.6 portrays BAM images of the 2DEGNH-DDSQ monolayers measured at different surface pressures. 2DEGNH-DDSQ formes rodlike assemblies at 0 mN/m (Figure 4.6A). The rod size increases longitudinally with the compression (Figure 4.6B). Then the rods were gathered to form a packed monolayer (Figure 4.6C) and were finally aggregated in three dimensions (Figure 4.6D,E). As shown in Chapter 2, the BAM images differ greatly from those observed in the 2DEG-DDSQ monolayer. The BAM images of the 2DEG-DDSQ monolayer show a tentative character as a liquidlike monolayer. The monolayer forms several domains with a smoothly curved boundary at low surface pressure. The domains are coalesced with compression.[24] The difference in monolayer morphology between 2DEG-DDSQ and 2DEGNH-DDSQ is derived from the urethane groups. The urethane groups at the end of the hydrophilic coronae form hydrogen bonds and increase the intermolecular interaction among 2DEGNH-DDSQs, which results in the formation of rodlike assemblies. Because the rods were observed at 0 mN/m, it is concluded that 2DEGNH-DDSQs self assembled to form the rods just after spreading the molecules at the air-water interface. 2DEGNH-DDSQ is a core-coronae type and rod-shape amphiphile, where hydrophobic core locates at the center and is sandwiched between the hydrophilic coronae. Because of the unique molecular structure, the molecule may easy to self-assemble through the short axis direction due to the hydrophobic-hydrophobic interaction working between the cores and hydrophilic-hydrophilic interaction working between the coronae to form sheets (Scheme 4.1). The sheets self-assemble to form the rods using the strong and well-ordered hydrogen bonding between the amides groups, which was confirmed by FT-IR measurements in section 4.3.3. 2DEGNH-DDSQ and 2DEG-DDSQ monolayers are unable to form LB films onto solid substrates. 2DEG-DDSQ and 2DEGNH-DDSQ are believed to be too soft and too rigid, respectively, for LB deposition.

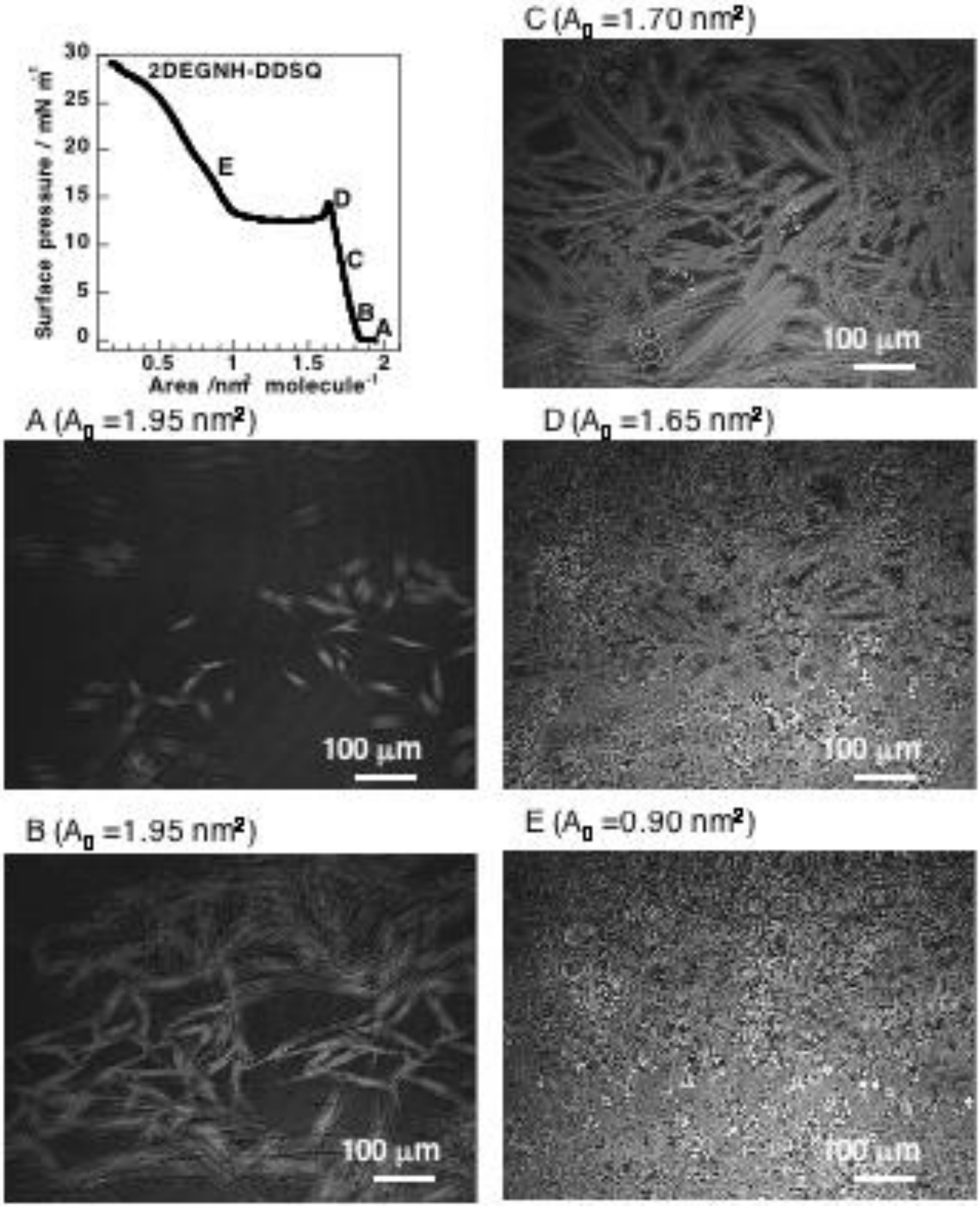

Figure 4.6. BAM images of 2DEGNH-DDSQ for different areas (A). Letters on the π–A isotherm indicate A values where each BAM image was taken. Actual surface areas are shown in parentheses above each image.

4.4.2. Monolayer Behavior of the 1:1 Mixture of 2DEGNH-DDSQ and 2DEG-DDSQ at the Air–water Interface

2DEGNH-DDSQ and 2DEG-DDSQ were dissolved in a chloroform solution at a 1:1 molar ratio and spread onto a water subphase. The π–A isotherm of the mixed film is given in Figure 7 together with those of pure 2DEG-DDSQ and 2DEGNH-DDSQ. In Figure 4.7, A is the average area permolecule. *A* remarkable feature of the mixed monolayer is the increase in A_{limt} (1.99 nm^2) compared to those of the single-component DDSQ amphiphiles (Figure 4.7a). The increase of A_{limt} suggests that 2DEG-DDSQ and 2DEGNH-DDSQ are not phase-separated but they are uniformly mixed. As mentioned in the previous section, the calculated cross-sectional areas of DDSQ core are 1.25-1.47 nm^2, whereas the calculated cross-sectional area of 2DEG-DDSQ assuming that DEG units take a fully stretched conformation is 2.49 nm^2. The lift-off point in the mixed film was 2.2 nm^2, which indicates that the ethylene glycol units in the amphiphilic DDSQs were partially stretched at the air-water interface as schematically shown in Figure 4.7b. The uniform mixing of the two molecules at the air–water interface was confirmed by BAM measurements (Figure 4.8). At larger surface areas (A) larger than the area of the lift-off point, the BAM image showed no formation of the rods indicating that the mixed monolayer may be a gas phase (Figure 4.8A). At the area of the lift-off of surface pressure, so-called island structures with smoothly curved boundaries indicate biphasic behavior in the mixed monolayer (Figure 4.8B). During the course of compression, the island coalesced and finally covered the entire measurement area (Figure 4.8C,D). These BAM images show general characteristics of a liquid-like monolayer. After the monolayer collapsed, the nucleation and growth of the rod like assemblies of 2DEGNH-DDSQ occurred (Figure 4.8E-G). Uniform mixing is induced by hydrogen bonding between the urethane in 2DEGNH-DDSQ and hydroxyl groups in 2DEG-DDSQ. The hydrogen bond formation is confirmed by FT-IR results in Section 4.3.3. A similar type of hydrogen bonding is observed in polyurethanes, and is known to enhance a homogeneous blending of hard and soft segments.[25] The intermolecular hydrogen bonding between urethane in 2DEGNH-DDSQ and hydroxyl groups in 2DEG-DDSQ reduces the solubility of the coronae into water.[26] Correspondingly, the hydrophilic chains are located at the air–water interface, which engenders the increase of A_{limt} (Figure 4.7b).

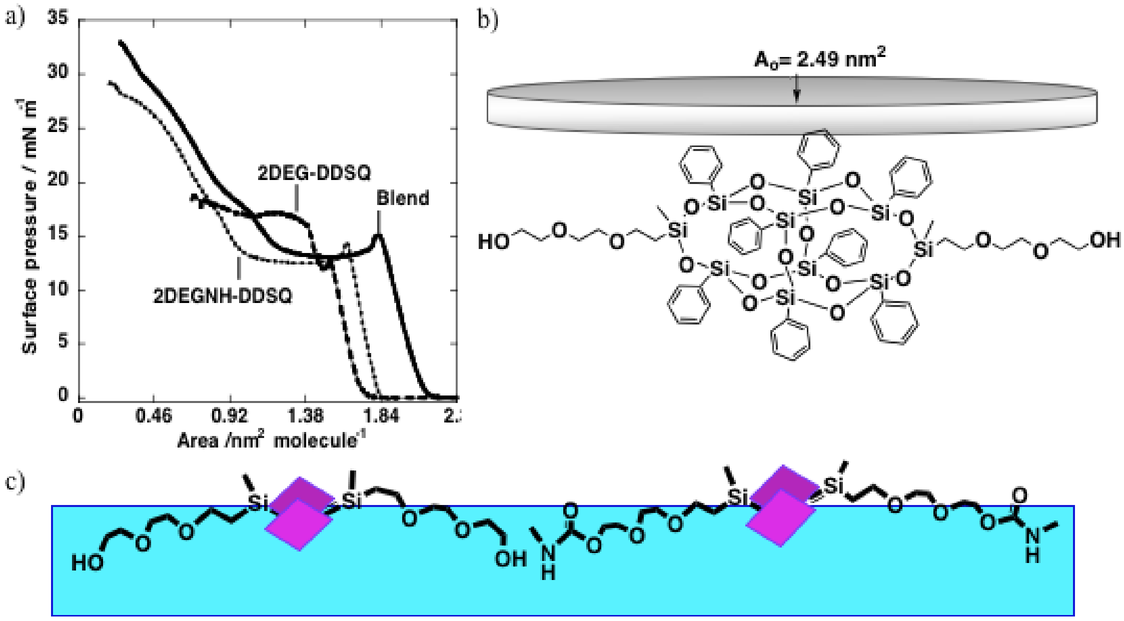

Figure 4.7. (a) Surface pressure (π) – area (A) isotherms for 2DEG-DDSQ (dashed line), 2DEGNH-DDSQ (dotted line), and their 1:1 molar mixture (solid line) at 20 °C. (b) Schematic illustration of the mixed monolayer at the air–water interface.

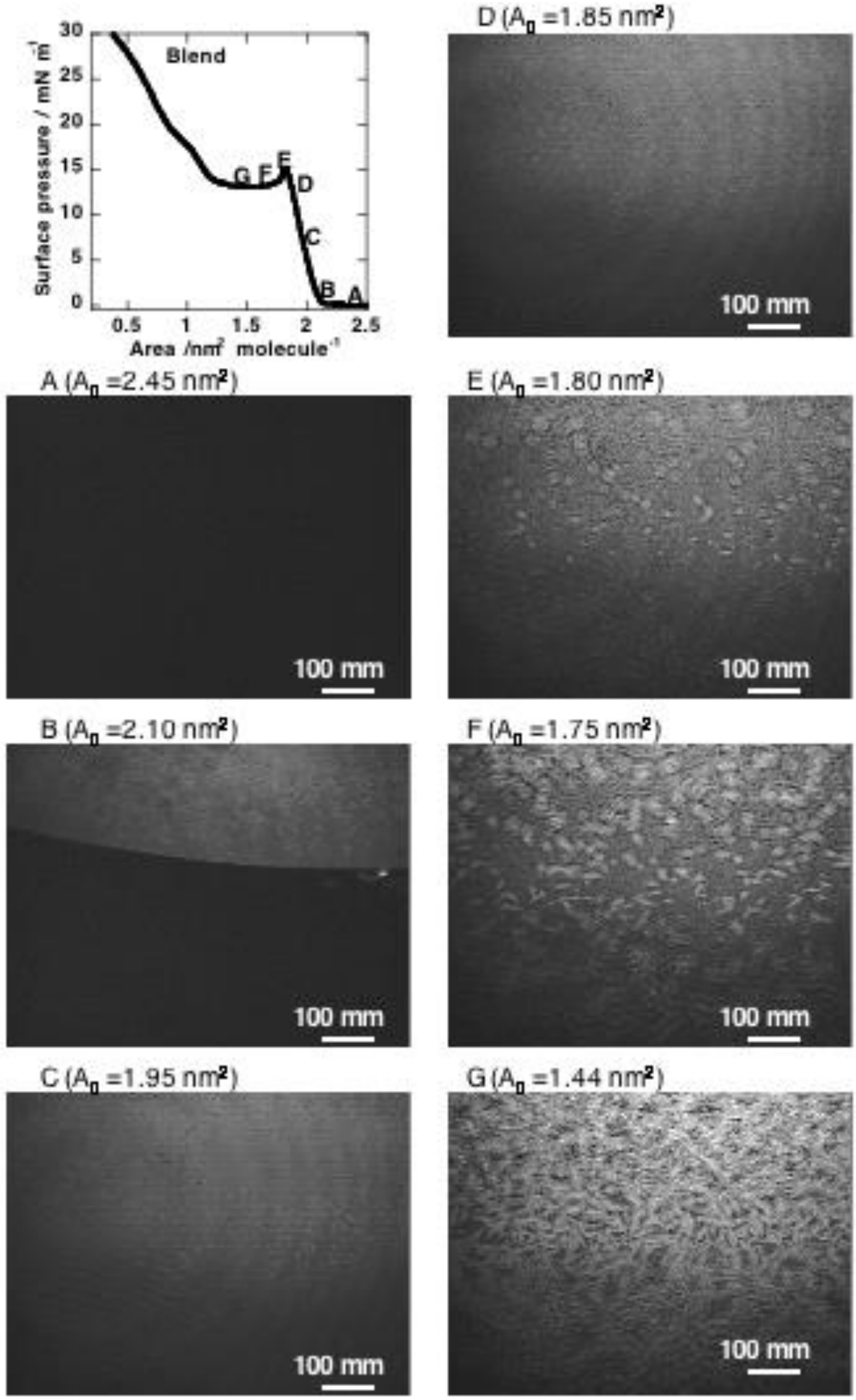

Figure 4.8. BAM images of the 1:1 mixture for different areas (*A*). Letters on the π–A isotherm correspond to the A values where the BAM images were taken. Actual surface areas are shown in parentheses above the images.

4.4.3. Morphological Studies of the Mixed LB Film

The mixed monolayer was deposited onto a solid substrate at 10 mN m^{-1} and 8°C by the LB technique. The transfer ratio of upward deposition was almost unity, but it was almost 0 in downward deposition (Z-type film). The morphological properties of the mixed films with one, two, and four layers deposited onto a hydrophilic silicon substrate were characterized using AFM (Figure 4.9). The AFM images respectively show a smooth and uniform surface with RMS values of 0.51 for the one-layer film and 0.21 for the two-layer film (Figure 9a,b). However, the four-layer film showed several dots whose heights were a few tens of nanometers (Figure 4.9c,d). Considering the monolayer structure portrayed schematically in Figure 7b, the weak van der Waals interaction among the DDSQ cores is the only positive force for building up the layers. 4DEG-DDSQ LB film forms a similar dotlike structure when the interlayer interaction is weak. The dotlike structure is formed by dewetting of the water absorbed during the transfer process. Therefore, it can be said that dewetting of absorbed water disrupted the layer structure in the multilayer film.

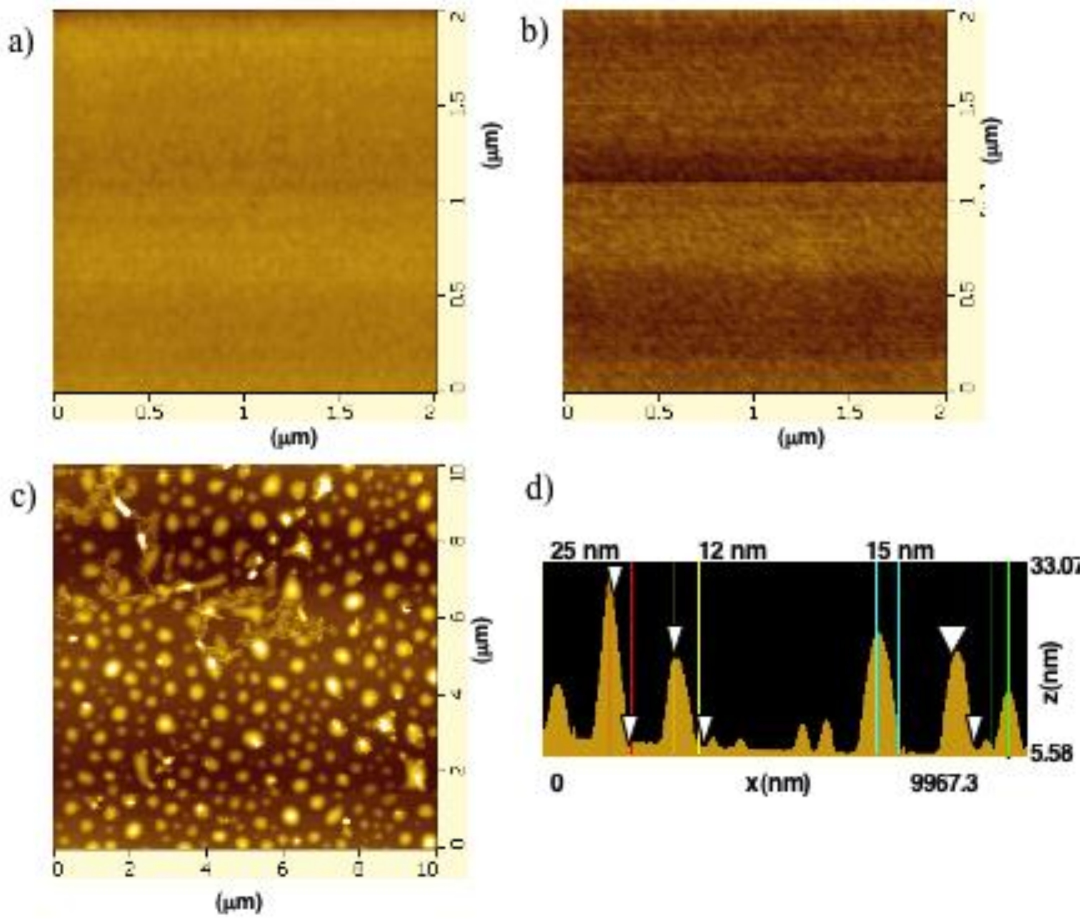

Figure 4.9. AFM images of mixed LB film deposited onto a hydrophilic silicon substrate at π = 10 mN m^{-1}(a) one layer, (b) two layers, and (c) four layers. (d) Cross-sectional profile of the dots for the mixed film with four layers on a hydrophilic substrate.

The surface composition of the deposited film was analyzed using X-ray photoelectron spectroscopy (XPS). The XPS spectrum shows peaks at 534, 400, 288, 155, and 102 eV, which respectively indicate the presence of oxygen (1s), nitrogen (1s), carbon (1s), silicon (2s), and silicon (1s) (Figure 4.10). The composition of the transferred film is discussed by comparing the atomic concentration ratio of [C] and [N]. The observed atomic concentration ratio of [N]/[C] is 1.21×10^{-2}, which is close to the theoretical value (1.54×10^{-2}). This agreement suggests that the transferred film was almost composed of 1:1 mixture of 2DEG-DDSQ and 2DEG-NHDDSQ.

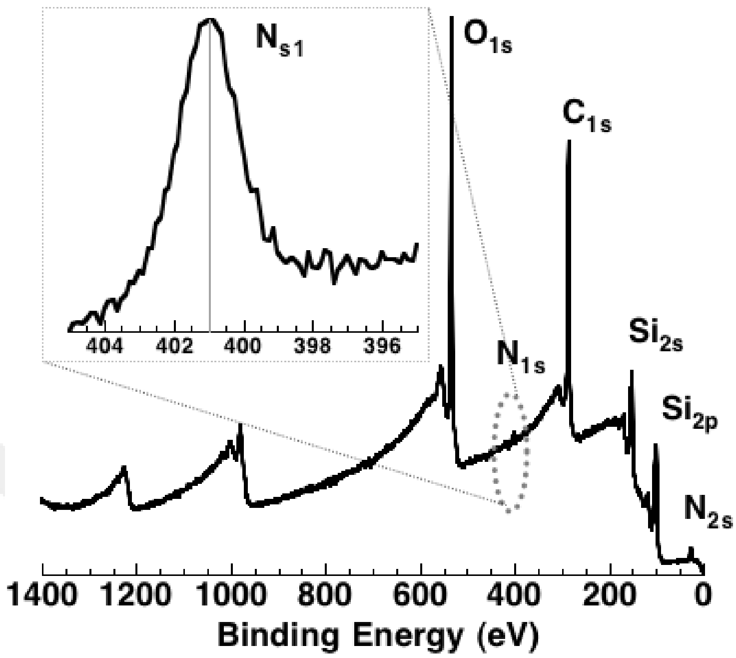

Figure 4.10. XPS spectrum of the mixed LB film.

FT-IR is well established as an analytical technique for functional group analysis and for the study of hydrogen bonding because mid-infrared spectral changes in band intensity and frequency shifts are known to reflect the presence and strength of hydrogen bonds.[25] Hydrogen bonding structure of 2DEGNH-DDSQ was established using FT-IR spectrophotometer methodology. Pure DDSQ monolayers did not form multilayer films. Therefore, cast films of the amphiphilic DDSQs and their 1:1 mixture were prepared.

Peaks related to carbonyl, N–H, and OH are well-known to be very sensitive to hydrogen-bonding effects.[27-29] Therefore, the N–H, OH and CO stretching regions were specifically addressed in the following discussion.

Coleman et al. reported that the IR spectrum of an aliphatic polyurethane showed three CO peaks at about 1684, 1699, and 1721 cm^{-1}. They assigned these peaks respectively to ordered and disordered hydrogen-bonded carbonyl groups and to "free" (non-hydrogen-bonded) carbonyl groups. Moreover, they reported that "free" N–H absorbed at 3444 cm^{-1} and that the peak shifted to a shorter wavenumber with increasing hydrogen bond strength. The full width at half-maximum intensity (fwhm) of the peak was proportional to the distribution of the hydrogen bond strength. It became smaller as the distribution narrowed.[28, 29]

The IR spectrum of 2DEGNH-DDSQ shows the CO absorption peak at 1684 cm^{-1} (hydrogen-bonded carbonyl groups) (Figure 4.11, spectrum b) and a sharp NH absorption peak at 3342 cm^{-1} (Figure 4.12, spectrum b) with a small FWHM (30 cm^{-1}). The peak positions and the small fwhm value confirm the formation of the ordered hydrogen bonds between NH and carbonyl groups as schematically shown in Scheme 4.3a. The amphiphilic nature of 2DEGNH-DDSQ as well as the hydrogen bonds further suggest a well-ordered structure. In contrast, the mixed film showed a CO peak at 1722 cm^{-1} ("free" CO) with a shoulder at 1705 cm^{-1} (disordered CO) and no contribution from the ordered hydrogen bonded carbonyl. Moreover, the broad absorption of the NH groups indicated that hydrogen bonding took place in an amorphous environment with a distribution of their length.[27]

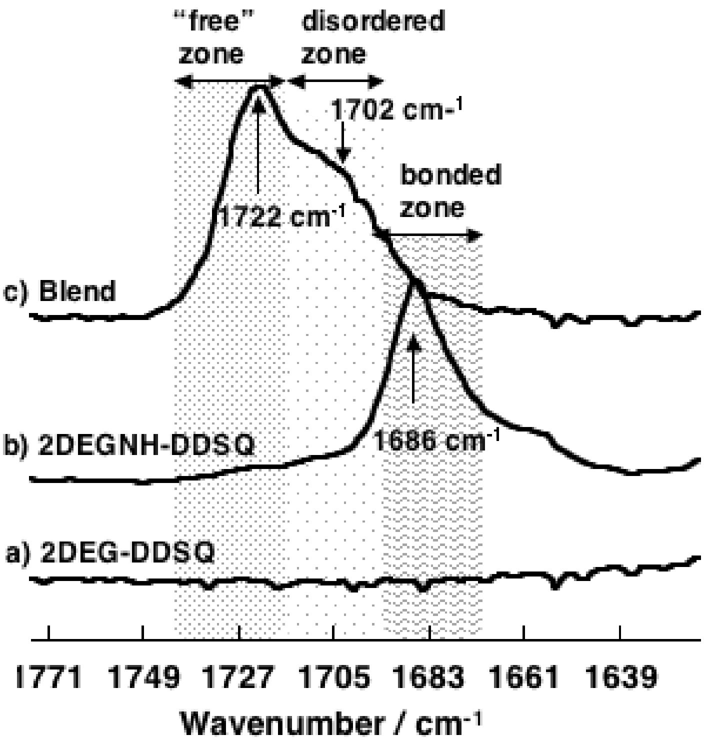

Figure 4.11. FT-IR spectra recorded at room temperature in the 1600–1775 cm^{-1} region for (a) 2DEG-DDSQ, (b) 2DEGNH-DDSQ, and (c) their 1:1 mixture.

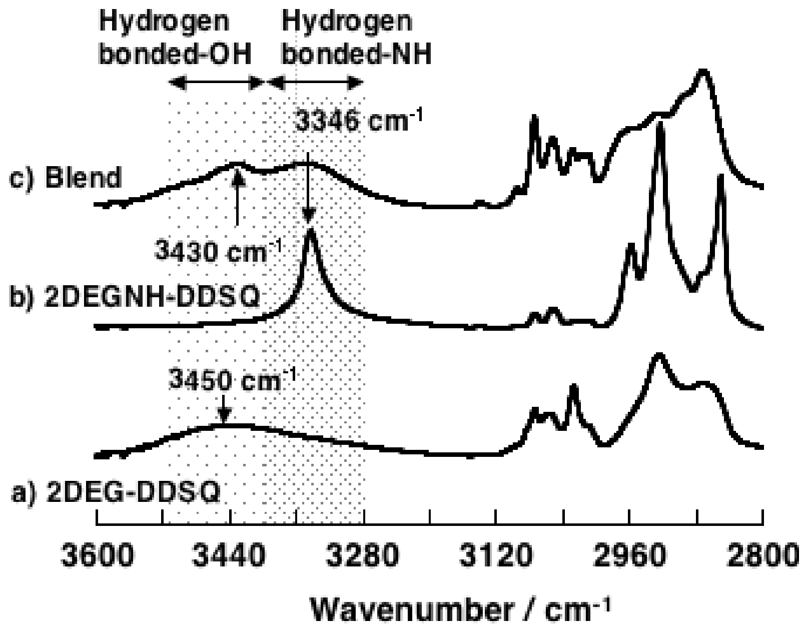

Figure 4.12. FT-IR spectra recorded at room temperature in the 2800–3600 cm^{-1} region for pure (a) 2DEG-DDSQ, (b) 2DEGNH-DDSQ, and (c) their 1:1 mixture.

The hydroxyl groups in 2DEG-DDSQ show broad absorption at 3450 cm^{-1} (Figure 4.12, spectrum a) because of the wide distribution of hydrogen bonding. The peak frequency of this broad band shifts to lower wavenumber (3430 cm^{-1}) (Figure 4.12, spectrum c) in the mixed film, which suggests that the OH groups predominantly form a hydrogen bond with CO, based on previous reports.[30, 31]

The IR peaks of the 1:1 mixed film indicate that 2DEGNH-DDSQ and 2DEG-DDSQ mixed uniformly through hydrogen bonding as schematically shown in Scheme 4.3b. Moreover, transformation of the hydrogen-bonded carbonyl group to "free" and disorder carbonyl groups, and the broadening of NH absorption in the mixed film indicate that the hydrogen bond structure is disordered, which likely produces liquidlike monolayer formation for the 1:1 mixed films.

a)

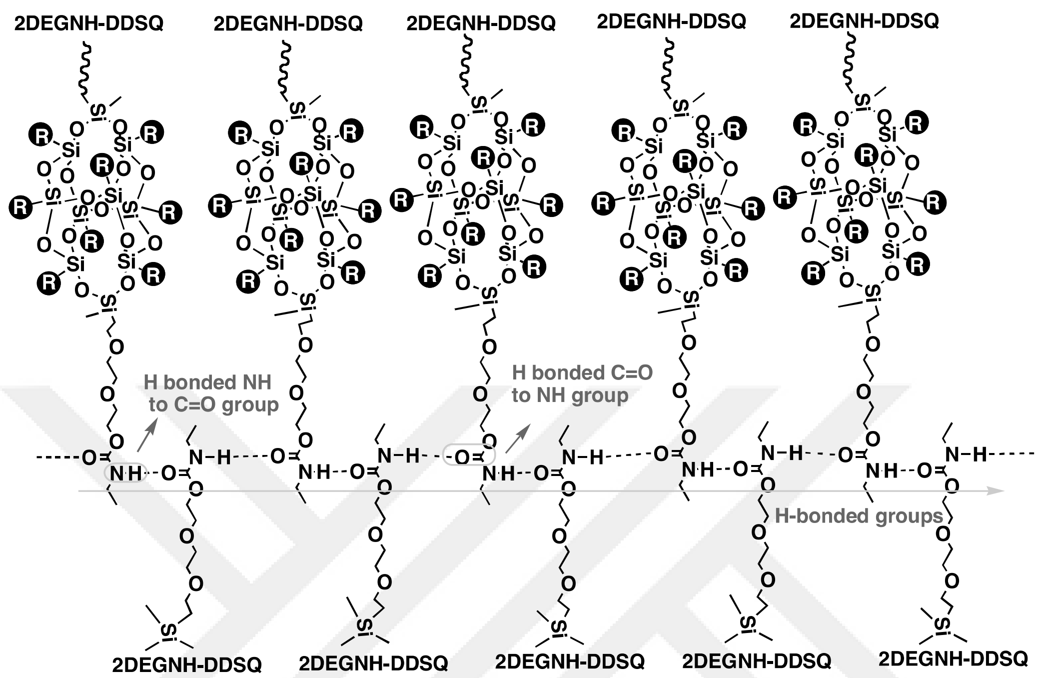

b)

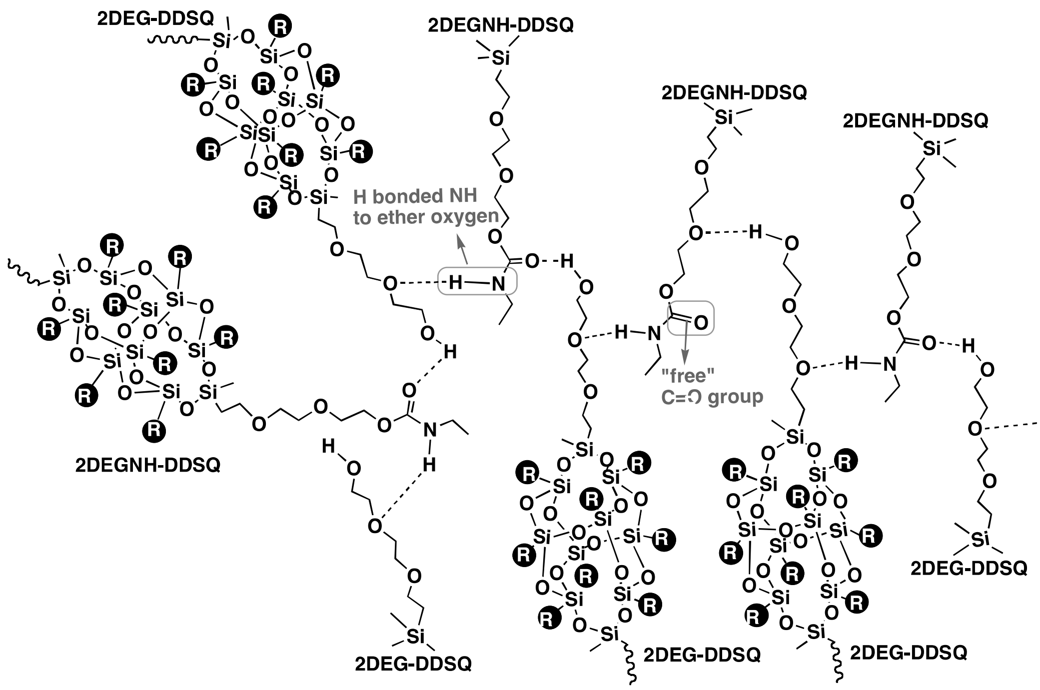

Scheme 4.3. Schematic illustration of film structure in (a) 2DEGNH-DDSQ, and (b) a 1:1 2DEG-DDSQ : 2DEGNH-DDSQ mixed film.

4.4.4. Monolayer Behavior of 4DEGNH-DDSQ at the Air–water Interface

A chloroform solution of amphiphilic DDSQs (1 mM) was spread on a water surface and π–A isotherms of the molecules were measured at 20 °C with a compression rate of 15 cm^2 min^{-1}. In Chapter 2, it has been shown that amphiphilic 4DEG-DDSQ formed a uniform monolayer. Compared to 4DEG-DDSQ (Figure 4.13a), the introduction of amide groups into the end of the DEG units (4DEGNH-DDSQ) engenders adecrease in the collapse pressure and increase in the area of lift-off the surface pressure. A_{limt} was found to be 2.50 nm^2 for 4DEG-DDSQ and 3.03 nm^2 for 4DEGNH-DDSQ. These values are greater than the calculated values of cross-sectional areas of DDSQ core based on the CPK model (Figure 4.13b). On the other hand, the calculated cross-sectional area of 4DEG-DDSQ is 3.96 nm^2 (Figure 4.15b), which is based on a model where DEG units take a fully stretched (all-trans) conformation. This result indicates that the hydrophilic DEG units are partially submerged in the water subphase (Figure 4.13c,d).

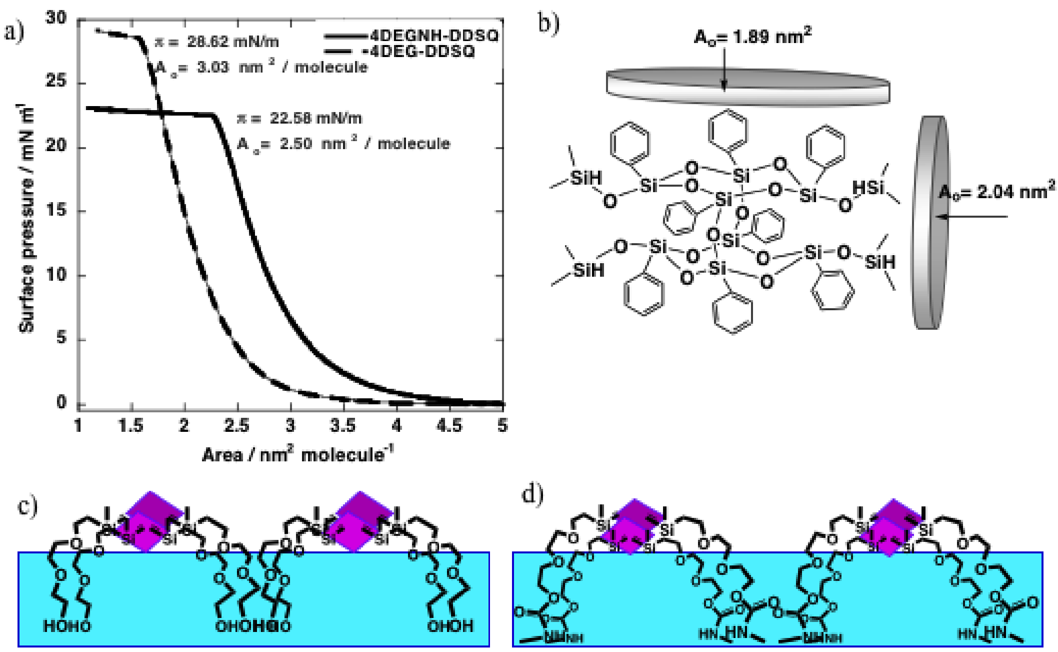

Figure 4.13 (a) Surface pressure (π)–area (A) isotherms for 4DEG-DDSQ (dotted line), and 4DEGNH-DDSQ (dashed line) at 20 °C. (b) Calculated cross-sectional areas of 4H-DDSQ using the CPK model. Schematic illustration of (c) 4DEG-DDSQ and (d) 4DEGNH-DDSQ monolayers at the air–water interface.

Figure 4.14 portrays BAM images of the 4DEGNH-DDSQ monolayers measured at different surface pressures. Although 4DEGNH-DDSQ has urethane groups at the end of the DEG units, no difference in monolayer morphology was observed. 4DEGNH-DDSQ shows a liquid-like monolayer formation similar to 4DEG-DDSQ. Because 4DEGNH-DDSQ with four DEGNH units will maybe diffucult to self assembled to form a rod structure as more DEGNH units attached one DDSQ core in 4DEGNH-DDSQ make the rearrangement of the molecules hard in one direction for 4DEGNH-DDSQ, the morphology of the monolayer is different in 2DEGNH-DDSQ.

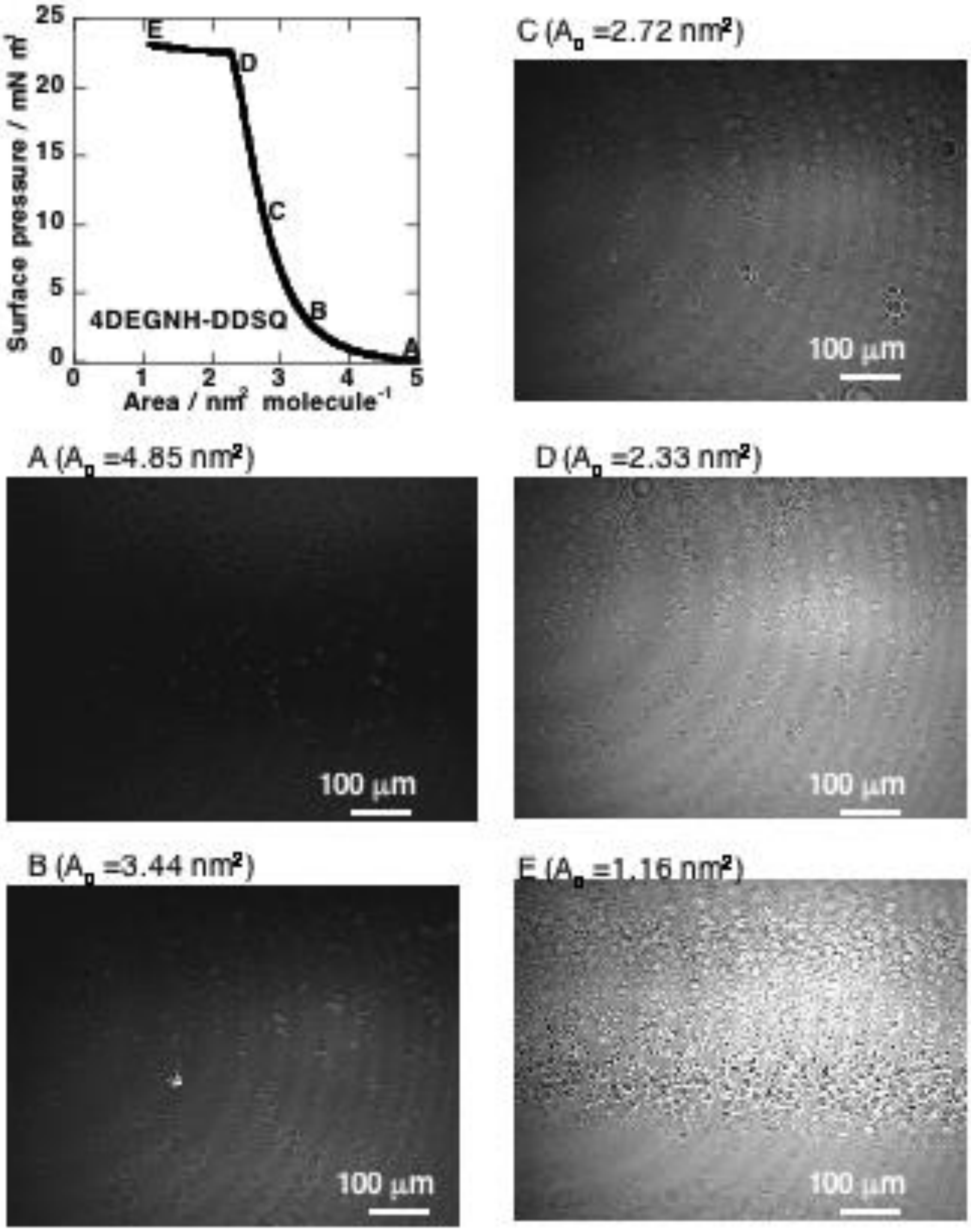

Figure 4.14 BAM images of 4DEGNH-DDSQ for different areas (A). Letters on the π–A isotherm correspond to the A values where the BAM images were taken. Actual surface areas are shown in parentheses above the images.

4.4.5. *Monolayer Behavior of the 1:1 Mixture of 4DEGNH-DDSQ and 4DEG-DDSQ at the Air–water Interface*

4DEGNH-DDSQ and 4DEG-DDSQ is dissolved in a chloroform solution at 1:1 molar ratio and spread onto a water subphase. The π–A isotherm of the mixed film is given in Figure 4.15 together with those of pure 4DEG-DDSQ and 4DEGNH-DDSQ. There is slight increase in A_{limt} (3.20 nm^2) and in the collapse pressure compared to 4DEGNH-DDSQ (Figure 4.15a).

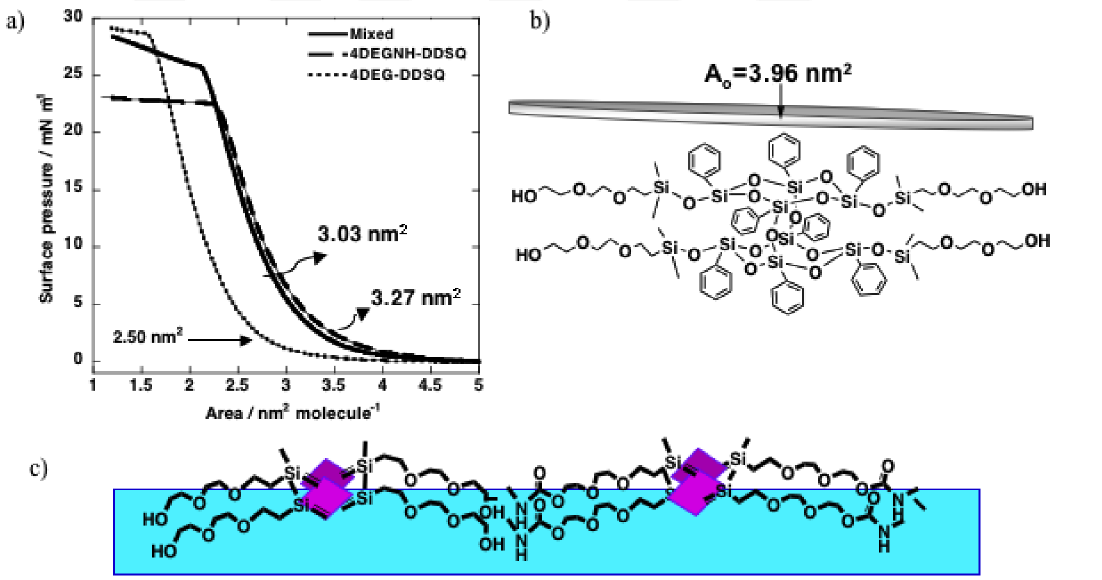

Figure 4.15 (a) Surface pressure (π) – area (A) isotherms for 4DEG-DDSQ (4DEGNH-DDSQ (dashed line), and their 1:1 molar mixture (solid line) at Calculated cross-sectional area of 4DEG-DDSQ using CPK model. (c) Schemati of the mixed monolayer at the air–water interface.

The increase of A_{limt} suggests that 4DEG-DDSQ and 4DEGNH-DDSQ are not phase-separated but they are uniformly mixed. The uniform mixing of the two molecules at the air–water interface was confirmed by BAM measurements (Figure 4.16). At larger surface area, the BAM image showed a gaseous phase (Figure 4.16A). At the area of the lift-off of surface pressure, the mixed monolayer formed a liquid-like monolayer (Figures 4.16B-D). After the monolayer collapses, the aggregation starts to occur (Figure 4.16E). Uniform mixing is induced by hydrogen bonding between the urethane in 4DEGNH-DDSQ and hydroxyl groups in 4DEG-DDSQ. The intermolecular hydrogen bonding between urethane in 4DEGNH-DDSQ and hydroxyl groups in 4DEG-DDSQ reduces the solubility of the coronae into water (Figure 4.15c).

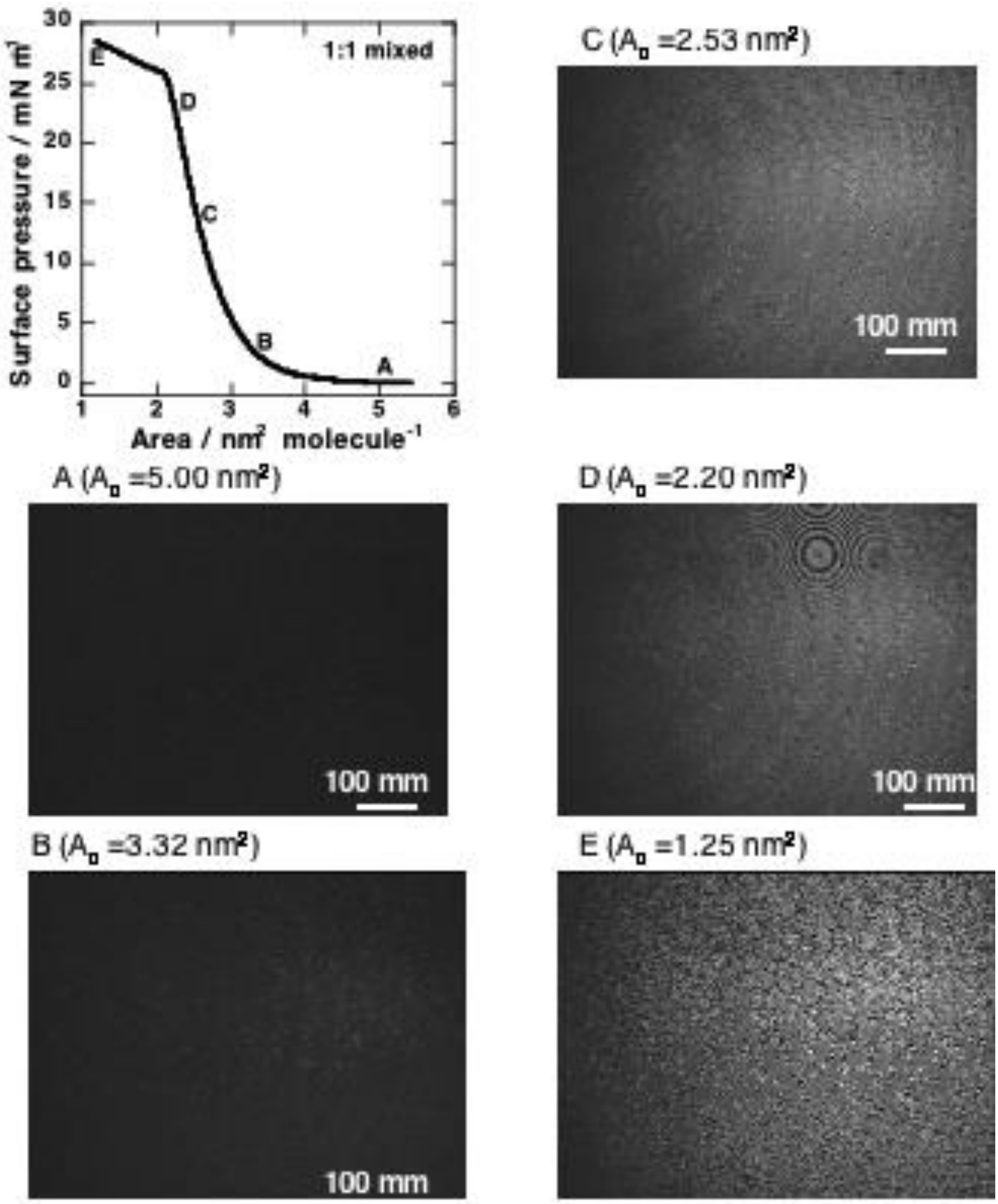

Figure 4.16 BAM images of the 1:1 mixture for different areas (A). Letters on the π–A isotherm denote each BAM image. Letter positions correspond to the A values where the BAM images were taken. Actual surface areas are shown in parentheses.

4.4.6. Morphological Studies of 4DEGNH-DDSQ and the Mixed LB Film

4DEGNH-DDSQ was transferred onto a hydrophilic substrate at 20 mN m^{-1}, and 8°C using LB technique. The transfer ratios of upward and downward depositions were almost unity (Y-type film). The surface morphology of the film was characterized using AFM (Figure 4.17). The AFM image showed smoother and uniform surface with RMS = 0.138 nm than that observed in 4DEG-DDSQ (RMS = 0.24 nm). On the other hand, two and four-layer films of 4DEGNH-DDSQ deposited on a hydrophobic substrate showed dot-like structures as observed before for 4DEG-DDSQ onto the hydrophobic substrate (Figures 4.18 and 4.19). This result can be attributed to the weak interaction between the hydrophobic substrate and DDSQ molecules and also dewetting process as mention in the Chapter 2.

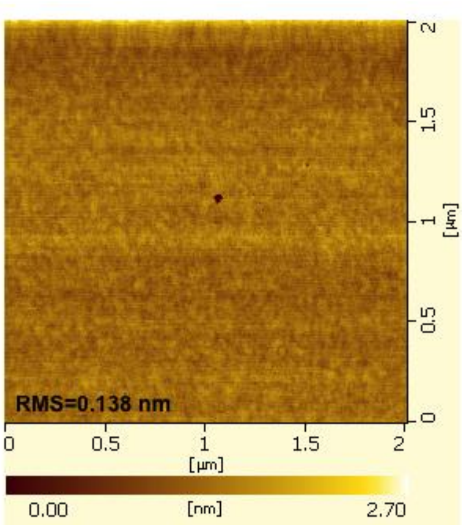

Figure 4.17 AFM images of one layer-4DEGNH-DDSQ LB film deposited onto hydrophilic substrate.

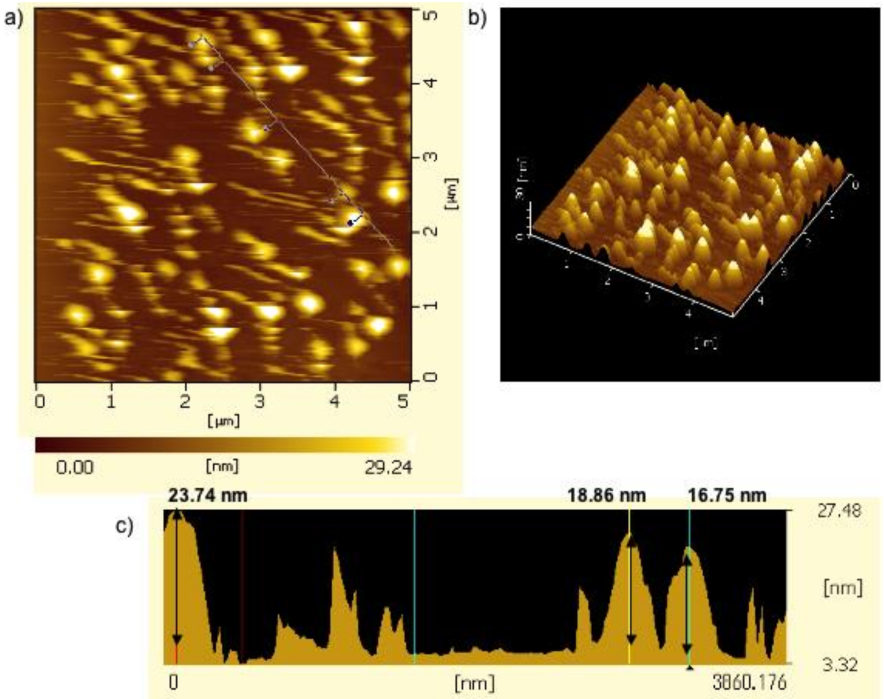

Figure 4.18 AFM images of two layer-4DEGNH-DDSQ LB film deposited onto hydrophobic substrate (a) Top view (b) three dimensional image (c) Cross-sectional profile of the dots.

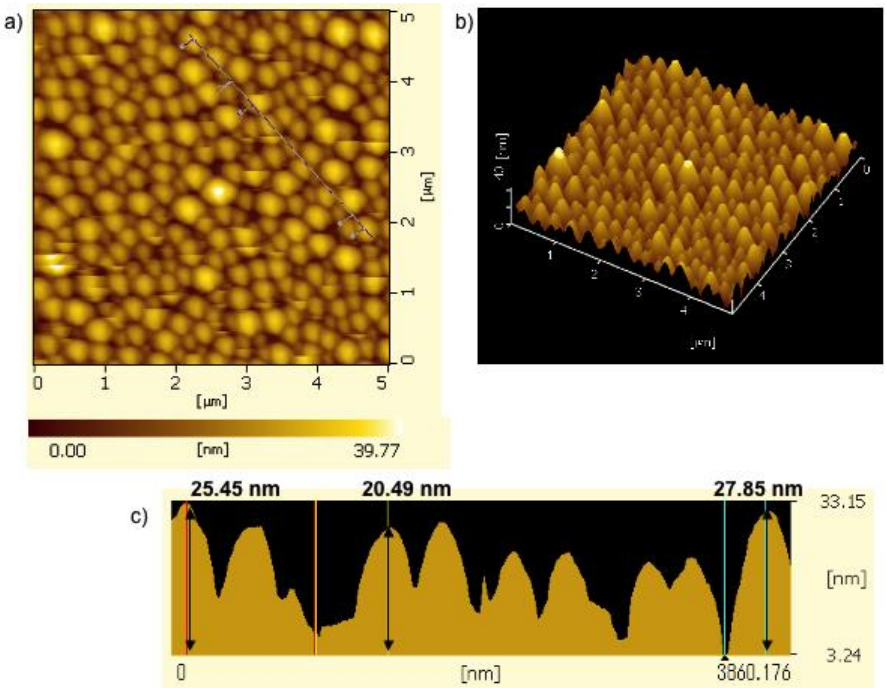

Figure 4.19 AFM images of four layer-4DEGNH-DDSQ LB film deposited onto hydrophobic substrate (a) Top view (b) three dimensional image (c) Cross-sectional profile of the dots

Moreover, to investigate the interaction between the hydroxyl groups in 4DEG-DDSQ and urethane groups in 4DEGNH-DDSQ, the mixed monolayer was deposited onto a solid substrate by the LB technique. The transfer ratios of upward and downward depositions were almost unity (Y-type film). The morphological properties of the mixed films with two layers deposited onto a hydrophobic and 1 layer deposited onto a hydrophilic silicon substrate were characterized using AFM (Figure 4.20). The AFM images respectively showed a dot-like structure onto the hydrophobic silicon substrate (Figure 4.20a) and smooth and uniform surface with RMS values of 0.26 onto the hydrophilic silicon substrate (Figure 4.20b). The heights of the dots are about 6 nm (Figure 4.20c). The mixed film showed a smaller heights and high density of dots compared to that of 4DEG-DDSQ. It can be attributed to the increasing hydrogen-bonding interaction between the urethane in 4DEGNH-DDSQ and hydroxyl groups in 4DEG-DDSQ and packed film formation.

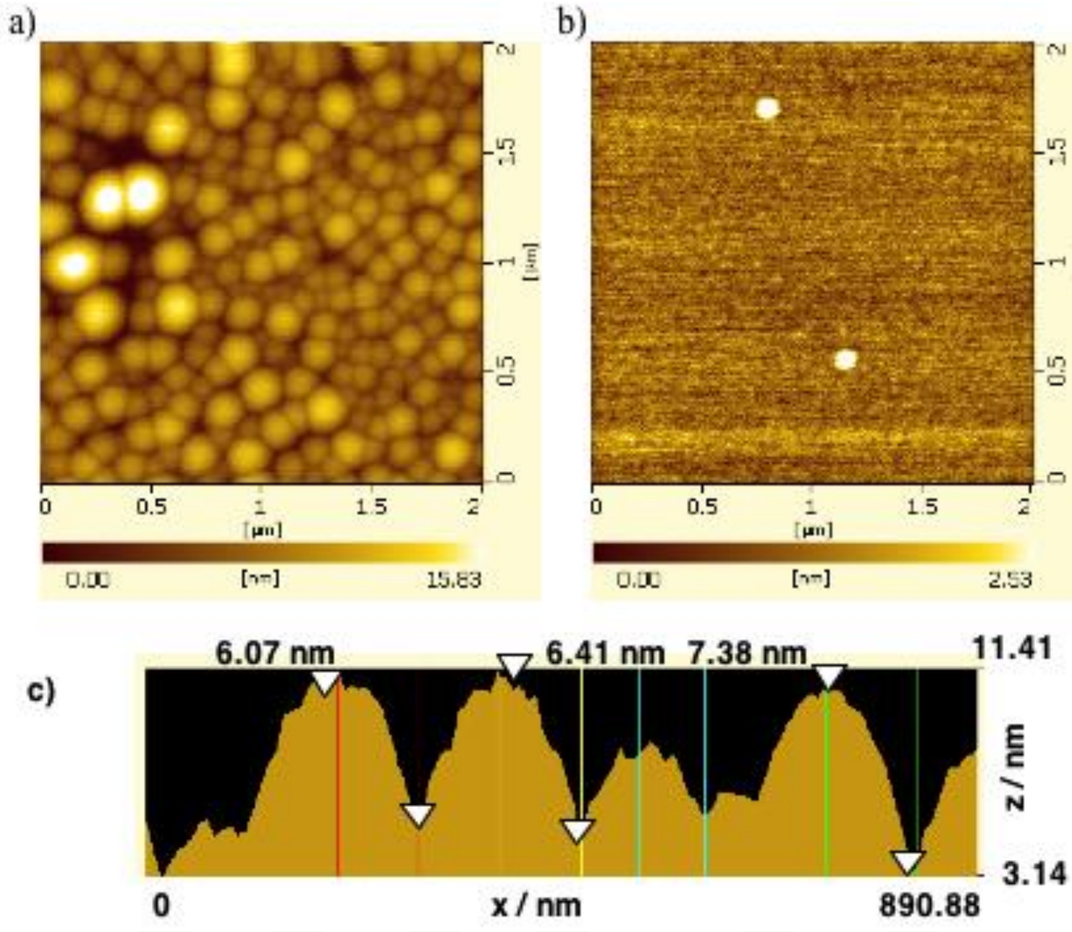

Figure 4.20 AFM images of mixed LB film deposited (a) two layers onto a hydrophobic silicon substrate (b) one layer onto a hydrophilic silicon substrate. (c) Cross-sectional profile of the dots for the mixed film with 2 layers on a hydrophobic substrate.

4.5. Summary

As described in this chapter, a core–corona type amphiphile, 2DEGNH-DDSQ, 4DEGNH-DDSQ, which contain a urethane group at the end of the coronae, were synthesized, and the monolayer properties were examined. The 2DEGNH-DDSQ formed a rodlike assembly at the air–water interface because of the strong hydrogen bond interaction among the urethane groups. The rigid monolayer structure renders the monolayer difficult to deposit onto a solid substrate using the LB technique. To overcome this problem, 2DEGNH-DDSQ was mixed with 2DEG-DDSQ at 1:1 molar ratio. The mixed film formed a uniform liquidlike monolayer at the air–water interface. The IR spectra indicated that the uniform film formation based on the intermolecular hydrogen bonding between the urethane groups of 2DEGNH-DDSQ and the hydroxyl group of 2DEG-DDSQ. The mixed monolayer deposited onto a solid substrate had a uniform surface with RMS= 0.24 nm.

4DEGNH-DDSQ forms liquid-like structure at the air water interface like 4DEG-DDSQ. 4DEGNH-DDSQ did not form rod-like structure because of the hard ordering in one direction. On the other hand, attachment of amide groups in 4DEGNH-DDSQ showed slight difference in film morphology and blending of 4DEGNH-DDSQ with 4DEG-DDSQ showed improvement of the film morphology.

4.5.1. Advantages of DDSQ compared to POSS

Based on the three chapters, Chapter 2, 3 and 4, the advantages of DDSQ compared to POSS can be stated as follows:

Recent studies showed that POSS derivatives that have cage-structures cannot form self-assembled monolayers at the air-water interface,[17] but only partially open-cage type POSS derivatives can.[32, 33] Besides DDSQs have similar features with other POSS members, the structural differences bring additional advantages such as; (i) DDSQ has relatively less reactive groups than conventional POSSs. On the preparation of amphiphilic molecules, having less reactive groups offers easy functionalization in addition to high yield and easy purification. (ii) Having double-decker structure offers less rigidness than cubic-cage POSSs. Too rigid molecules are easy to aggregate and less compatible for monolayer study. (iii) The double-decker–structure of DDSQs enables to prepare "core-coronae" type amphiphiles. Commercial available DDSQ molecules consist of Si-O core with peripheral phenyl groups, which form hydrophobic part. In order to prepare amphiphilic structure, hydrophilic part should be attached to the core using reactive groups. These groups are just in the two edges of the core. Therefore, hydrophilic and hydrophobic parts can take place easily and separately in DDSQ monolayer.

4.6. References

1. Zhu, J.; Eisenberg, A.; Lennox, R. B. *Macromolecules* **1992,** 25, 6547-6555.

2. Zhu, J.; Eisenberg, A.; Lennox, R. B. *Journal of the American Chemical Society* **1991,** 113, 5583-5588.

3. Gabrielli, G.; Puggelli, M.; Faccioli, R. *Journal of Colloid and Interface Science* **1973,** 44, 177-180.

4. Wijekoon, W. M. K. P.; Wijaya, S. K.; Bhawalkar, J. D.; Prasad, P. N.; Penner, T. L.; Armstrong, N. J.; Ezenyilimba, M. C.; Williams, D. J. *Journal of the American Chemical Society* **1996,** 118, 4480-4483.

5. Sackmann, E. *Science* **1996,** 271, 43-48.

6. Lo, M. Y.; Zhen, C. G.; Lauters, M.; Jabbour, G. E.; Sellinger, A. *Journal of the American Chemical Society* **2007,** 129, 5808-+.

7. Lichtenhan, J. D. *Comments on Inorganic Chemistry* **1995,** 17, 115-130.

8. Gonzalez, R. I.; Phillips, S. H.; Hoflund, G. B. *Journal of Spacecraft and Rockets* **2000,** 37, 463-467.

9. Leu, C.-M.; Chang, Y.-T.; Wei, K.-H. *Macromolecules* **2003,** 36, 9122-9127.

10. Leu, C.-M.; Chang, Y.-T.; Wei, K.-H. *Chemistry of Materials* **2003,** 15, 3721-3727.

11. Mantz, R. A.; Jones, P. F.; Chaffee, K. P.; Lichtenhan, J. D.; Gilman, J. W.; Ismail, I. M. K.; Burmeister, M. J. *Chemistry of Materials* **1996,** 8, 1250-1259.

12. Cassagneau, T.; Caruso, F. *Journal of the American Chemical Society* **2002,** 124, 8172-8180.

13. Wu, G. J.; Su, Z. H. *Chemistry of Materials* **2006,** 18, 3726-3732.

14. Nicholson, K. T.; Zhang, K.; Banaszak Holl, M. M.; McFeely, F. R.; Calzaferri, G.; Pernisz, U. C. *Langmuir* **2001,** 17, 7879-7885.

15. Owens, T. M.; Nicholson, K. T.; Fosnacht, D. R.; Orr, B. G.; Banaszak Holl, M. M. *Langmuir* **2006,** 22, 9619-9622.

16. Deng, J. J.; Hottle, J. R.; Polidan, J. T.; Kim, H. J.; Farmer-Creely, C. E.; Viers, B. D.; Esker, A. R. *Langmuir* **2004,** 20, 109-115.

17. Deng, J. J.; Polidan, J. T.; Hottle, J. R.; Farmer-Creely, C. E.; Viers, B. D.; Esker, A. R. *Journal of the American Chemical Society* **2002,** 124, 15194-15195.

18. Deng, J. J.; Viers, B. D.; Esker, A. R.; Anseth, J. W.; Fuller, G. G. *Langmuir* **2005,** 21, 2375-2385.

19. Deng, J. J.; Farmer-Creely, C. E.; Viers, B. D.; Esker, A. R. *Langmuir* **2004,** 20, 2527-2530.

20. Yin, W.; Deng, J.; Esker, A. R. *Langmuir* **2009,** 25, 7181-7184.

21. Hottle, J. R.; Kim, H.-J.; Deng, J.; Farmer-Creely, C. E.; Viers, B. D.; Esker, A. R. *Macromolecules* **2004,** 37, 4900-4908.

22. Hottle, J. R.; Deng, J.; Kim, H.-J.; Farmer-Creely, C. E.; Viers, B. D.; Esker, A. R. *Langmuir* **2005,** 21, 2250-2259.

23. Kim, H.-J.; Deng, J.; Hoyt Lalli, J.; Riffle, J. S.; Viers, B. D.; Esker, A. R. *Langmuir* **2005,** 21, 1908-1916.

24. Kucuk, A. C.; Matsui, J.; Miyashita, T. *Journal of Colloid and Interface Science* **2011,** 355, 106-114.

25. Mishra, A. K.; Chattopadhyay, D. K.; Sreedhar, B.; Raju, K. V. S. N. *Progress in Organic Coatings* **2006,** 55, 231-243.

26. Corti, M.; Minero, C.; Degiorgio, V. *Journal of Physical Chemistry* **1984,** 88, 309-317.

27. Christenson, C. P.; Harthcock, M. A.; Meadows, M. D.; Spell, H. L.; Howard, W. L.; Creswick, M. W.; Guerra, R. E.; Turner, R. B. *Journal of Polymer Science, Part B: Polymer Physics* **1986,** 24, 1401-1439.

28. Coleman, M. M.; Lee, K. H.; Skrovanek, D. J.; Painter, P. C. *Macromolecules* **1986,** 19, 2149-2157.

29. Coleman, M. M.; Skrovanek, D. J.; Hu, J.; Painter, P. C. *Macromolecules* **1988,** 21, 59-65.

30. Kuo, S. W.; Chang, F. C. *Macromolecules* **2001,** 34, 5224-5228.

31. Kuo, S. W.; Chang, F. C. *Macromolecules* **2001,** 34, 4089-4097.

32. Ferguson-McPherson, M. K.; Low, E. R.; Esker, A. R.; Morris, J. R. *The Journal of Physical Chemistry B* **2005,** 109, 18914-18920.

33. Deng, J.; Hottle, J. R.; Polidan, J. T.; Kim, H.-J.; Farmer-Creely, C. E.; Viers, B. D.; Esker, A. R. *Langmuir* **2003,** 20, 109-115.

5. CHAPTER 5: Proton Conducting Behavior of Amphiphilic DDSQ Containing Covalently Bonded Phosphonic Acid Groups at the End of the DEG Units

5.1. Introduction

Recently, polymer electrolyte fuel cells with proton-conductive polymers used as solid electrolytes have been an active area of research because of their wide applications in vehicles, portable electric devices, and so on. Proton-conductive polymer electrolytes used in fuel cell applications are most often perfluorosulfonic acid polymers such as Nafion®. However, production of fluorinated polymers is expensive and they are environmentally inadaptable. Therefore, many studies have examined non-fluorinated polymers such as poly(arylene ether sulfone)s,[1-4] poly(arylene ether ketone)s,[2, 3, 5-7] polyimides,[2, 8] and others[2, 9-13] for use as a base skeleton for sulfonated polymer synthesis. Moreover, the high proton conductivity of Nafion® depends strictly on the presence of water, and its operations are limited to temperatures below 100 ˚C in a wet medium.[14, 15] Fuel cell systems that can be operated at intermediate temperatures (100-200 ˚C) under low or non-humid conditions might enable high power–generation efficiency, lower cost, simpler heat management, and better tolerance of catalysts against poisoning.[16] Therefore, these benefits have spurred studies to identify and develop a proton-conducting material that can conduct protons efficiently in widely various operation conditions without loss of performance over time.

Regarding intermediate temperature fuel cells, the systems[17-21] containing amphoteric liquids such as imidazole,[22, 23] pyrazole,[23] and sulfuric or phosphoric acid have been used as proton conductive sources instead of water because of their higher boiling temperature. Initially, these molecules were doped in basic[24-26] or acid polymer[27] and dopand leakage occurring at lower temperatures caused difficulties. Subsequently, several groups reported covalent bonding of amphoteric groups to polymers.[28-31] In the covalent bonded polymer electrolyte, amphoteric molecules mainly transport protons through rapid hydrogen bond breaking and forming processes through intrinsic structure diffusion.[29] To facilitate structural diffusion to attain high conductivities, hydrophilic poly(ethylene oxide) (PEO) units have been incorporated onto a polymer backbone. For example, PEO–terminated imidazole-based proton–conductors show that conductivity depends on the motion of structural defects of the hydrogen-bond system. [32-34] Armand and coworkers reported that proton conductivity of phosphoric–acid–doped PEO film increases concomitantly with increasing segmental motions of PEO chains.[35]

POSSs are organic-inorganic hybrid materials composed of an inorganic $SiO_{1.5}$ core with organic coronae. The $SiO_{1.5}$ provides good thermal and mechanical stability, whereas organic coronae provide compatibility with polymer materials. Therefore it has been used as a nanofiller to improve the thermal and structural stability of polymer electrolytes.[36-38] For example, Choudhury et al.[39] incorporated sulfonated POSS into Nafion® using layer-by-layer technique. They reported that incorporation of sulfonated POSS into Nafion® not only improves thermal and mechanical properties; it also increases proton conductivity in non-humid conditions. They also reported that addition of POSS as a filler in sulfonated poly(ether ether ketone) (SPEEK) engendered a three-fold increase in proton–conductivity.[37] However, a direct application of sulfonated POSS as a proton–conductive film is rare because of the high crystallinity of POSS. [40]

Chapter 5 describes a proton-conductive film based on double-decker-shaped silsesquioxane (DDSQ). In the Chapter 2 and 4, it is reported that new "core-coronae" type hybrid amphiphiles using DDSQs as a hydrophobic core and DEG units as hydrophilic coronae were synthesized.[41] For the present study, phosphonic acid was bonded covalently to DDSQ with two or four DEG (2DEG-DDSQ, 4DEG-DDSQ) to synthesize hybrid proton–conductive materials. The obtained compounds (2PHOS-DDSQ and PHOS-DDSQ) were characterized using ^{1}H, ^{31}P NMR, FT-IR and MALDI-TOF MS spectrometry. It is found that PHOS-DDSQ is stable against to the water, whereas 2PHOS-DDSQ is not. PHOS-DDSQ formed an amorphous film by drop casting. Then the proton conductivities of the cast film under humid and non-humid conditions were studied using impedance spectra measurements. Results show that the synthesized material (PHOS-DDSQ) exhibits proton conductivity of 0.12 S cm^{-1}, which is as high as Nafion®[36] in humid conditions, as well as maximum conductivity of 3.6×10^{-4} S cm^{-1} in non-humid conditions.

5.2. *Experimental Section*

5.2.1. *Materials.*

Double-decker-shaped silsesquioxanes containing four SiH groups (4H-DDSQ) are kindly donated by Chisso Corp. Anhydrous tetrahydrofuran (THF) and toluene are purchased respectively from Aldrich and Nacalai Tesque, Inc. They were used without further purification. Platinum divinyltetramethyldisiloxane (Pt(dvs), 3 wt% in xylene solution) is obtained from Umicore. Dichloromethane, chloroform and acetone are purchased from Kanto Chemical Co. Inc. and distilled before use. Spectroscopic grade chloroform (Dojindo Laboratories) was used as a casting solvent. $POCl_3$ and pyridine are purchased from Aldrich Chemical Co. and used as received.

5.2.2. *Instrumental Analysis.*

^{1}H and ^{31}P NMR measurements were conducted using a spectrometer (JNM-AL 400; JEOL). Thermogravimetric analysis (TGA) was performed under nitrogen at a heating rate of 10°C min^{-1} using a Shimadzu TGA-50H. Transition and melting temperatures were measured using a differential scanning calorimetric (DSC-2C; Perkin-Elmer Inc., Norwalk, CT) under nitrogen flow (20 mL/min) with a heating rate of 10 ˚C/min. All samples were first heated from 0 to 200 °C (first scan) and held for 2-3 min to erase the thermal history. Then they were quenched to -50 °C (second scan), and finally heated to 200 °C (third scan). Atomic force microscopy (SPA400; Seiko Instruments Inc.) was used to characterize the surface morphology. A silicon cantilever (14 nN m^{-1} and 132 kHz, Si-DFM20; Seiko Instruments Inc.) was used. Images were taken using the non-contact mode. All measurements were conducted at room temperature. Glass substrates were washed with chloroform and acetone and dried with flowing nitrogen. Electrodes were deposited onto the substrate using thermal deposition of Cr/Au with a metal mask onto the glass substrate. Two electrode elements that are 0.5 mm wide and 1 mm long are separated from each other by 50 μm. PHOS-DDSQ/chloroform solution (1 wt%) was drop cast onto the glass substrate to form a film. In–plane proton conductivity (σ) of the cast films was measured using electrochemical impendence spectroscopy (EIS). Impedance measurements of the polymer were conducted using impedance analyzers (1260 Impedance/Gain-Phase Analyzer with a 1296 Dielectric Interface system; Solartron Analytical) over the frequency range of 1–10^6 Hz at ac amplitude of 10 mV. Proton–conductivity measurements under different temperature and humidity conditions were taken using a climate chamber (LHU-113; Espec Corp.). The sample was put in the chamber with defined humidity at 35 °C for 2 h. Then temperature was varied from 35 to 85 °C at 10 °C intervals. Conductivity was measured 15–20 min after the temperature reached the set point. The proton conductivity measurements in non-humid conditions were carried out in an oven (Vacuum oven vos-201SD, EYELA) heated from 100 to 190 °C. Samples were initially kept initially at 100 °h for at least 1 h to dry the film. The conductivity was calculated using equation (1),

$$\sigma = L / R \times T \times W \qquad (1)$$

where L (50 μm) signifies the distance between two electrodes, W denotes the length of the electrode (1 mm), T stands for the PHOS-DDSQ film thickness (1 μm) (Figure 5.1), and R represents the film resistance determined from AC impedance spectra, respectively. Film thickness was determined using a laser scanning microscope (VK-9700; Keyence Co.).

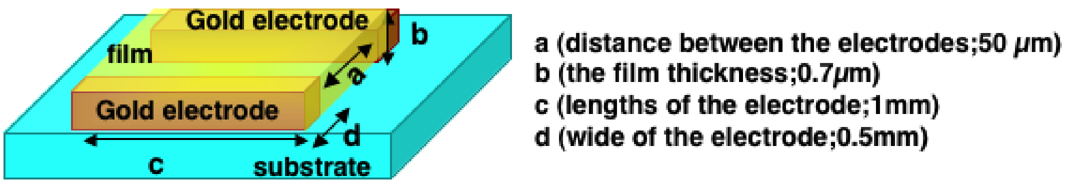

Figure 5.1 Prepared electrode for the proton conductivity measurement

5.3. Synthesis and Characterization

5.3.1. Functionalization of Di(ethylene glycol) Units of 2DEG-DDSQ with Phosphoric Acid (2PHOS-DDSQ).

2DEG-DDSQ (2 g, 1.41 mmol) was dissolved in pyridine (10 ml) under nitrogen atmosphere. To the solution was added $POCl_3$ (2.63 ml, 28.20 mmol) at 0 ^oC and then the mixture was stirred at 45 ^oC for 24 h. The reaction mixture was cooled to rt, H_2O (1 ml) was added and then the suspension was stirred at rt for 6 h. After 6 h, the mixture was extracted with CH_2Cl_2 (x3). The combined organic layers were dried over Na_2SO_4, filtered and then concentrated. 2PHOS-DDSQ was obtained in 60% yield as yellowish viscose (Scheme 5.1).

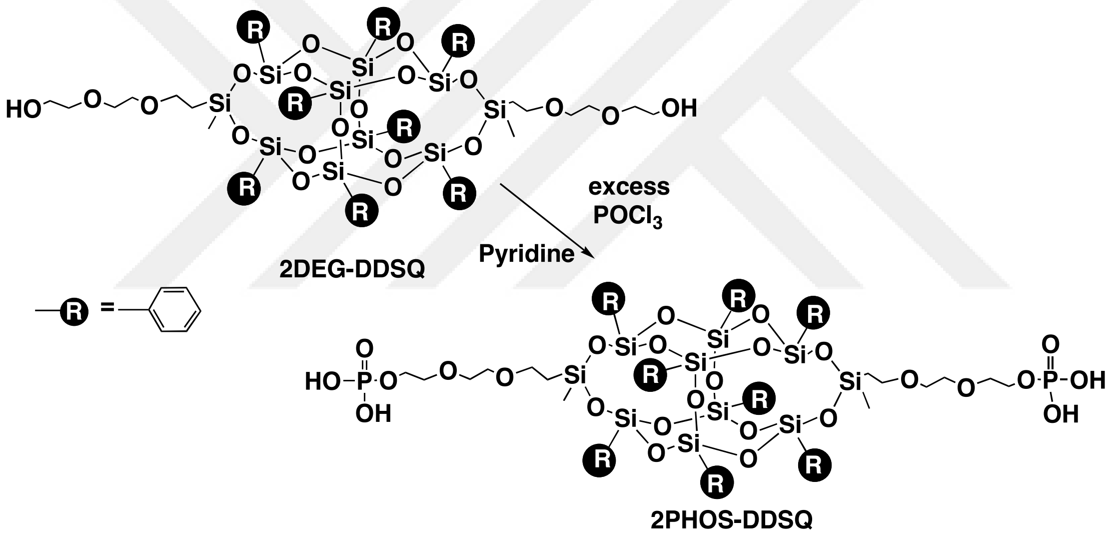

Scheme 5.1 Synthesis of 2PHOS-DDSQ.

5.3.2. FT-IR Spectrum of 2PHOS-DDSQ

The FT-IR spectrum of 2PHOS-DDSQ shows wide absorption peak centered at 3430 cm^{-1} comparing to the spectrum of the 2DEG-DDSQ due to the wide distributions of the hydrogen-bonded OH groups. On the other hand, Si-O-Si stretching of DDSQ core appears in each spectrum, suggesting that that DDSQ core remained unchanged during the synthesis (Figure 5.2). [FTIR (cm^{-1}), ν =3430 - 3230 (broad, free and hydrogen bonded O-H), ν =2974, 2935, 2879 (aliphatic C-H), ν =1256 (CH_2-O), ν =1098 (Si-O)].

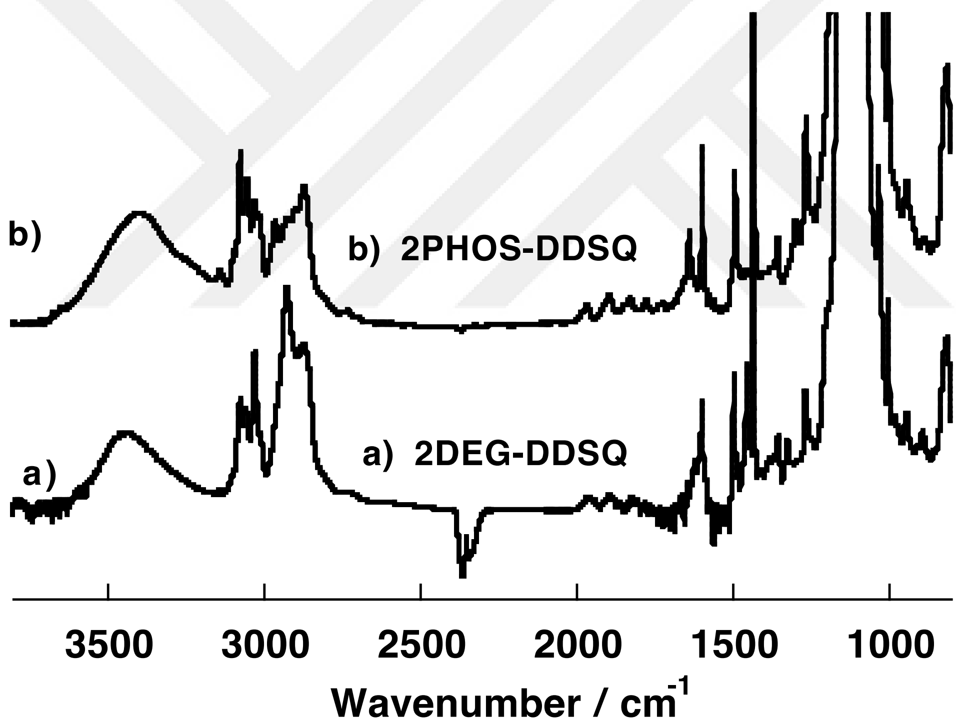

Figure 5.2 FT-IR spectra of a) 2DEG-DDSQ, b) 2PHOS-DDSQ

5.3.3. **^{1}H NMR Spectrum of 2PHOS-DDSQ**

^{1}H NMR spectra were taken in $CDCl_3$ solvent (Figure 5.3). The ^{1}H NMR spectrum of 2PHOS-DDSQ shows just shifting of methyl protons to a higher magnetic filed. [^{1}H NMR (ppm) (400 MHz, $CDCl_3$, $CHCl_3$ ref) 7.25-7.60 (m, 40H, Ph), 3.41-3.57 (t, 20H CH_2-O), 1.17 (t, 4H, CH_2-Si), 0.30 (s, 6H, $Si(CH_3)$)].

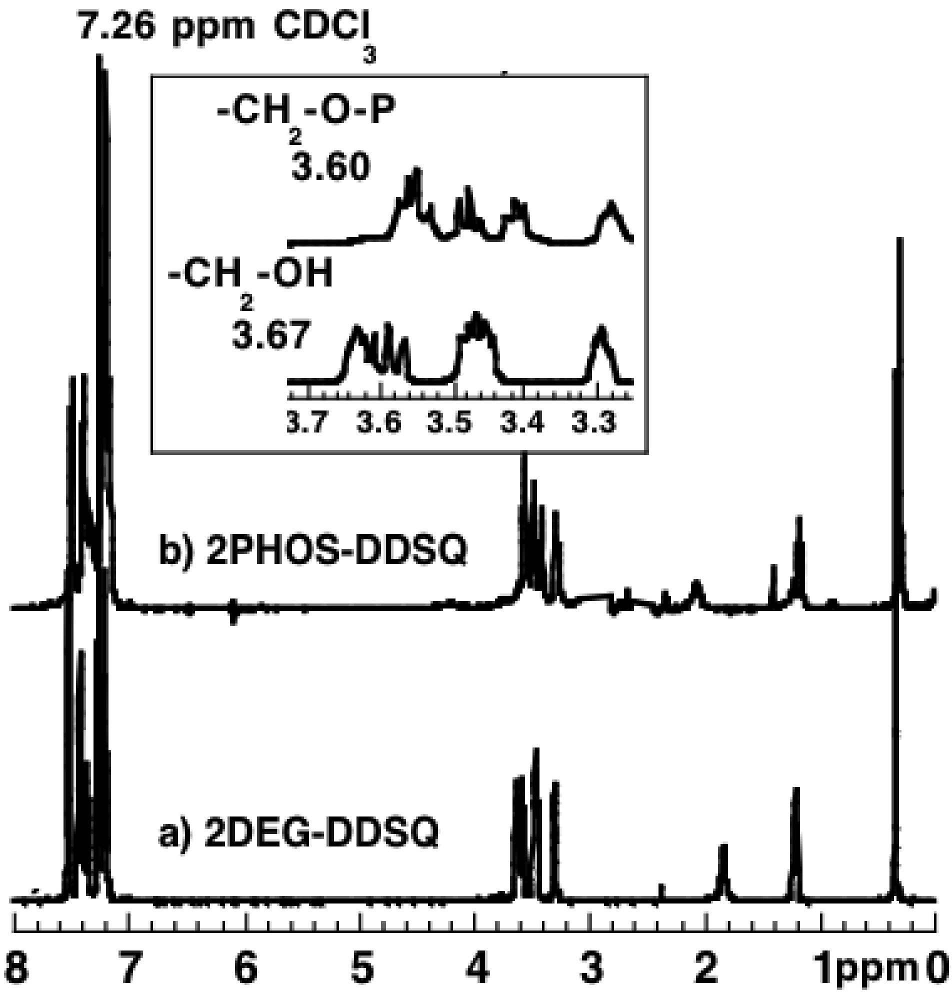

Figure 5.3 ^{1}H NMR of (a) 2DEG-DDSQ, (b) 2PHOS-DDSQ in $CDCl_3$.

5.3.4. ^{31}P NMR Spectrum of 2PHOS-DDSQ

Figure 5.4 shows the ^{31}P NMR spectra of 2PHOS-DDSQ taken in CDC3. After 2nd time washing of 2PHOS-DDSQ with water, the peak of phosphor atom at 5.6 ppm disappeared. This result shows that ester bond in 2PHOS-DDSQ was hydrolyzed by several treatments with water. [^{31}P NMR (ppm), (161.9 MHz, 85 % H_3PO_4 ref), 5.6 (CH_2O-*P*O-$(OH)_2$)].

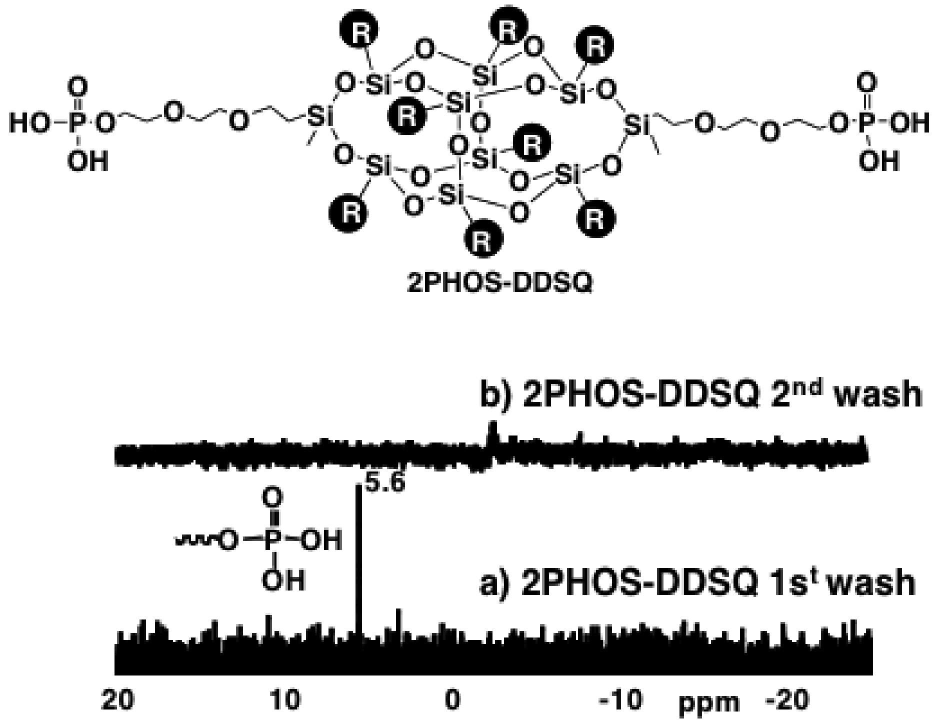

Figure 5.4 ^{31}P NMR of 2PHOS-DDSQ in $CDCl_3$ after (a) 1st washing, (b) 2nd washing with water.

5.3.5. Functionalization of Di(ethylene glycol) Units of 4DEG-DDSQ with Phosphoric Acid (PHOS-DDSQ).

4DEG-DDSQ (1 g, 0.54 mmol) was dissolved in pyridine (10 ml) under nitrogen atmosphere. To the solution was added $POCl_3$ (2.02 ml, 21.60 mmol) at 0 °C and then the mixture was stirred at 45 °C for 24 h. The reaction mixture was cooled to rt, H_2O (1 ml) was added and then the suspension was stirred at rt for 6 h. After 6 h, the mixture was extracted with CH_2Cl_2 (x3). The combined organic layers were dried over Na_2SO_4, filtered and then concentrated. 4(DEG-PHOS)-DDSQ was obtained in 70% yield as yellowish viscose (Scheme 5.2).

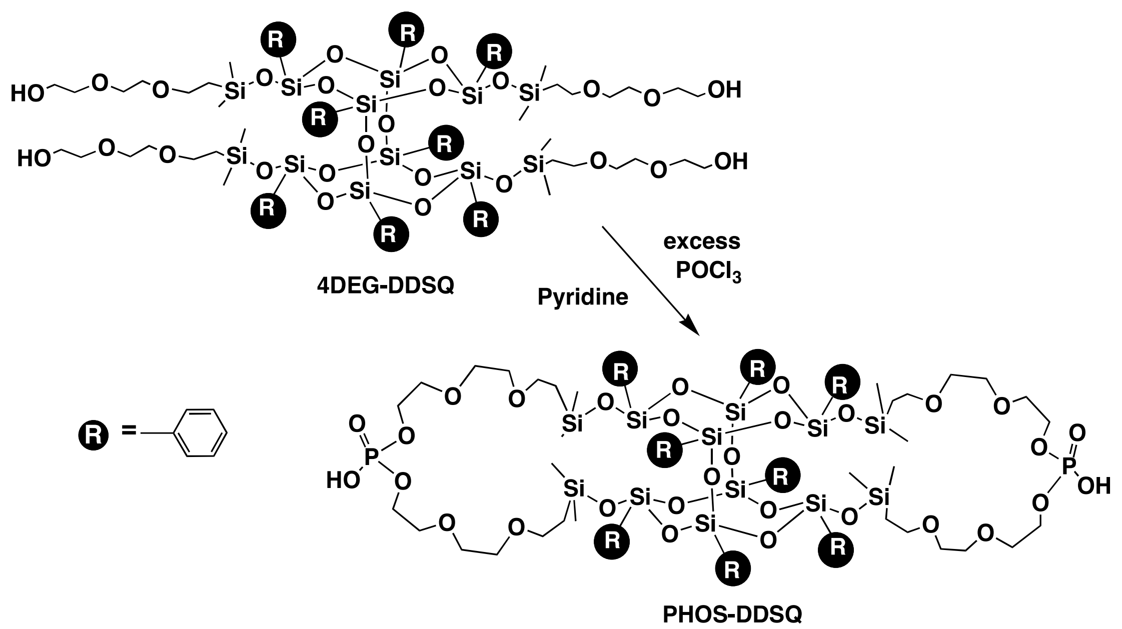

Scheme 5.2. Synthesis of PHOS-DDSQ.

5.3.6. **FT-IR Spectrum of PHOS-DDSQ**

The FT-IR spectrum of PHOS-DDSQ shows OH absorption peak at 3430 cm^{-1} and wide absorption peak centered at 3380 cm^{-1} due to the wide distributions of the hydrogen-bonded OH groups (Figure 5.5). On the other hand, Si-O-Si stretching of DDSQ core appears in each spectrum, suggesting that that DDSQ core remained unchanged during the synthesis. [FT-IR (cm^{-1}), ν =3430 - 3230 (broad, free and hydrogen bonded O-H), n =2958, 2910, 2870 (aliphatic C-H), ν =1253 (P=O), ν =1256 (CH_2-O), ν =1057 (Si-O), ν =1150 (Si-C)].

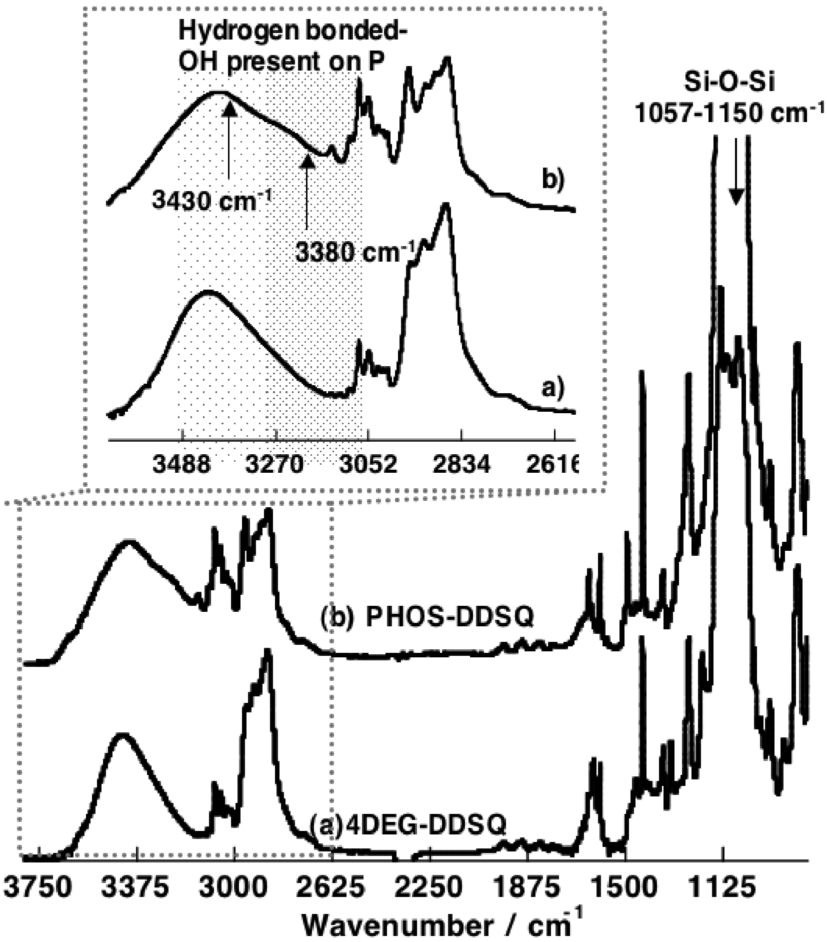

Figure 5.5 FT-IR spectra of a) 4DEG-DDSQ, b) PHOS-DDSQ

5.3.7. ^{1}H NMR Spectrum of PHOS-DDSQ

^{1}H NMR spectra were taken in $CDCl_3$ solvent (Figure 5.6). The ^{1}H NMR spectrum of PHOS-DDSQ shows just shifting of methyl protons to a higher magnetic filed. [^{1}H NMR (ppm), (400 MHz, $CDCl_3$, $CHCl_3$ ref) 7.26-7.76 (40H, Ph), 3.13-3.62 (40H, CH_2-O), 0.90 (8H, CH_2-Si), 0.01 (12H, Si(CH_3)$_2$].

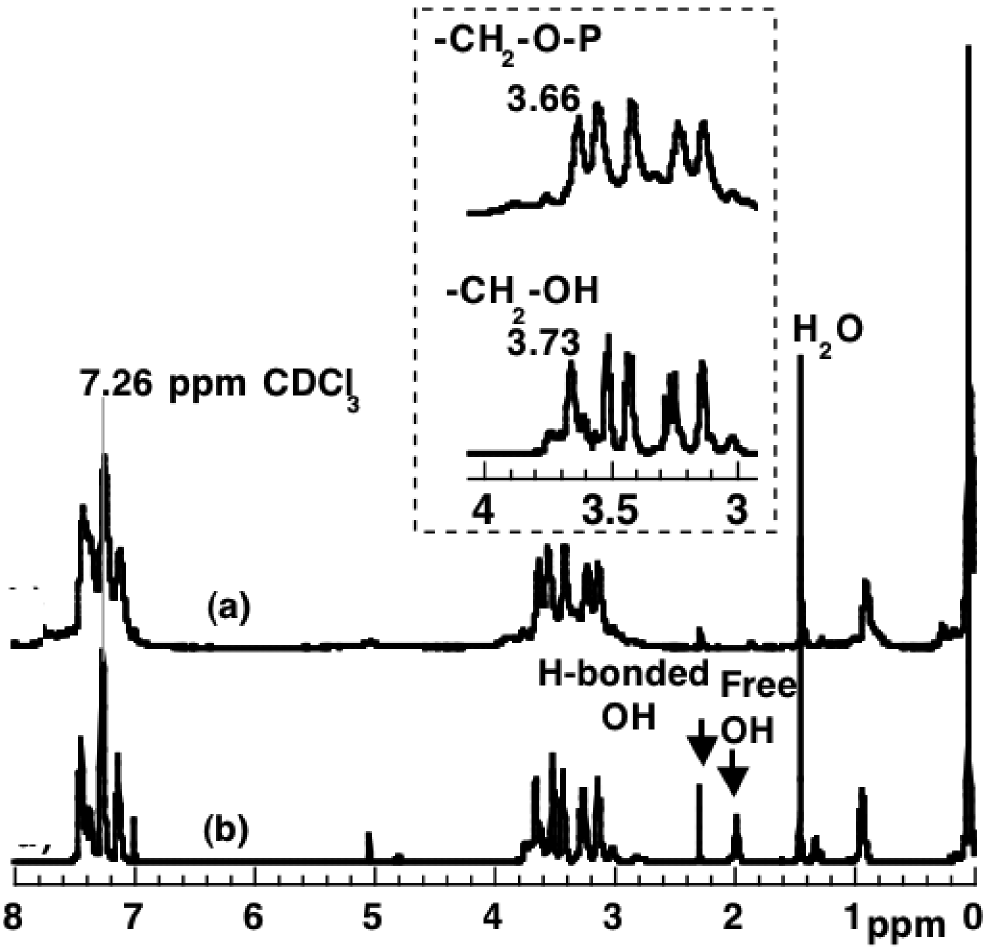

Figure 5.6 ^{1}H NMR spectra of (a) 4DEG-DDSQ, (b) PHOS-DDSQ.

5.3.8. *^{31}P NMR* **Spectrum of PHOS-DDSQ**

Figure 5.7 shows the ^{31}P NMR spectra of PHOS-DDSQ taken in CDC_3. ^{31}P NMR shows one phosphor atom peak, and this peak position or intensity did not change after 2nd time washing with water, which related to the phosphor atom is stable against to the water. [^{31}P NMR (ppm), (161.9 MHz, 85 % H_3PO_4 ref), - 21.4 (($CH_2O)_2$-*P*O-OH)].

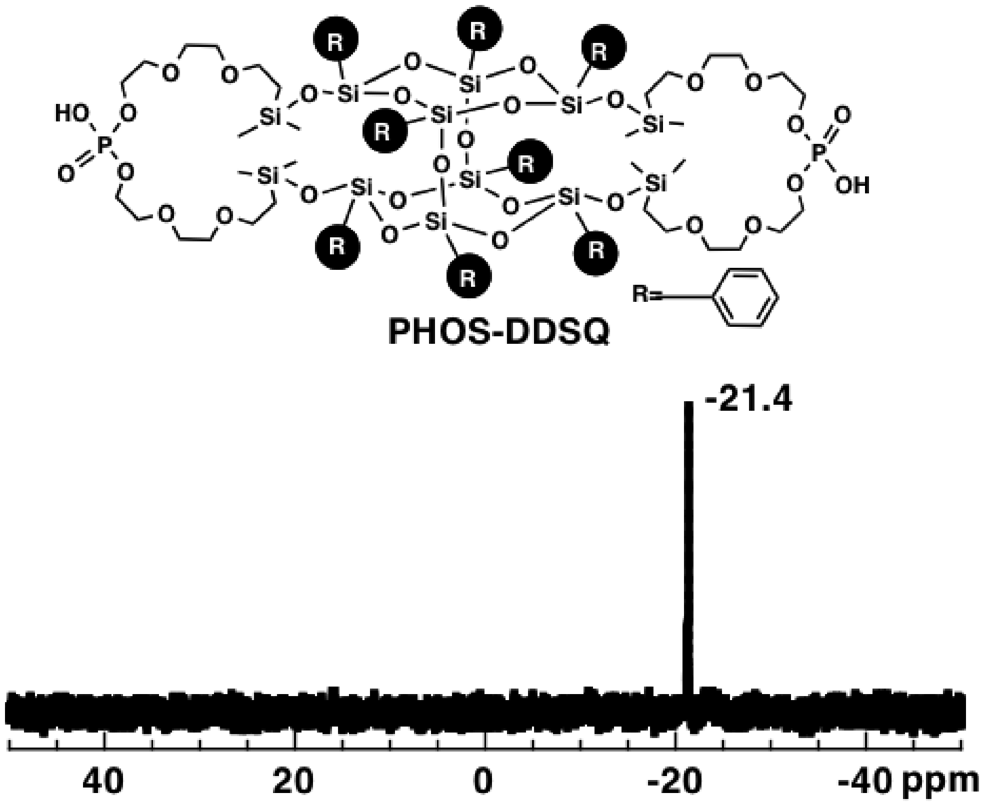

Figure 5.7 ^{31}P NMR spectrum of PHOS-DDSQ.

5.3.9. Maldi-Tof MS Spectrum of PHOS-DDSQ

MALDI-TOF mass spectrum, which shows molecular ions at 2058.50 g mol^{-1} for [M+Ag+, calculated value 2060.27, strongly supports successfully functionalization of 4DEG-DDSQ with phosphonic acid (Figure 5.8). [MALDI-TOF MS =2058.50 (M + Ag^{+}, calculated value 2060.27)].

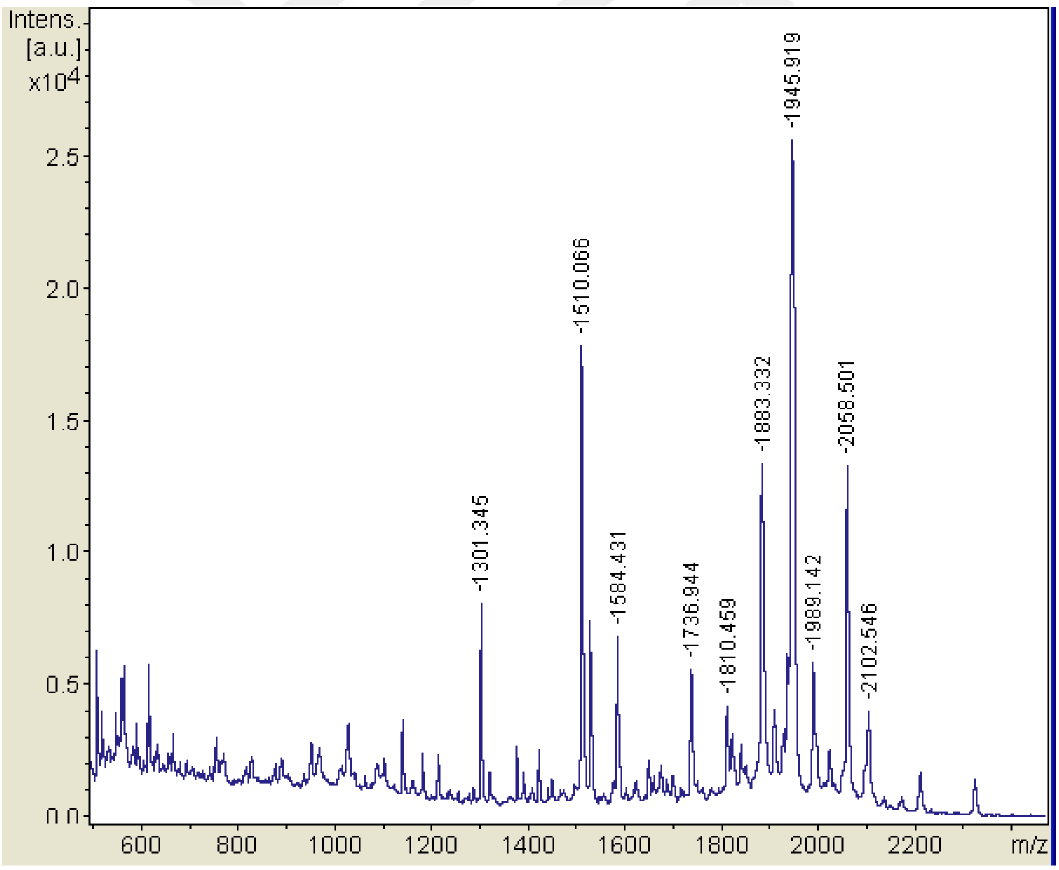

Figure 5.8 Maldi-Tof spectrum of PHOS-DDSQ

5.3.10. XPS Spectrum of PHOS-DDSQ

XPS spectrum shows that the energy binding of phosphor 2p is appeared at 134 eV (Figure 5.9).

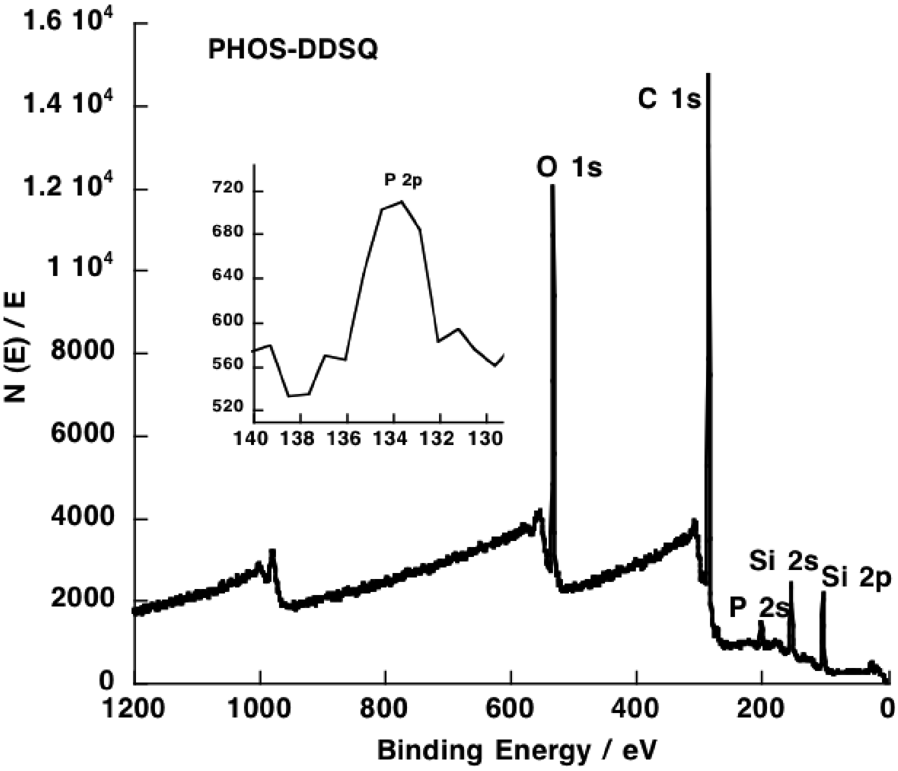

Figure 5.9 XPS spectrum of PHOS-DDSQ.

5.4. Results and Discussion

5.4.1. Syntheses and Characterization of PHOS-DDSQ.

DDSQ (PHOS-DDSQ) containing phosphonic acid was synthesized by reaction of 4DEG-DDSQ with excess $POCl_3$ at 45 ^{o}C (Scheme 5.2). Then the mixture was washed with water to remove $POCl_3$. The FT-IR spectrum of PHOS-DDSQ shows Si-O-Si stretching of DDSQ core at 1057-1150 cm^{-1}, suggesting that DDSQ core remained unchanged during the synthesis (Figure 5.5). The formation of circular structure of PHOS-DDSQ was determined by the following NMR, FT-IR, and XPS spectra and titration measurements results. After the reaction of 4DEG-DDSQ with $POCl_3$, the protons peak related to OH protons, which appeared at 2.24 ppm (hydrogen bonded OH) and 1.85 ppm (free OH) had almost disappeared and methane protons of DEG groups were shifted 0.07 ppm to a higher magnetic field, which indicates that all of the OH groups were reacted with $POCl_3$ (Figure 5.6). The presence of phosphor atoms was also confirmed by ^{31}P-NMR and XPS spectra. The ^{31}P-NMR spectrum of PHOS-DDSQ shows a single peak at -21.4 ppm (Figure 5.7). Moreover, the XPS spectrum of phosphor 2p appeared at 134 eV (Figure 5.9). This binding energy corresponds to that of phosphate group.[42] To determine the acid amount, PHOS-DDSQ was titrated with 0.014 M of NaOH solution using phenolphthalein as an indicator. PHOS-DDSQ was not dissolved in water. Therefore, we applied a two-phase titration. PHOS-DDSQ was dissolved in chloroform and small amount of NaOH solution was added to the chloroform solution. The mix solution was stirred vigorously and the color of NaOH aq was observed. This process was carried out repeatedly until the NaOH solution's color changed from transparent to purple red. The amount of acid in one PHOS-DDSQ molecule was determined to be 1.82 from the titration measurement. According to the spectra and titration measurements, we concluded that the PHOS-DDSQ formed a crown–ether–like conformation. The structure was also supported by MALDI-TOF MS spectra, which showed several peaks because of fragmentation during the measurements. However, the peaks at (1945.91) and (2058.50) can be attributed to M (1952.40) and M+Ag^+ (2060.27), respectively (Figure 5.8). It is noteworthy that the ester bond (C-O-P) is sensitive to hydrolysis. Indeed, when we carried out similar reaction with 2DEG-DDSQ (Scheme 5.1), which has two DEG groups as coronae, results showed that the ester bond was hydrolyzed by several treatments with water. The result of 2DEG-DDSQ reaction indicated that the crown–ether–like structure in PHOS-DDSQ prevents the hydrolysis reaction.

5.4.2. Thermal Properties of PHOS-DDSQ

Thermal properties of PHOS-DDSQ were evaluated by TGA and DSC measurements (Figures 5.10 and 5.11). The temperature of 5% weight loss (T_{d5}) of 4DEG-DDSQ was 316 ˚C whereas that of PHOS-DDSQ was 222 ˚C. The decrease was attributed to the readily occurring decomposition of phosphonic acid groups. Although the temperature stability was decreased about 30%, the decomposition temperature up to 220 ˚C is beneficial for use an intermediate proton–conductive membrane application.

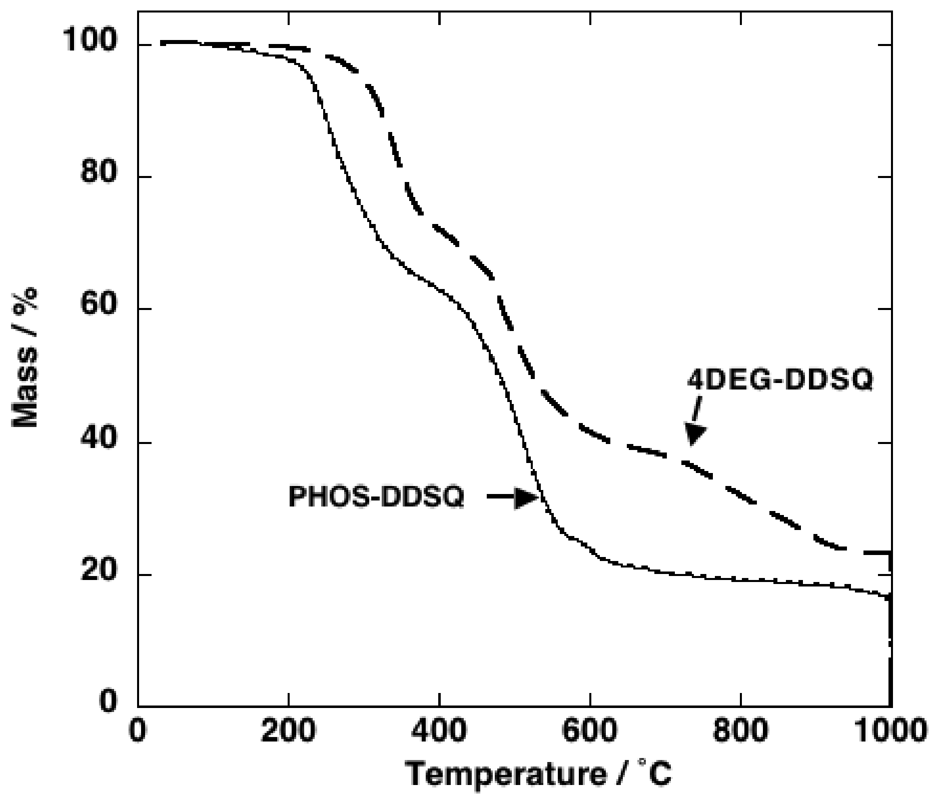

Figure 5.10. TGA thermograms of (a) 4DEG-DDSQ, (b) PHOS-DDSQ.

The DSC third heating curve of PHOS-DDSQ is shown in Figure 5.11 together with those of 4DEG-DDSQ. Both molecules showed a glass transition, which is attributed to amorphous phase transition. The glass transition temperatures are below room temperature (-18 ˚C for 4DEG-DDSQ and -24 ˚C for PHOS-DDSQ). Therefore, both molecules are rubbery solids in room temperature conditions.

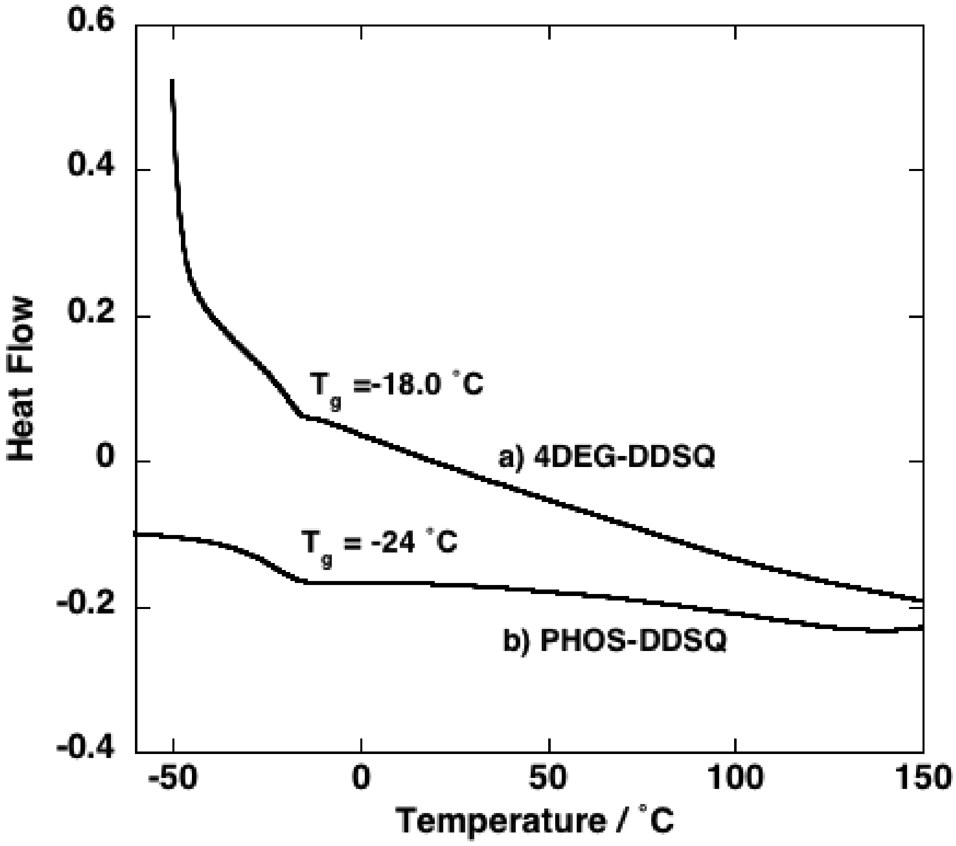

Figure 5.11. DSC thermograms of (a) 4DEG-DDSQ, (b) PHOS-DDSQ.

The amorphous structure was confirmed also using AFM. An AFM image of the PHOS-DDSQ cast film (Figure 5.12) presents a smooth and homogeneous surface morphology showing no phase separation.

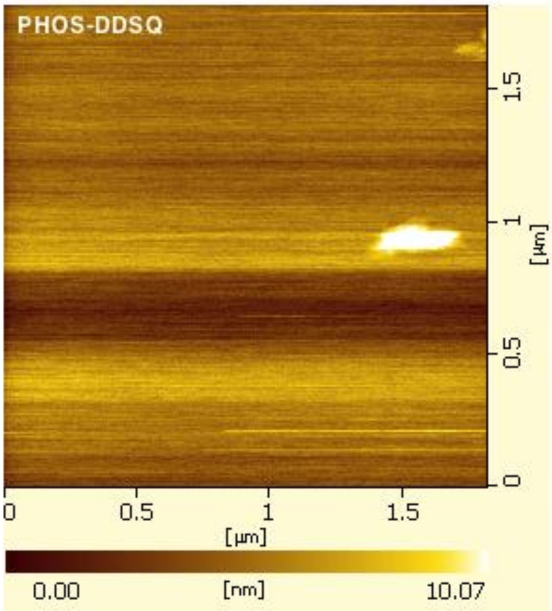

Figure 5.12. AFM image of PHOS-DDSQ cast film.

5.4.3. Proton Conductivity of PHOS-DDSQ.

Drop cast film of 4DEG-DDSQ and PHOS-DDSQ was fabricated onto a glass substrate, where a parallel gold electrode is patterned and the proton conductivity of the cast film was measured by changing relative humidity and temperature. The proton conductivity of 4DEG-DDSQ was too low to be measured in the present condition. However, Cole-Cole plots of PHOS-DDSQ showed tentative semicircle spectra, which indicate that PHOS-DDSQ is a proton–conductive film (Figures 5.13a,b). The film resistance was given directly by the intersection of a semicircle with the real axis in the complex plane of Cole–Cole plots.

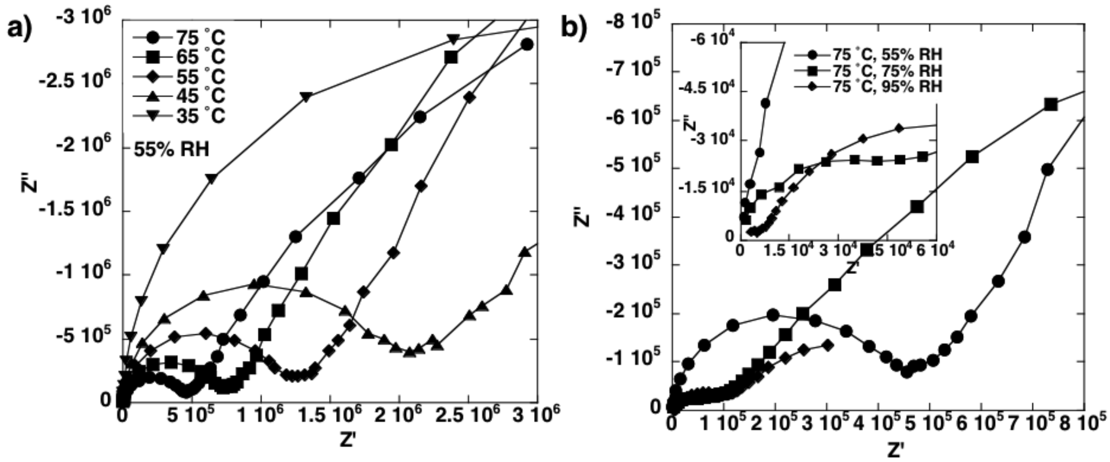

Figure 5.13. The impedance response of the PHOS-DDSQ cast film (a) at the different temperature at 55% RH, (b) at different RH at 85˚C.

The proton conductivity (σ) of the samples was calculated using equation (1). PHOS-DDSQ showed reasonable good conductivity at 85 ˚C in the present measurement relative humidity conditions; 1.2×10^{-3} S cm^{-1} at 55% RH, 1.3×10^{-2} S cm^{-1} at 75% RH, and 1.2×10^{-1} S cm^{-1} at 95 % RH respectively (Figure 5.14a). It is noteworthy that the conductivity at 55–85 ˚C at 95% RH is comparable to that of Nafion.[36] The proton transport in the film occurs via Grotthuss and Vehicle mechanism. In PHOS-DDSQ, the Grotthuss mechanism will be “forming–breaking–forming” hydrogen bonding process among phosphonic acids and between phosphonic acid and water or ether in DEG groups. In the low RH, the hydrogen bonding process between phosphonic acid and water as well as diffusion of water amount decrease, which results in low proton conductivity. The activation energy of PHOS-DDSQ was 40 kJ mol^{-1} at 95% RH (Figure 5.14b, Table 5.1), which is about twice as large as Nafion at 100% RH.[43] The higher activation energy might result from formation of a non-uniform proton–conductive channel.

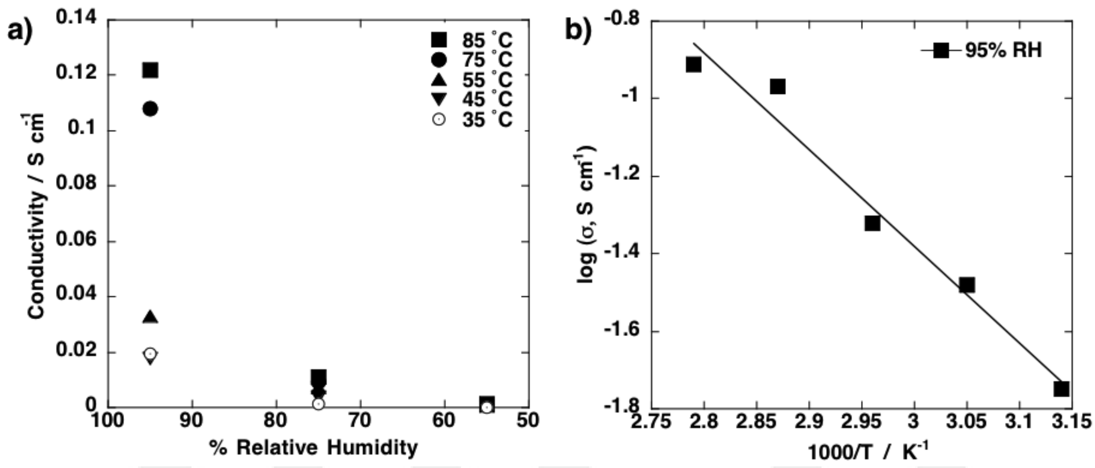

Figure 5.14. (a) Relative humidity dependence of conductivity for the PHOS-DDSQ cast film at 35, 45, 55, 75, 85 °C, (b) Arrhenius plots of proton conductivities of the PHOS-DDSQ cast film measured at 95% RH condition.

The proton conductivity of PHOS-DDSQ in non-humid conditions was also studied. PHOS-DDSQ was cast onto a substrate, where gold electrode is patterned and the substrate was put in a heat chamber and keep at 100 °C for 1 h to dry the film. Then the proton conductivity of the film was measured by changing the temperature. The Cole-Cole plot of the cast film showed a clear semicircle, which indicates that the PHOS-DDSQ showed proton conductivity in non-humid conditions (Figure 5.15a). The conductivity increases concomitantly with increasing temperature up to 170 ˚C. It reaches the value of 3.6×10^{-4} S cm^{-1}, then it drops to a low conductive value. The decrease in conductivity at temperatures higher than 170 ˚C (Figure 5.15b) is attributed to loss of phosphonic acid units caused by self-condensation of these groups.[28] In the non-humid conditions, the amount of water was very low. Therefore protons were transported via hydrogen-bond breaking and forming processes among phosphonic acids and between phosphonic acid and ether oxygen of DEG groups. Results suggest that movements of flexible DEG chains support the process. The conductivity followed the Arrhenius relation in the range of 100–165 ˚C and the activation energy was calculated as 70 kJ mol^{-1} (Figure 5.15c). The activation energy is comparable with other phosphonic acid based polymers value in non-humid conditions.[44]

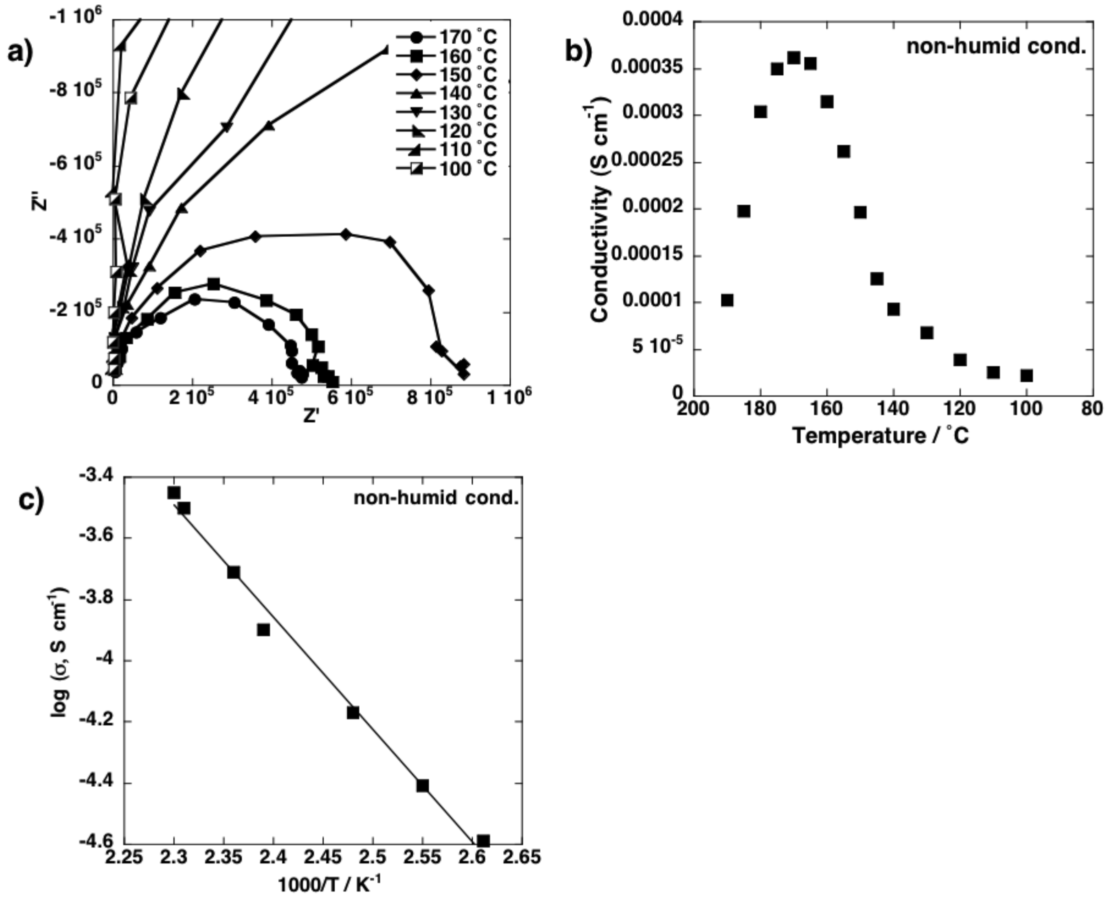

Figure 5.15. (a) The impedance response of the PHOS-DDSQ cast film in non-humid condition, (b) proton-conductivity responds of increasing temperature (c) Arrhenius plot of proton conductivity of the PHOS-DDSQ cast film measured in non-humid condition.

Table 5.1 Arrhenius Relations

	55%	75%	95%	Non-humid
E_a (kJ /mol)	44.0	41.2	44.9	70.8

5.5. Summary

In this study, phosphonic acid group was introduced covalently into DDSQ using DEG as a spacer. According to the spectra and titration measurements, it was concluded that PHOS-DDSQ formed a crown–ether–like confirmation. PHOS-DDSQ showed a high degradation temperature (Td5=222 ˚C) and was stable against hydrolysis reactions. PHOS-DDSQ cast film showed high conductivity (0.12 S cm^{-1} at 85 ˚C) in humid conditions (95% RH). This value is comparable with Nafion. Moreover, proton conductivity of 3.6×10^{-4} S cm^{-1} was achieved in non-humid conditions at 170 ˚C. This report is the first describing a proton–conductive film prepared using only POSS compounds. Now, PHOS-DDSQ is not suitable for fuel cell applications because of their softness. The improvement for increasing mechanical stability by photocrosslinking of the phenyl groups is in progress. The high proton conductivity in humid conditions and moderate to good proton conductivity in non-humid condition as well as the high thermal stability of PHOS-DDSQ present important advantages for fuel cell applications.

5.5.1. **Contribution of DDSQ to High Proton Conductivity**

The contributions of DDSQ to the high proton conductivity can be listed as follows: (i) 'thermal stability' is required to overcome the high temperature proton conductivity without any degradation, (ii) 'flexibility' of DDSQ core contribute the chain movements, (iii) 'double–decker structure' supplies connection of four short chain DEG units, which are functionalized by phosphonic acid in one structure. Moreover, crown ether like structure in PHOS-DDSQ make the phosphonic acid groups stabile against to the hydrolysis in high humidity conditions. The contribution of phosphonic acid attached to end of the DEG units is to provide amorphous film and efficient hydrogen bonding between the architectures. Because of the efficient interaction among phosphonic acid groups or between phosphonic acid and DEG units in amorphous structure,[46] Grotthuss-type mechanism especially in non-humid conditions effectively takes a main role on the proton transportation.

5.6. References

1. Bae, B.; Hoshi, T.; Miyatake, K.; Watanabe, M. *Macromolecules* **2011,** 44, 3884-3892.

2. Hickner, M. A.; Ghassemi, H.; Kim, Y. S.; Einsla, B. R.; McGrath, J. E. *Chemical Reviews* **2004,** 104, 4587-4611.

3. Rikukawa, M.; Sanui, K. *Progress in Polymer Science* **2000,** 25, 1463-1502.

4. Karlsson, L. E.; Jannasch, P. *Journal of Membrane Science* **2004,** 230, 61-70.

5. Xing, P. X.; Robertson, G. P.; Guiver, M. D.; Mikhailenko, S. D.; Kaliaguine, S. *Journal of Polymer Science Part a-Polymer Chemistry* **2004,** 42, 2866-2876.

6. Gil, M.; Ji, X. L.; Li, X. F.; Na, H.; Hampsey, J. E.; Lu, Y. F. *Journal of Membrane Science* **2004,** 234, 75-81.

7. Tian, S. H.; Shu, D.; Wang, S. J.; Xiao, M.; Meng, Y. Z. *Fuel Cells* **2007,** 7, 232-237.

8. Yasuda, T.; Li, Y.; Miyatake, K.; Hirai, M.; Nanasawa, M.; Watanabe, M. *Journal of Polymer Science Part a-Polymer Chemistry* **2006,** 44, 3995-4005.

9. Fujimoto, C. H.; Hickner, M. A.; Cornelius, C. J.; Loy, D. A. *Macromolecules* **2005,** 38, 5010-5016.

10. Kim, D. S.; Robertson, G. P.; Guiver, M. D.; Lee, Y. M. *Journal of Membrane Science* **2006,** 281, 111-120.

11. Schuster, M.; Kreuer, K. D.; Andersen, H. T.; Maier, J. *Macromolecules* **2007,** 40, 598-607.

12. Seesukphronrarak, S.; Ohira, A. *Chemical Communications* **2009**, 4744-4746.

13. Laberty-Robert, C.; Valle, K.; Pereira, F.; Sanchez, C. *Chemical Society Reviews* **2011,** 40, 961-1005.

14. Ianniello, R.; Schmidt, V. M.; Stimming, U.; Stumper, J.; Wallau, A. *Electrochimica Acta* **1994,** 39, 1863-1869.

15. Kreuer, K. D. *Chemphyschem* **2002,** 3, 771-+.

16. Peckham, T. J.; Holdcroft, S. *Advanced Materials* 22, 4667-4690.

17. Schuster, M.; Rager, T.; Noda, A.; Kreuer, K. D.; Maier, J. *Fuel Cells* **2005,** 5, 355-365.

18. Kotov, S. V.; Pedersen, S. D.; Qiu, W. M.; Qiu, Z. M.; Burton, D. J. *Journal of Fluorine Chemistry* **1997,** 82, 13-19.

19. Yamabe, M.; Akiyama, K.; Akatsuka, Y.; Kato, M. *European Polymer Journal* **2000,** 36, 1035-1041.

20. Meng, Y. Z.; Tjong, S. C.; Hay, A. S.; Wang, S. J. *Journal of Polymer Science Part a-Polymer Chemistry* **2001,** 39, 3218-3226.

21. Allcock, H. R.; Hofmann, M. A.; Ambler, C. M.; Morford, R. V. *Macromolecules* **2002,** 35, 3484-3489.

22. Sevil, F.; Bozkurt, A. *Journal of Physics and Chemistry of Solids* **2004,** 65, 1659-1662.

23. Kreuer, K. D.; Fuchs, A.; Ise, M.; Spaeth, M.; Maier, J. *Electrochimica Acta* **1998,** 43, 1281-1288.

24. Xiao, L. X.; Zhang, H. F.; Scanlon, E.; Ramanathan, L. S.; Choe, E. W.; Rogers, D.; Apple, T.; Benicewicz, B. C. *Chemistry of Materials* **2005,** 17, 5328-5333.

25. He, R. H.; Li, Q. F.; Jensen, J. O.; Bjerrum, N. J. *Journal of Polymer Science Part a-Polymer Chemistry* **2007,** 45, 2989-2997.

26. Kawahara, M.; Morita, J.; Rikukawa, M.; Sanui, K.; Ogata, N. *Electrochimica Acta* **2000,** 45, 1395-1398.

27. Yamada, M.; Honma, I. *Polymer* **2005,** 46, 2986-2992.

28. Ingratta, M.; Elomaa, M.; Jannasch, P. *Polymer Chemistry* **2010,** 1, 739-746.

29. Steininger, H.; Schuster, M.; Kreuer, K. D.; Kaltbeitzel, A.; Bingol, B.; Meyer, W. H.; Schauff, S.; Brunklaus, G.; Maier, J.; Spiess, H. W. *Physical Chemistry Chemical Physics* **2007,** 9, 1764-1773.

30. Bock, T.; Mohwald, H.; Mulhaupt, R. *Macromolecular Chemistry and Physics* **2007,** 208, 1324-1340.

31. Granados-Focil, S.; Woudenberg, R. C.; Yavuzcetin, O.; Tuominen, M. T.; Coughlin, E. B. *Macromolecules* **2007,** 40, 8708-8713.

32. Schuster, M.; Meyer, W. H.; Wegner, G.; Herz, H. G.; Ise, M.; Kreuer, K. D.; Maier, J. *Solid State Ionics* **2001,** 145, 85-92.

33. Goward, G. R.; Schuster, M. F. H.; Sebastiani, D.; Schnell, I.; Spiess, H. W. *The Journal of Physical Chemistry B* **2002,** 106, 9322-9334.

34. Schuster, M. E.; Meyer, W. H. *Annual Review of Materials Research* **2003,** 33, 233-261.

35. Donoso, P.; Gorecki, W.; Berthier, C.; Defendini, F.; Poinsignon, C.; Armand, M. B. *Solid State Ionics* **1988,** 28-30, 969-974.

36. Decker, B.; Hartmann-Thompson, C.; Carver, P. I.; Keinath, S. E.; Santurri, P. R. *Chemistry of Materials* **2009,** 22, 942-948.

37. Chhabra, P.; Choudhary, V. *Journal of Applied Polymer Science* 118, 3013-3023.

38. Phillips, S. H.; Haddad, T. S.; Tomczak, S. J. *Current Opinion in Solid State and Materials Science* **2004,** 8, 21-29.

39. Subianto, S.; Mistry, M. K.; Choudhury, N. R.; Dutta, N. K.; Knott, R. *ACS Applied Materials & Interfaces* **2009,** 1, 1173-1182.

40. Cui, L.; Collet, J. P.; Xu, G.; Zhu, L. *Chemistry of Materials* **2006,** 18, 3503-3512.

41. Kucuk, A. C.; Matsui, J.; Miyashita, T. *Journal of Colloid and Interface Science* **2011,** 355, 106-114.

42. Viornery, C.; Chevolot, Y.; Léonard, D.; Aronsson, B.-O.; Péchy, P.; Mathieu, H. J.; Descouts, P.; Grätzel, M. *Langmuir* **2002,** 18, 2582-2589.

43. Asano, N.; Aoki, M.; Suzuki, S.; Miyatake, K.; Uchida, H.; Watanabe, M. *Journal of the American Chemical Society* **2006,** 128, 1762-1769.

44. Parvole, J.; Jannasch, P. *Macromolecules* **2008,** 41, 3893-3903.

45. Sacca, A. P., R.; Carbone, A.; Gatto, I.; Passalacqua, E. . *ECS Trans* **2004,** 11, 357-366.

46. Hickner, M. A. P., B. S. *Fuel Cells* **2005,** 5, 213-229.

6. Chapter 6: Summary and Conclusion

Polyhedral oligomeric silsesquioxanes (POSSs) have attracted much interest because of their unique chemical structures and well-defined geometric shapes. The well-defined organic-inorganic architecture is suitable for constructing a hybrid nano building block. Controlling a structure in nanometer scale provides higher homogeneity, which gives an opportunity to tailor the properties of the materials precisely.

This thesis mainly focuses on preparing nano hybrid double-decker shaped silsesquioxane (DDSQ, one of POSS members) assemblies using Langmuir-Blodgett technique and application of DDSQ derivatives as proton-conducting materials.

This thesis is composed of six chapters as follows:

Chapter 1 provides basic information about silsesquioxane, synthesis of DDSQ molecules and functionalization of them. The preparation process of Langmuir monolayer and Langmuir-Blodgett film and advantages of Langmuir-Blodgett technique are discussed in detail. The technological applications of POSS based on the fuel cell and the background about fuel cell applications are introduced.

In Chapter 2, new "core-coronae" amphiphilic DDSQs were synthesized, and their monolayer behavior on water surface and Langmuir-Blodgett (LB) film formation were studied. Two kinds of amphiphilic DDSQ molecules, which have two or four di(ethylene glycol) units (2DEG-DDSQ and 4DEG-DDSQ, respectively), were synthesized by direct hydrosilylation of di(ethylene glycol) vinyl ether with DDSQs. Surface pressure (π)–area (A) isotherms and Brewster angle microscope (BAM) measurements indicate that both amphiphilic DDSQs form a stable monolayer at the air-water interface.

The 4DEG-DDSQ monolayer on a water surface was deposited on a solid substrate by the LB technique. Atomic force microscope (AFM) images of a one-layer 4DEG-DDSQ film show a homogenous uniform surface on a hydrophilic silicon substrate, whereas nanometer scale dots are formed on a hydrophobic silicon substrate. Multilayer deposition on a hydrophobic substrate result in an increase of dot size with increasing deposition number of layers. Moreover, homogenous multilayer films with a few voids are obtained on a hydrophilic substrate. The results indicate that "core-coronae" type amphiphile 4DEG-DDSQ, in which DDSQ is the hydrophobic core and DEG units are the hydrophilic coronae, is a good candidate for preparing hybrid nanoassemblies.

In Chapter 3, the effect of solutes on monolayer properties of a new "core–coronae" type amphiphile was studied. The "core–coronae" type hybrid amphiphile comprises double-decker-shaped polyhedral silsesquioxane (DDSQ) as a core and four di(ethylene glycol) (DEG) units as coronae (4DEG-DDSQ). The molecule was spread onto a water subphase containing phosphoric acid, 1,3-bis(hydroxymethyl)urea, or potassium chloride. Then monolayer properties were studied using π–A and BAM measurements. Addition of phosphoric acid and 1,3-

bis(hydroxymethyl)urea to the water subphase increased the limiting surface area of the 4DEG-DDSQ monolayer compared to that prepared in the pure water surface. The surface area increase is attributed to formation of strong hydrogen–bonding between OH groups of DEG units and solutes. Although addition of KCl showed a negligible change in the π–A isotherm, and DEG units coordinate with K^+ ions. The monolayer spread on the different subphase was transferred onto a solid substrate and the morphology of the transferred film was observed using AFM. The AFM images show a dot-like structure, irrespective of the subphase composition, whereas the dot size decreases and the dot density increases with addition of solutes.

In Chapter 4, "core–corona" amphiphiles, 2DEGNH-DDSQ, 4DEGNH-DDSQ, which have a urethane group at the end of the coronae, were synthesized to elucidate the effects of hydrogen bonding on monolayer properties. BAM revealed that 2DEGNH-DDSQ formed unique rod-like assemblies. 2DEGNH-DDSQs are well ordered in the rod-like assembly because of the strong hydrogen bonds among the urethane groups, as confirmed by FT-IR spectra. Although the monolayer was not transferred onto a solid substrate, mixing of 2DEGNH-DDSQ with 2DEG-DDSQ, which has already been reported to form a liquid-like monolayer, overcame this problem. The 1:1 molar mixture of 2DEGNH-DDSQ and 2DEG-DDSQ forms a uniform liquid-like monolayer. The mixed monolayer was transferred onto a solid substrate as a Z-type Langmuir–Blodgett film. AFM images of the mixed-bilayer film showed a uniform surface with RMS = 0.21. The intermolecular hydrogen bonds between the urethane groups in 2DEGNH-DDSQ and the hydroxyl groups in 2DEG-DDSQ improve the monolayer properties, which enable successful transfer of the LB film. On the other hand, 4DEGNH-DDSQ forms liquid-like structure at the air water interface similar to 4DEG-DDSQ.

In Chapter 5, phosphonic-acid-containing double-decker-shaped polysilsesquioxane (PHOS-DDSQ) was synthesized and the proton conductivity of PHOS-DDSQ cast film was studied under humid and non-humid conditions. PHOS-DDSQ was synthesized by direct hydrosilylation of di(ethylene glycol) (DEG) vinyl ether with double-decker shaped polyhedral silsesquioxane (DDSQ), with subsequent phosphate esterification of hydroxyl groups. NMR, XPS, and MALDI–TOF MS spectra and titration measurements revealed that two hydroxyl groups of DEG were esterified with one phosphate to form a crown-ether-like structure. That structure prevents hydrolysis of the phosphate ester bond. PHOS-DDSQ showed high thermal stability, with decomposition temperature exceeding 220 °C, because of its inorganic DDSQ core. A uniform film of PHOS-DDSQ can be fabricated by drop casting. The cast film showed high proton conductivity (0.12 S cm^{-1}) in humid conditions, which is comparable to that of a Nafion® membrane. Moreover, the cast film offered good proton conductivity in non-humid conditions (3.6×10^{-4} S cm^{-1} at 170 °C). The conductivity and thermal stability indicate that PHOS-DDSQ is a good candidate for use as a proton-conductive membrane in hydrated type fuel cells as well as fuel cells operated at intermediate temperatures (100–200 °C) in non-humid conditions.

In conclusion, this thesis reports a study of "core-coronae" type amphiphiles based on DDSQ. The self-assembly properties of the synthesized amphiphiles indicates that DDSQ derivatives are good candidates for hybrid nanobuilding block. As described in Chapter 2, 3 and 4, besides the similar features with POSS, DDSQ provides additional advantages such as high yield, easy purification, relatively less rigidness and enables to prepare "core-coronae" type amphiphiles. In addition to this, phosphonic acid containing DDSQ shows high proton conductivity in humid condition and acceptable conductivity in non-humid condition as well as the high thermal stability. The contributions of DDSQ to the high proton conductivity (described in Chapter 5) can be listed as follows: thermal stability, flexibility, and double–decker structure. These properties make DDSQ derivates (PHOS-DDSQ) as an important candidate for proton conductive material in hydrated type fuel cells as well as fuel cells operated at intermediate temperatures (100-200 ˚C) in non-humid condition.

PUBLICATIONS RELATED TO THE THESIS

JOURNAL PAPERS

- 1) **Asuman C. Kucuk**, Jun Matsui, and Tokuji Miyashita, Proton-conducting electrolyte film based on Phosphonic acid Functionalized Double-decker-shaped Polyhedral Silsesquioxanes, Chem. Mater. (to be submitted)
- 2) **Asuman C. Kucuk**, Jun Matsui, and Tokuji Miyashita. Effects of Subphase Composition on the Monolayer Properties of "Core-coronae" Type Hybrid Amphiphiles Langmuir, (to be submitted)
- 3) **Asuman C. Kucuk**, Jun Matsui, and Tokuji Miyashita. Effects of Hydrogen Bonding on the Monolayer Properties of Amphiphilic Double-decker Shaped Polyhedral Silsesquioxanes. Langmuir, 2011, 27 (10), pp 6381–6388, (DOI: 10.1021/la200604w).
- 4) **Asuman C. Kucuk**, Jun Matsui, and Tokuji Miyashita. Langmuir-Blodgett Films Composed of Amphiphilic Double-Decker Shaped Polyhedral Oligomeric Silsesquioxanes. Journal of Colloid and Interface Science, Volume 355, Issue 1, 1 March 2011, Pages 106-114.

CONFERENCE PAPERS

- 1) **Asuman C. Kucuk**, Jun Matsui, and Tokuji Miyashita. "Core-Coronae" Type Amphiphilic Double- Decker Shaped Polyhedral Oligomeric Silsesquioxane. 60th SPSJ Spring Annual Meeting. 25-27 May, 2011, Osaka, JAPAN (Polymer Preprints, Japan Vol.60. No 1(2011))
- 2) **Asuman C. Kucuk**, Jun Matsui, and Tokuji Miyashita. Hydrogen-bonding Effect to the Monolayer Behavior of Amphiphilic Double-Decker Shaped Polyhedral Oligomeric Silsesquioxane. 60th SPSJ Spring Annual Meeting. 25-27 May, 2011, Osaka, JAPAN (Polymer Preprints, Japan Vol. 60. No 1(2011)) (oral presentation)
- 3) **Asuman C. Kucuk**, Jun Matsui, and Tokuji Miyashita. Fabrication of High-Quality Ultrathin Hybrid Film with Blending of Newly Synthesized Amphiphilic POSSs. International conference on Nanoscopic Colloids, September 19-22, 2010, Makuhari, Chiba, JAPAN (oral presentation)
- 4) **Asuman C. Kucuk**, Jun Matsui, and Tokuji Miyashita. Blends of Newly Synthesized Amphiphilic POSSs to form Ultrathin Film, Global COE conference, 2010, Sendai, JAPAN (oral presentation)
- 5) **Asuman C. Kucuk**, Jun Matsui, and Tokuji Miyashita. Morphological Studies of Amphiphilic Polyhedral Oligomeric Silsesquioxane Ultrathin Films Prepared by Langmuir Blodgett Technique, 59th SPSJ Spring Annual Meeting. 2010, Yokohama, JAPAN (oral presentation)

- 6) **Asuman C. Kucuk**, Jun Matsui, and Tokuji Miyashita. Homogenous Monolayer Formation of Amphiphilic Double-Decker-shaped Polyhedral Oligomeric Silsesquioxane by Langmuir Blodgett Technique, JSPS/NRF 2nd Joint Seminar co-located with Young Scientist Meeting February 24, 2010, Yokohama, JAPAN
- 7) **Asuman C. Kucuk**, Jun Matsui, and Tokuji Miyashita. Monolayer Behaviors of Amphiphilic Double-Decker-Shaped Polyhedral Oligomeric Silsesquioxanes, International FAPS conference October 21, 2009, Nagoya, JAPAN (oral presentation)

PATENT

- Tokuji Miyashita, Jun Matsui, **Asuman Celik Kucuk**, Proton-Conducting Membrane Based on Newly Synthesized Silsesquioxane Derivatives, Application date: 27.06.2011, JP2011-142262)

ACKNOWLEDGEMENTS

I would like to acknowledge my advisor, **Professor Tokuji Miyashita** for his guidance, support, appreciation, and encouragement for my research work at Tohoku University.

I would like to thank the committee members, Professor Shin-ichiro Shoda and Professor Tomoyuki Akutagawa for their valuable comments, suggesting, and discussions.

I would like to express my appreciation and give many thanks to Assistant Prof. Jun Matsui for his helpful guidance and discussion in carrying out research.

I have special thanks to Associate Prof. Masaya Mitsuishi and Associate Prof. Akira Watanabe for their kind co-operation and helpful advises.

I also acknowledge fellow graduate students that I had frequent interactions with during my experiments: Rinko Kudo, Takeo Suzuki, Ryosuke Fujii, Shimpei Morita, and Takahiro Ogawa.

Moreover, I appreciate all the past and current members of the Miyashita lab for their friendship and good working atmosphere and all kind of help. I also thank to my friends in the chemistry department for their friendship, refreshing talk, and sharing of their devices and chemicals.

I would like to thank Grants-in-Aid for Scientific Research and

MONBU-KAGAKUSHO Scholorship for supporting this work. I thank Chisso Corp. for supplying DDSQs.

I dearly thank my parents who brought me up and encouraged my pursuit of higher knowledge. I am very grateful to my husband, Dr. Fuat Kucuk, for being patient and tolerant.